Max-Planck-Institut
für Meteorologie

MAX-PLANCK-GESELLSCHAFT

International Max Planck Research School
on Earth System Modelling

A 1D model study of brine dynamics in sea ice

Philipp Johannes Griewank

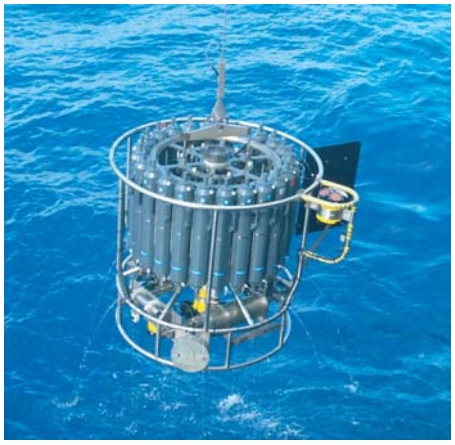

Berichte zur Erdsystemforschung 144/2014

Reports on Earth System Science

Hinweis

Die Berichte zur Erdsystemforschung werden vom Max-Planck-Institut für Meteorologie in Hamburg in unregelmäßiger Abfolge herausgegeben.

Sie enthalten wissenschaftliche und technische Beiträge, inklusive Dissertationen.

Die Beiträge geben nicht notwendigerweise die Auffassung des Instituts wieder.

Die "Berichte zur Erdsystemforschung" führen die vorherigen Reihen "Reports" und "Examensarbeiten" weiter.

Notice

The Reports on Earth System Science are published by the Max Planck Institute for Meteorology in Hamburg. They appear in irregular intervals.

They contain scientific and technical contributions, including Ph. D. theses.

The Reports do not necessarily reflect the opinion of the Institute.

The "Reports on Earth System Science" continue the former "Reports" and "Examensarbeiten" of the Max Planck Institute.

Anschrift / Address

Max-Planck-Institut für Meteorologie
Bundesstrasse 53
20146 Hamburg
Deutschland

Tel.: +49-(0)40-4 11 73-0
Fax: +49-(0)40-4 11 73-298
Web: www.mpimet.mpg.de

Layout:

Bettina Diallo, PR & Grafik

Titelfotos:
vorne:
Christian Klepp - Jochem Marotzke - Christian Klepp
hinten:
Clotilde Dubois - Christian Klepp - Katsumasa Tanaka

Berichte zur Erdsystemforschung 144/2014

A 1D model study of brine dynamics in sea ice

Philipp Johannes Griewank

aus Dallas

Hamburg 2013

Reports on Earth System Science 144/2014

ISSN 1614-1199

Philipp Johannes Griewank
Max-Planck-Institut für Meteorologie
Bundesstrasse 53
20146 Hamburg

Als Dissertation angenommen
vom Department Geowissenschaften der Universität Hamburg

auf Grund der Gutachten von
Prof. Dr. Jochem Marotzke
und
Dr. Dirk Notz

Hamburg, den 8. November 2013
Prof. Dr. Christian Betzler
Leiter des Departments für Geowissenschaften

ISSN 1614-1199

A 1D model study of brine dynamics in sea ice

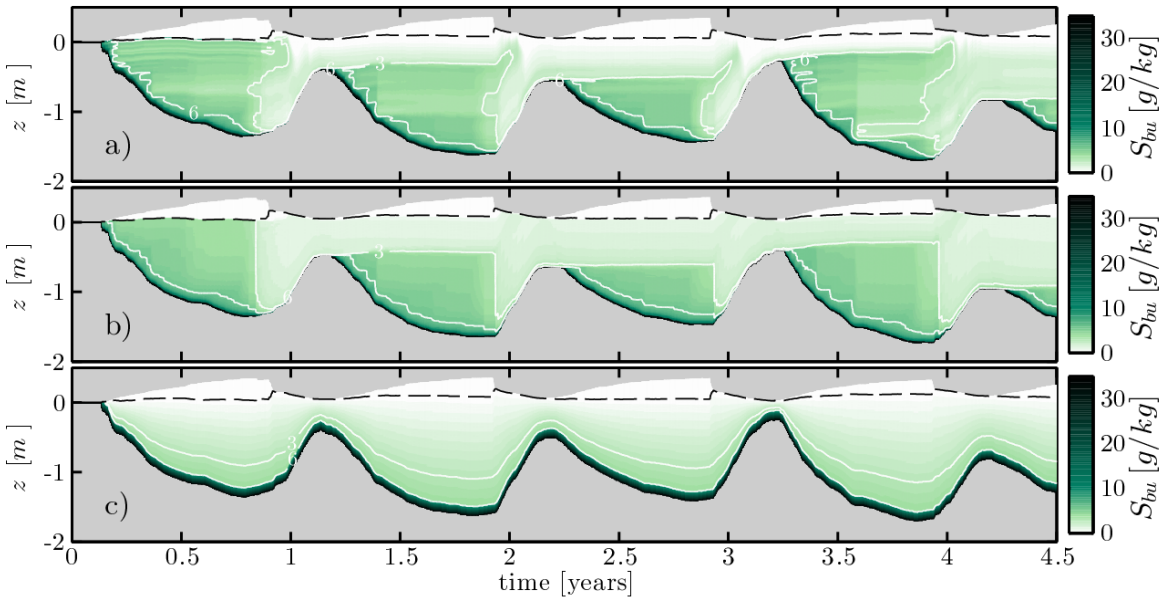

Philipp Johannes Griewank

Hamburg 2013

Abstract

In this thesis I develop a new 1D thermodynamic sea-ice model with parametrized brine dynamics to study brine movement inside sea ice and the evolution of sea-ice salinity. Brine dynamics, which have never been measured directly, are poorly understood and determine the evolution of sea-ice salinity which in turn influences the phase composition and thermodynamic properties of sea ice as well as the stratification of the ocean. The newly developed 1D Semi-adaptive Multi-phase Sea-Ice Model SAMSIM has many unique properties, such as a semi-adaptive grid, a gas volume fraction, different densities of ice and brine, and slush formation during snow melt. The thermodynamic properties and phase composition are calculated according to mushy-layer theory. SASMIM uses a finite volume approach to explicitly conserve enthalpy and mass.

I introduce parametrizations for each of the three desalination processes which occur in sea ice, namely gravity drainage, flushing, and flooding. Our gravity drainage parametrization takes the convective nature of the process into account and is able to reproduce laboratory measurements and fulfill theoretical expectations, a feat unaccomplished by previously proposed parametrizations. In contrast to other attempts, my flushing parametrization explicitly accounts for horizontal flows close to the ice surface. Flooding is the least well understood of the three processes, and no data or theory are available to evaluate the performance of the model. SAMSIM's parametrized salinity evolution agrees well with sea-ice characteristics derived from ice-core data.

By forcing SAMSIM with atmospheric reanalysis data from the Arctic I learn that the depth of gravity drainage varies strongly over time and can span the full ice depth. I also discover that gravity drainage is not restricted to the growth season as previously thought, but is also present as the ice warms and begins to melt. While gravity drainage is most effective in the lower half of warming sea ice, flushing desalinates the upper half of sea ice once surface melt sets in. By comparing the reanalysis forced runs with and without salinity parametrizations I find that prescribing a depth dependent salinity profile characteristic of multi-year ice leads to deviations below 5 % on average. I also introduce a second set of parametrizations which aim to imitate the salinity profile of the original more complex parametrizations but at a reduced computational cost. These simplified parametrizations only reduce the absolute error of the prescribed salinity profile by approximately 1 %.

Contents

Chapter 1

Introduction

Sea ice is a multi-phase material consisting of almost pure fresh water ice, salty brine, and entrapped gas bubbles (Weeks, 2010). It forms a thin and brittle skin on the polar ocean's surface spread across approximately 5 % of our planet. Although sea ice was traditionally only of interest to those who lived and travelled in the coastal regions of the Arctic, scientists quickly recognized the critical role sea ice plays in our global climate system. Sea ice severely dampens the heat flux from the ocean to the atmosphere in winter, and the ice surface reflects the majority of incoming short wave radiation in spring. Sea ice has such a large impact on ocean-atmosphere fluxes and the surface albedo that all atmosphere-ocean models need to include sea ice in some way if they hope to simulate the global ocean and atmosphere circulation with any degree of precision. Aside from these two major effects sea ice also plays a significant role in many other aspects, such as the freshwater and salinity cycle, ocean-atmospheric momentum transfer, biogeochemical processes, and ocean waves.

Public and economic interest in sea ice are increasing. The strong decline of summer sea ice in the Arctic is one of the most visible consequences of anthropogenic greenhouse gas emissions and opens the resources of the Arctic to human development. In the last decade commercial ships have begun sailing the Northern Sea Route and the Northwest Passage. Both routes are expected to become economically viable for shipping over the next decades as sea ice decreases further. Populations along the Arctic coasts are faced with changing sea-ice and climate conditions. Especially hunters and fishers are affected by the rapid decline of sea ice.

1.1 Sea-ice research

There are, broadly speaking, five possible approaches to study sea ice. Field measurements are the most direct and comprehensive approach, as no simplifications or approximations affect the results. However, the logistical, technical, and legal obstacles which need to be overcome in the Arctic and Antarctic make field work costly, dangerous, and unpredictable. A further hindrance is that it is difficult to measure what happens inside sea ice. While the internal temperature profile of ice can be measured with various thermometers, the only common method used to measure the small-scale

physical and chemical properties of sea-ice is ice coring. Taking ice cores is a highly invasive process which is non-repeatable and has not been automated. As a result of these limitations and the general difficulties of conducting sea-ice research in the field, the observational record of ice cores is sparse in both time and space. The quality of the observational record is further degraded by the high heterogeneity of sea ice which requires multiple cores to deduce representative values (as described by Gough et al., 2012). As a result of these issues, much of what occurs inside and below sea ice and the scale of many processes can not be deduced from available field data. A fundamental limitation of field measurements as a tool for scientific inquiry is its irreproducibility and the inability of the investigator to set boundary conditions. This is where the second approach truly shines, namely laboratory studies.

In a laboratory experiments can be repeated and the boundary conditions controlled to accommodate the needs of the investigator. However, even under laboratory conditions sea ice is a difficult substance to sample, and the time and length scales over which sea-ice processes occur make many processes unfeasible to study. For example, it can require months to grow sea ice a meter thick, and individual ice flows can be kilometers wide. An additional limitation is that many common field conditions are difficult to reproduce in a laboratory. Snow for example is of fundamental importance to sea ice, but can not be easily recreated and applied in a controlled fashion.

The third approach used to study sea ice is by analysing satellite retrievals. Researchers have derived sea-ice concentrations from satellite measurements since the late seventies onwards, from which they can compute ice location, drift, extent, and area in both the Arctic and Antarctic (Carsey, 1992). Over the last decade advances have been made to deduce ice thickness from remote sensing data, which is much more difficult to measure than concentration (e.g. Kwok et al., 2004; Kaleschke et al., 2012; Maas et al., 2013). Although satellites are invaluable tools to gain a comprehensive overview of sea-ice conditions in the Arctic and Antarctic, they are plagued by retrieval uncertainty, have a limited resolution, and can only measure radiative properties.

The remaining two approaches are theory and simulation, and sea ice has proven itself to be rather resistant to both. The only aspect of sea ice fully captured theoretically is the thermodynamics of a small mass integral of ice large enough to contain a balanced sample of ice and salty brine. The thermodynamics on this scale are well captured by mushy layer theory, which assumes that the temperature and solid fraction are in balance via the freezing point of the brine (Feltham et al., 2006). Simulations of sea-ice aspects other than thermodynamics are very dependent on parametrizations and approximations. For ice dynamics, a further complication is that even on large scales sea ice becomes very stiff and brakes when sufficiently compressed. This behavior is very difficult to capture numerically, and requires large amounts of iterations and computational resources to solve (e.g. Lemieux et al., 2010; Losch and Danilov, 2012). These theoretical and numerical issues have led to sea ice being represented as simply as possible in climate models. The first and still widely used method of representing sea ice in coupled atmosphere-ocean models is to assign each ocean cell an ice cover fraction and thickness. If no ice is present, both are zero. When ice is present, the ice fraction defines how much of the ocean cell surface is covered by a vertically and horizontally homogeneous slab of ice with a constant salinity. The amount of ice is

given by the ice fraction times the thickness. Ice melt, growth, horizontal transport, and compression are derived from the atmospheric and oceanic boundary conditions in accordance with the ice state, leading to a new thickness and fraction for each new time step. Over the last decades climate models have begun increasing the complexity of the sea-ice components of climate models in the hope of better simulating the Arctic and Antarctic. One proposed method to advance sea-ice models is to move away from the assumption that sea-ice salinity is constant over time (e.g. Vancoppenolle et al., 2007).

That sea-ice salinity varies over time and depth has been well known for a long time (Malmgren, 1927). However, only relatively recently were the processes which desalinate ice clearly identified (Notz and Worster, 2009). Changes of bulk salinity in sea ice are all caused by brine movements in the ice which advect salt. These brine movements are collectively referred to as brine dynamics and are one of the aspects of sea ice which is poorly understood, as brine movements can not be measured directly and can only be inferred indirectly from salinity measurements. Field measurements of salinity are scarce as they require ice coring, and laboratory studies of salinity are mostly restricted to small-scale ice growth experiments which do not capture the full salinity evolution (Cox and Weeks, 1974; Cottier et al., 1999; Notz, 2005). 2D numerical simulations and analytical models of brine fluxes exist, but only for growing sea ice under idealized conditions (e.g. Oertling and Watts, 2004; Petrich et al., 2004; Wells et al., 2010; Rees Jones and Worster, 2013a).

1.2 Thesis outline

In this thesis I study brine fluxes in sea ice and the resulting salinity evolution by parametrizing brine dynamics in a 1D model based on the mushy-layer theory. The new model and parametrizations I develop are used to quantify and analyze the salinity evolution and the brine dynamics. The insights I gain from these studies allow me to quantify the impact the salinity evolution has on sea-ice characteristics relevant to climate models, from which I can deduce which level of salinity representation is ideal for climate models. The insights into brine dynamics are also of great importance to sea-ice biogeochemistry, as the chemical composition in sea ice is highly dependent on the advection of dissolved tracers in the brine. The three key questions my thesis seeks to answer are:

1. How and with which precision can brine fluxes be parametrized in a 1D sea-ice model?

2. When and how do brine movements occur in sea ice, and how does sea-ice salinity evolve over time as a result?

3. How much could climate models benefit from fully parametrizing salinity, and which salinity approach provides the best improvement at a reasonable computational cost?

My PhD research consists of two main components. The first is model and parametrization development, and the second is using the newly developed tools to analyze and study the resulting salinity evolution and its effects. Instead of separating these two components I decided to split the thesis thematically. Chapter 2 focuses on sea ice during growth, and chapter 3 focuses on surface melt and the full salinity cycle. In chapter 2 only the technical aspects and model description are introduced which are needed to simulate sea-ice growth. The remaining model description follows in chapter 3. As a result both chapters consist of equal parts model description and results. Chapters 2 and 3 are written in the style of journal publications. Accordingly, they contain their own abstracts, introductions, and conclusions. Chapter 2 was already published and chapter 3 which is an extension of chapter 2 is currently being prepared for submission.

- In **chapter 2** I focus on gravity drainage during ice growth, the most thoroughly studied and strongest desalination process. Gravity drainage is the convective exchange of cold and dense brine with fresher seawater and occurs mostly in growing sea ice close to ice-ocean interface. Gravity drainage is crucial to the biogeochemistry of sea ice as it replenishes the ice with nutrients. In chapter 2 I introduce SAMSIM, the 1D Semi-Adaptive Multi-phase Sea-Ice Model along with two parametrizations of gravity drainage. I use laboratory salinity measurements to tune my parametrizations and show that my salinity simulations are in better agreement with numerical, theoretical, and observational findings than previous attempts. SAMSIM is then used to study how gravity drainage behaves under a range of conditions. This chapter was published in the Journal of Geophysical Research: Ocean in 2013 and will be referred to as (Griewank and Notz, 2013) in chapter 3.

- In **chapter 3** I implement surface melt and parametrizations of flooding and flushing into SAMSIM and use the newly expanded model to study the salinity of Arctic sea ice. Flooding occurs when enough snow accumulates on the ice surface to push the ice underwater so that ocean water floods the snow. Flushing occurs when melt water percolates downward or flows horizontally into flaws or melt ponds. The inclusion of surface melt, flooding, and flushing, enables SAMSIM to simulate the complete sea-ice evolution. I use SAMSIM to simulate many years of simulated Arctic sea ice, from which I draw conclusions on the transformation of first-year to multi-year ice, on the relationship between bulk salinity and sea-ice thickness, on the characteristics of flushing and gravity drainage, and on the variability of sea-ice salinity. I choose to focus on Arctic sea ice because the newly-developed flooding parametrization poorly reproduces strong flooding events, which are very widespread in the Antarctic. Finally, I study how various salinity approaches implemented in SAMSIM affect sea-ice properties relevant to climate models to asses the impact fully parametrizing the temporal salinity evolution would have on climate models.

- In the final **chapter 4** I summarize the results of chapters 2 and 3 to answer the three questions of my thesis and provide a brief outlook.

Chapter 2

Insights into brine dynamics and sea-ice desalination from a 1D model study of gravity drainage

We study gravity drainage using a new one-dimensional, multi-phase sea-ice model. A parametrization of gravity drainage based on the convective nature of gravity drainage is introduced, whose free parameters are determined by optimizing model output against laboratory measurements of sea-ice salinity evolution. Optimal estimates of the free parameters as well as the parametrization performance remain stable for vertical grid resolutions from 1 to 30 mm. We find a strong link between sea-ice growth rate and bulk salinity for constant boundary conditions, but only a weak link for more realistic boundary conditions. We also demonstrate that surface warming can trigger brine convection over the whole ice layer. Over a growth season, replacing the convective parametrization with constant initial salinities leads to an overall 3 % discrepancy of stored energy, thermal resistance, and salt release. We also derive from our convective parametrization a simplified, numerically cheap and stable gravity-drainage parametrization. This parametrization results in an approximately 1 % discrepancy of stored energy, thermal resistance, and salt release compared to the convective parametrization. A similarly low discrepancy to our complex parametrization can be reached by simply prescribing a depth-dependent salinity profile.

2.1 Introduction

Gravity drainage, which is the convective exchange of cold and dense brine with fresher seawater, is the dominant desalination process in sea ice (Notz and Worster, 2006, 2009) and plays a crucial role in sea-ice biogeochemistry by replenishing the ice with nutrients (Vancoppenolle et al., 2010). Gravity drainage can also be used to efficiently desalinate sea water (Gu et al., 2012). In this paper, we study gravity drainage using the newly developed 1D thermodynamic sea-ice model SAMSIM (Semi-Adaptive Multi-phase Sea-Ice Model) with a convective gravity-drainage parametrization. The model is used in particular to quantify how gravity drainage affects the thermodynamic

properties of sea ice. We also present a simplified salinity parametrization based on our convective parametrization that is suitable for climate models.

Our current understanding of gravity drainage is far from complete, partly because detailed measurements of brine flow in sea ice are largely lacking. Most of our current understanding stems from evaluating salinity measurements from ice cores and laboratory studies of growing multi-phase materials (e.g. Chen, 1995; Wettlaufer et al., 1997; Cottier et al., 1999). However, growing and measuring sea ice in the laboratory over many weeks is a practical challenge, and (to our knowledge) no laboratory sea-ice experiments lasting longer than a month have been conducted.

Detailed field studies of growing sea ice through ice core series are rare owing to the severe logistical issues of taking and processing ice cores under inhospitable climate conditions. Hence, only few such studies exist, most notably those conducted by Nakawo and Sinha (1981), Lei et al. (2010) and Gough et al. (2012). Unfortunately, measuring salinity by ice cores has many drawbacks. These include brine loss from cores, low temporal resolution, and the inability to sample repeatedly due to the destructive nature of core extraction. Gough et al. (2012) conducted a very thorough analysis of their core data showcasing that multiple cores are necessary to obtain representative values. This is due to the high horizontal variability of sea ice, and because salinity measurements from the same core at different heights can not be treated as independent due to a high vertical correlation of measured salinity anomalies.

In this paper, we study gravity drainage numerically. Previous numerical studies can be split into 2D approaches, which simulate the flow field of brine in a vertical slice of growing sea ice, and 1D approaches, which parametrize the brine flow and its effects on the vertical sea-ice profile. 2D models have the drawback of being computationally expensive and/or limited to well defined test cases (see Oertling and Watts, 2004; Petrich et al., 2004; Wells et al., 2010). Proposed 1D parametrizations are either based on the quantitative estimates of Cox and Weeks (1988), or treat gravity drainage as a diffusive process similar to turbulent diffusion in a mixed layer (Vancoppenolle et al., 2010; Jeffery et al., 2011). However, both of these 1D methods are inconsistent with laboratory experiments and 2D simulations from which we know that gravity drainage is not a turbulent process. Saenz and Arrigo (2012) were the first to take the convective nature of gravity drainage partially into account, but their gravity drainage parametrization is still based on the simplified estimates of Cox and Weeks (1988). Our approach extends the findings of small-scale laboratory experiments and 2D numerical simulations to large and longer scales using a 1D thermodynamic model based on mushy-layer theory and a convective gravity drainage parametrization derived from research on brine fluxes from solidifying binary alloys (Wells et al., 2010). A key property of the newly developed thermodynamic multi-phase model SAMSIM is a semi-adaptive grid, which gives us an advantage over previous attempts to parametrize gravity drainage. Instead of prescribing an explicit ice-ocean front, as in the Maykut and Untersteiner model (Maykut and Untersteiner, 1971) and all its descendants (e.g. Semtner, 1976; Bitz and Lipscomb, 1999; Huwald et al., 2005a), the grid ensures that the ice-ocean interface is always well approximated without imposing any assumptions of salinity, temperature or growth rate. Open questions we address in this paper are the link between sea-ice growth speed and bulk salinity, whether gravity drainage can

penetrate deep into the ice, and how gravity drainage can be represented in climate models.

Our new convective parametrization is ill-suited for earth system models as it requires a small time step to avoid instabilities. As an alternative we derive a simpler parametrization from the convective parametrization which can improve sea-ice thermodynamics and salt release into the ocean for climate models. In this paper we refer to the simpler salinity parametrization as the simple parametrization and to the more complex parametrization that calculates brine fluxes as the convective parametrization.

Section 2.2 provides a brief description of SAMSIM. In section 2.3 we introduce the full convective parametrization. Based on it, we also devise the simple salinity parametrization. Section 2.4 contains a description of the Levenberg-Marquadt optimization algorithm and data used to determine the free parameters of our parametrizations. In section 2.5 we conduct our first experiments using idealized boundary conditions. Here we study how growth speeds influence bulk salinity and how deep convection can be triggered. These findings are then compared to a more realistic growth season simulated by forcing the model with three-hourly ERA-reanalysis data in section 2.6. Using this growth season, we study how the thermal properties of the sea ice vary when the salinity is either prescribed, or simulated using the simple parametrization that we introduced in section 2.3. Finally, in section 2.7, we present a summary of our results and conclusions, and discuss how gravity drainage can be represented in climate models.

2.2 SAMSIM description

In the following section we provide a brief overview of SAMSIM, our semi-adaptive multi-phase sea-ice model. The thermodynamic core of SAMSIM is derived from the mushy-layer equations of sea ice (Feltham et al., 2006). Our approach is similar to that of Notz and Worster (2006), but was extended to also include a gas phase and gravity drainage. For an in depth discussion on multi-phase sea-ice models see Hunke et al. (2011).

In contrast to commonly used front tracking models (see Maykut and Untersteiner, 1971; Semtner, 1976; Bitz and Lipscomb, 1999; Huwald et al., 2005a; Saenz and Arrigo, 2012), SAMSIM has no prescribed ice-ocean front. In a front tracking method ice grows by changing the position of the ice-ocean interface at each time step. In contrast, in SAMSIM the solid fraction increases in a grid layer which has a constant thickness at each time step. Although there are many reasons to prefer the front-tracking approach, our approach grants us some additional freedom which we exploit when parametrizing brine dynamics. Additionally, there is a simple theoretical elegance in directly representing sea ice and water as a continuum of varying solid fraction, consistent with the mushy layer nature of sea ice.

SAMSIM is a finite-volume model to allow simple conservation of all conserved properties, such as mass, energy, and tracers. Currently, the spatial and temporal discretisation schemes that are used to solve the heat transport equation

$$q = -k\frac{\partial T}{\partial z}$$

are explicit and of first-order. The time integrated heat flux between the layer i and $i+1$ over a time step of length dt is

$$\int_t^{t+dt} q\,\mathrm{d}t = -k\frac{T^i - T^{i-1}}{\frac{\triangle z^i + \triangle z^{i-1}}{2}} \cdot dt$$

which requires a small time step to satisfy the CFL condition for heat diffusion

$$\frac{k\ dt}{\rho c \triangle z^2} < 0.5$$

. Higher order and implicit schemes can be implemented if a longer time step is needed, but were unnecessary for this study as we require a small time step to resolve the brine dynamics.

2.2.1 Layer properties

SAMSIM is a 1D finite-volume model, in which each layer is horizontally and vertically homogeneous and all phases are in local thermal equilibrium with each other. Each layer is defined by four core variables: absolute salinity S_{abs}, absolute enthalpy H_{abs}, mass m, and thickness $\triangle z$. The absolute enthalpy is the total Joules of enthalpy, and the absolute salinity is the total salt content in the layer in grams. From the absolute salinity, absolute enthalpy, and mass we derive temperature T and solid mass fraction ψ by numerically solving the following set of equations for enthalpy (H), bulk salinity (S_{bu}), brine salinity (S_{br}), and ψ:

$$H = \frac{H_{abs}}{m} = -\psi L + f(T) \tag{2.1}$$

$$S_{bu} = \frac{S_{abs}}{m} = S_{br}(1-\psi) \tag{2.2}$$

$$S_{br} = g(T) \tag{2.3}$$

The appropriate value of latent heat (L), the integral of the heat capacity with respect to temperature ($f(T)$), and the brine salinity as a function of temperature ($g(T)$) are material specific and their accuracy can be varied as desired. By approximating gas as massless, we can derive the solid, liquid, and gas phase volume fractions (ϕ_s, ϕ_l, and ϕ_g) from ψ, $\triangle z$, and m.

Salt is treated as a massless tracer but brine density is a function of brine salinity. When brine moves between layers, salt advection is calculated via the simple upstream method. The simple upstream method is artificially diffusive, especially when the tracer concentration has steep gradients. Since the brine salinity is determined by the temperature and since the temperature profile in sea ice is rather smooth, the artificial diffusion for salinity is small. If passive tracers were introduced, a more sophisticated advection method might be needed.

The thermal conductivity of each layer is simply the volume weighted sum of the solid and liquid fractions $k = \phi_s k_s + \phi_l k_l$. The gas fraction is treated as a perfect insulator and does not contribute to the layer's conductivity.

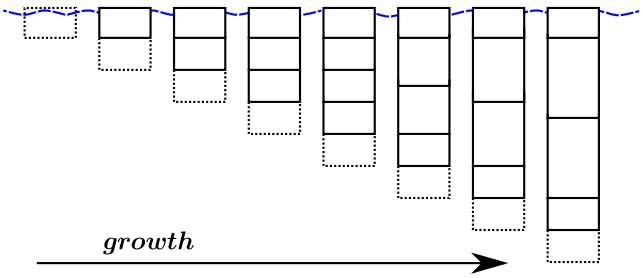

Figure 2.1: Semi-adaptive grid evolution during growth for N=5, N_{top}=1, N_{mid}=2, N_{bot}=2 (see subsection 2.2.2).

2.2.2 Semi-adaptive grid

SAMSIM employs an irregular 1D grid which we refer to as a semi-adaptive grid for lack of a better term. This grid consists of a set number of top and bottom layers (N_{top} and N_{bot}) with a constant thickness of $\triangle z_0$, and a variable number of adaptive middle layers (N_{mid}) which grow and shrink in steps of $\triangle z_0/N_{mid}$ as needed. When the ice is so thin that not all layers are needed surplus layers are deactivated. When the number of active layers (n) is less than the maximum number of layers (N=$N_{top}+N_{mid}+N_{bot}$), all active layers share the thickness $\triangle z_0$. If no ice is present at all, SAMSIM shrinks to a single layer. The layers are indexed from top to bottom. This means that the index i of the top layer is 1, the lowest active layer has the index n, and when all layers are active the lowest layer has the index N.

Figure 2.1 shows how SAMSIM's semi-adaptive grid evolves during growth for N=5, N_{top}=1, N_{mid}=2, N_{bot}=2. Starting from a single layer of open water (n=1), the grid grows to ensure that the solid volume fraction ϕ_s^n in the lowest active layer always lies below a certain fixed value ($\phi_s^n < \phi_s^{min}$). When ϕ_s^n increases beyond the limit value ϕ_s^{min} a new layer of underlying ocean water is added. If not all layers are activated ($n < N$) the new layer is created by activating one of the previously deactivated layers. If $n = N$ then the uppermost bottom layer is merged into the middle layers, and all the bottom layers are shifted downwards by one. When this occurs all middle layers grow thicker by $\triangle z_0/N_{mid}$. The resulting changes of the core variables in the middle layers is calculated using simple upstream advection. For example, if only two middle layers exist both layers grow by $\triangle z_0/2$, and a mass of $\triangle z_0/2$ times the density of the lower middle layers is reallocated to the upper middle layer. Conversely, the lowest layer is dissolved when ϕ_s^n=0 and $\phi_s^{n-1} < \phi_s^{min}/2$. The lowest layer is dissolved only when $\phi_s^{n-1} < \phi_s^{min}/2$ to ensure that new layers are not dissolved shortly after forming, when ϕ_s^n=0 and $\phi_s^{n-1} \approx \phi_s^{min}$. It is possible to set ϕ_s^{min} to zero, but under certain conditions this can lead to many bottom layers with very low solid fractions. In nature these very low solid fractions would indicate free floating ice crystals. ϕ_s^{min} can be understood physically as the minimum amount of ice needed for the ice crystals to form a connected mushy layer.

All tests performed in this paper use a value of 0.05 for ϕ_s^{min}, which results in a slight artificial cut off at vertical resolutions of 1 or 2 mm. Raising ϕ_s^{min} up to 0.10 barely effects results, but instabilities occurred at values lower than 0.03.

The semi-adaptive grid has three major advantages. First, it allows SAMSIM to keep

the spatial resolution constantly high at the ice-ocean and ice-atmosphere boundaries without exceeding a set maximum amount of layers. The second advantage is that no numerical diffusion occurs in the bottom layers due to moving layer boundaries. Instead, newly formed bottom layers retain their salinity, enthalpy and mass as they are shifted upwards in steps until they are merged into the middle layers. The final advantage is that the lowest layer —which represents the water at the ice-ocean interface— can evolve freely, which lets SAMSIM imitate processes such as underplating to a certain extent. Underplating refers to the collection of relatively light freshwater below the ice and above the denser underlying ocean water.

For the aims of this study, these advantages of the semi-adaptive grid far outweigh its disadvantages. These disadvantages include temporal discontinuities in the simulations caused by the finite-size, step-wise addition and removal of layers. Additionally, vertical tracer advection across the transition from thin to thicker layers can cause nonphysical tracer transport. However, these numerical artifacts are small and can safely be neglected in this paper, since gravity drainage is mostly localized to the thin bottom layers. A further disadvantage of SAMSIM's grid are possible difficulties in its horizontal advection, which, again, is irrelevant for our one-dimensional study. Finally, SAMSIM's grid causes a somewhat larger computational burden compared to traditional grids, because the thin top and bottom layers limit the time step.

For specific purposes, such as calculating the ice thickness, we require a defined ice-ocean front which is not provided a-priori by SAMSIM's grid. For such purposes we linearly interpolate a value from the solid volume fraction of the lowest layer. For example, if $\phi_s^n = \phi_s^{min}/3$, we would assume the upper third of the bottom layer to contain sea ice. The diagnosed ice-ocean front does not move smoothly, especially during melt. The impact of these steps on the Rayleigh number is discussed in subsection 2.5.2.

For the purpose of this paper, snow is treated as a single layer of varying thickness with constant density and constant thermal conductivity. Although this simple setup is still standard for sea-ice components of earth system models, there have been recent efforts to include more sophisticated representations of snow in climate models since the snow has such a low and varying thermal conductivity (Lecomte et al., 2011).

2.2.3 Brine expulsion

Because the density of ice is lower than that of water, freezing sea ice expels excess brine. This process is known as brine expulsion and was once believed to be an important desalination process in thin ice (Cox and Weeks, 1975). Notz and Worster (2006, 2009) have demonstrated that although brine expulsion redistributes salt in the sea ice, the amount of salt that leaves the ice is negligibly small. However, brine expulsion is crucial to the density evolution of sea ice.

SAMSIM determines the amount of brine which is expelled by checking if the summed volume of liquid brine and solid ice exceeds the volume of the layer at each time step. If the volume does exceed the layer volume SAMSIM assumes that the excess brine is always moved to the layer below, regardless of the properties of the lower layers. The same approach was used in the 1D model of Maksym and Jeffries (2000). In

reality, brine can move upwards as well. Upward displaced brine can cause thin skins of extremely salty brine on top of the sea ice, a behavior Roscoe et al. (2011) captured with time-lapse photography. However, since it has been shown analytically and numerically that the total amount of salt transported downward by expulsion leads to maximum deviations of roughly 1 ppt (Chiareli and Worster, 1995; Notz, 2005) and the amount of upward displaced brine is likely much smaller than the amount of downward displaced brine, we expect the bulk salinity errors in SAMSIM introduced by our unidirectional implementation of brine expulsion to be far below 1 ppt.

2.3 Gravity drainage parametrizations

In contrast to 2D or 3D models, a 1D model is incapable of resolving a convective process and gravity drainage can only be parametrized. Previous one-dimensional parametrizations of gravity drainage were presented by Cox and Weeks (1988),Vancoppenolle et al. (2010),Jeffery et al. (2011), and Saenz and Arrigo (2012). The empirical approach of Cox and Weeks (1988) calculates desalination in growing ice as a combination of initial salt entrapment, brine expulsion and gravity drainage. However, we know now from experiments and theory that both initial salt entrapment and brine expulsion do not desalinate the ice (Notz and Worster, 2009). Both Vancoppenolle et al. (2010) and Jeffery et al. (2011) treat gravity drainage as a diffusion caused by brine mixing, similar to turbulent mixing in boundary layers. However, both of these approaches are in contrast to studies of growing mushy layers which have shown that gravity drainage is a convective process linked to chimney formation (e.g. Tait and Jaupart, 1992; Chen, 1995; Wettlaufer et al., 1997; Notz and Worster, 2008). In sea ice, these chimneys are commonly referred to as brine channels. Saenz and Arrigo (2012) were the first to incorporate some limited convective aspects of gravity drainage into a 1D parametrization. However, the parametrization of Saenz and Arrigo (2012) relies heavily on empirical values, both to determine initial desalination and stable solid fractions. We have developed two new one-dimensional parametrizations of gravity drainage; a *convective* parametrization and, derived from it, a *simple* parametrization. The convective parametrization attempts to simulate brine movement as accurately as possible based on a few core assumptions. The simple parametrization is an attempt to produce a realistic salinity evolution at a lower computational cost.

2.3.1 Rayleigh number

Following previous studies (e.g. Tait and Jaupart, 1992; Wettlaufer et al., 1997), the onset and strength of gravity drainage in our parametrizations is linked to a porous-medium/mushy-layer Rayleigh number (R). In general, such a Rayleigh number describes the ratio of driving buoyancy to both thermal diffusion and viscous resistance in a porous medium. However, the specific formulations used to calculate R vary considerably and are highly dependent on the assumed permeability. Due to this high variability in definitions, it is difficult to compare Rayleigh number values from different studies. A clear distinction should be made between Rayleigh numbers that represent

the whole vertical sea-ice profile, and discretized local Rayleigh numbers that represent the convective flow from a specific single horizontal layer to the underlying ocean. We use R^i to refer to the Rayleigh number of the layer i. As many of our assumptions are based on the results of Wells et al. (2010), we strive to keep our definition of the Rayleigh number qualitatively similar to their definition.

R^i can be regarded as the ratio of two representative timescales; the advective timescale t_A^i and the diffusive timescale t_D^i. The advective timescale is defined by the amount of time that the buoyancy driven brine in layer i needs to reach the ice-ocean interface. According to Darcy's law the brine moves at a characteristic speed of

$$v = \frac{g \triangle \rho \Pi}{\mu}$$

in which g is the gravitational acceleration, $\triangle\rho$ is the density difference between the brine and the underlying ocean water, μ the dynamic viscosity of the brine, and Π the sea-ice permeability which is discussed in subsection 2.3.4. Accordingly, the time needed for brine to move the distance h^i from layer i to the ice-ocean interface equals

$$t_A^i = \frac{h^i \mu}{\tilde{\Pi}^i g \triangle \rho^i} \ .$$

Instead of the permeability of the layer i we use the minimal permeability of the layers beneath i,

$$\tilde{\Pi}^i = \min(\Pi^i, \Pi^{i+1}, ..., \Pi^n),$$

as the most impermeable layer acts as a bottleneck to the flow. Using the minimal permeability is a simplification of the harmonic mean, which is the correct approach to determine the bulk permeability for a Darcy flow through a stack of layers.

The diffusive timescale

$$t_D^i = \frac{(h^i)^2}{\kappa}$$

represents the diffusion time of thermal anomalies over the distance h^i for a given thermal diffusivity κ. The diffusive timescale reflects the time necessary for the relatively cold brine traveling downward in the channels to warm to the temperature of the surrounding sea-ice.

To calculate the thermal diffusivity representative values of thermal conductivity, thermal capacity, and density must be chosen $\kappa = k/(\rho c)$. Often the phase-averaged values of sea-ice are chosen in accordance with mushy-layer theory (e.g Vancoppenolle et al., 2006; Wells et al., 2010, 2011). However, as mushy-layer theory is based on the phase liquidus relation at thermal equilibrium, it can not capture the non-equilibrium thermal interactions between the cold brine in the channels and the warmer surrounding sea ice. The heat flux from the sea ice to the brine channels depends on the geometry of the brine channels, the flow field in the channels, and the speed with which the salty brine dissolves the channel walls. Instead of the phase-averaged values of sea ice we use the thermal conductivity, capacity, and density of the brine to calculate the

thermal diffusivity for the following reasons. Firstly, due to the fact that the mass of the surrounding sea-ice is much greater than the mass of the brine flowing through the channels, the surrounding sea ice cools much less than the brine in the channels warms and can be considered thermally inert. Secondly, as the thermal diffusivity of the brine in the channels is up to eight times smaller than the phase-averaged values of the surrounding sea-ice, thermal anomalies in the brine channel persist longer than in the surrounding sea ice. Both of these considerations indicate that the heat flux from the surrounding sea ice to the cold brine in the channels is limited by the thermal diffusivity of the brine itself and not by the thermal diffusivity of the surrounding sea ice. Our reasoning focuses on the thermal imbalance in the brine channels, but it is possible that the thermal dissipation of the upwelling brine in the surrounding mush dominates. However, until a more detailed 2-D or 3-D analysis of gravity drainage can conclusively resolve the issue, we will use the brine thermal diffusivity as a working assumption.

By computing density differences via the difference of brine salinity to the salinity of the lowest active layer n which represents the water at the ice-ocean interface, $\triangle\rho^i = \rho_l\beta\triangle S^i = \rho_l\beta\triangle(S^i_{br} - S^n_{br})$, the resulting Rayleigh number is

$$R^i = \frac{t^i_D}{t^i_A} = \frac{g\triangle\rho^i\tilde{\Pi}^i h^i}{\kappa\mu} = \frac{g\rho_l\beta\triangle S^i\tilde{\Pi}^i h^i}{\kappa\mu}. \tag{2.4}$$

A high Rayleigh number indicates that the moving brine flows quicker than thermal diffusion can enforce thermal equilibrium. As long as the moving brine is colder than the surrounding brine, it remains saltier and heavier and keeps descending. A low Rayleigh number indicates that thermal diffusion acts quicker than advection, returning the brine to thermal equilibrium and negating its buoyancy. Assuming both timescales are identical, brine in the ice would be brought into thermal (and salinity) equilibrium just as quickly as it moves, resulting in a neutral buoyancy. This dependence of the convective strength on the Rayleigh number is the core of the convective parametrization we now turn to.

2.3.2 Convective parametrization

The convective parametrization strives to simulate the convective brine fluxes as accurately as possible. Our approach was heavily inspired by the 2D numerical studies of growing mushy layers conducted by Petrich et al. (2004) and Wells et al. (2010). By assuming that chimney spacing in growing mushy layers maximizes potential energy transport, Wells et al. (2010) linked solute flux to the Rayleigh number of the convecting mushy layer. They concluded that the solute flux increases approximately linearly with the Rayleigh number when the Rayleigh number is above a critical value. Below that value the circulation breaks down. Rees Jones and Worster (2013a) found an analytically derived linear relationship of solute flux to Rayleigh number for 2D planar flows. Rees Jones and Worster (2013a) numerically extended their approach to 3D flows to discover some nonlinear behavior between solute flux and Rayleigh number.

However, despite these nonlinear effects Rees Jones and Worster (2013b) still recommend parametrizing gravity drainage using a linear relationship of Rayleigh number to solute flux.

Wells et al. (2010) imitate a growing mushy layer with constant and well defined boundaries using a quasi-steady-state approach. As SAMSIM aims to simulate sea ice under all the variable conditions of the Arctic and Antarctic, our 1D parametrization must be able to deal with a much wider range of changing boundary conditions. We adopt the Wells et al. (2010) 2D results to a 1D parametrization using the following assumptions:

1. If the Rayleigh number of a layer is above a critical value, brine leaves the ice via brine channels into the underlying ocean.
2. The amount of brine leaving each layer i is proportional to $R^i - R_{crit}$.
3. All brine which leaves through channels is replaced by brine moving upward through the mush from the ocean.
4. Brine moving upward transports salt and thermal energy from layer to layer.
5. Brine leaving the sea ice downward through channels moves quickly enough that thermal interactions with the surrounding ice can be neglected.

Although we have strong support for all of these assumptions from 2D simulations and experiments, the more the conditions in the 1D model differ from the conditions simulated by Wells et al. (2010), the less confident we are in our assumptions. This is especially relevant for deep convection in thick ice. The first assumption implies that brine channels always exist when the Rayleigh number exceeds the critical value. Although this can be safely assumed near the ice-ocean interface, we have no evidence this assumption is always valid in thick ice. Cole and Shapiro (1998) found that brine channels typically extended 30 to 50 centimeters into 1.4 meter thick slices of first-year ice taken from two locations near Barrow. However, no channels were found that extended completely through the ice sheet. To truly validate or invalidate our assumption a much more thorough study of brine channels would be necessary.

The second assumption results in two free parameters, the critical Rayleigh number R_{crit} and a proportionality constant α which has the physical dimension of $kg/(m^3 s)$. How we estimate these parameters is described in section 2.4. This second assumption is not identical to the findings of Wells et al. (2010), because Wells et al. (2010) linked the total brine flux to a non-local Rayleigh number and we link the brine flux of each layer to a local Rayleigh number. As no data or theory exists on how gravity drainage interacts with entrapped gas bubbles, our gravity drainage parametrization simply ignores the gas fraction.

Assumptions three and four are similar to those of the channel-active-passive-zone model proposed by Rees Jones and Worster (2013b) and are justified by the results of Wells et al. (2010) and Rees Jones and Worster (2013a). Figure 2.2 contains a sketch of the resulting brine and salt fluxes at the bottom of growing sea ice. In the sketch, the second to fourth lowest layers are equally unstable ($R^{n-1} = R^{n-2} = R^{n-3} > R_{crit}$)

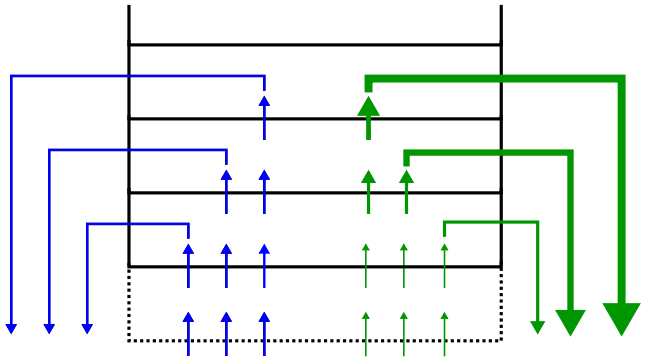

Figure 2.2: Sketch of brine fluxes (blue) and resulting salinity fluxes (green) of the convective gravity drainage parametrization in the bottom ice layers during growth (see subsection 2.3.2). The blue arrows leaving the column represent brine leaving the ice through brine channels and entering the ocean. The short blue arrows represent the upwelling brine which replaces the brine leaving the ice. Arrow thickness indicates flux strength. Although the brine fluxes are of the same strength, the resulting salt flux are stronger from the colder upper layers as the brine salinity is higher.

which leads to identical mass fluxes. Although the brine fluxes are of the same strength, the resulting salt flux are stronger from the colder upper layers because the brine salinity is higher. The resulting heat fluxes would be opposite to the salt fluxes, with the warmer lower layers moving heat upward into the colder layers.

The model calculates the temperature, volume fractions and brine salinity of all active layers from 1 to n at the beginning of each time step according to equations (2.1), (2.2), and (2.3). Using those values the Rayleigh number of each layer (besides the lowest) is calculated. If $R^i > R_{crit}$ we consider the layer i convectively unstable. The mass of brine that flows from layer i ($br^i_\downarrow$) into the ocean in a time step of length dt is

$$br^i_\downarrow = \alpha(R^i - R_{crit}) \triangle z^i \cdot dt.$$

The downward flowing brine is scaled by the time step dt and the layer thickness $\triangle z$, and has the temperature and salinity of the layer it originated from. Note that what we refer to as brine mass flow is synonymous with liquid mass flow. After $br_\downarrow$ has been computed for all layers, the resulting upward brine fluxes from layer $i+1$ to layer i resulting from mass conservation are

$$br^i_\uparrow = br^{i-1}_\uparrow + br^i_\downarrow = \sum_{k=1}^{k=i} br^k_\downarrow$$

The amount of brine entering the layer i from below is $br^i_\uparrow$ which equals the sum of brine leaving that layer. Since we advect salt with the upstream method, the amount of salt which enters the layer i per time step is $br^i_\uparrow \cdot S^{i+1}_{br}$ and the amount of salt leaving the layer i is $(br^{i-1}_\uparrow + br^i_\downarrow) \cdot S^i_{br}$. The resulting change in absolute salinity is

$$\triangle S^i_{abs} = br^i_\uparrow \cdot S^{i+1}_{br} - (br^{i-1}_\uparrow + br^i_\downarrow) \cdot S^i_{br} = br^i_\uparrow \cdot (S^{i+1}_{br} - S^i_{br}). \tag{2.5}$$

An implication of these assumptions is that brine movement occurs in convectively stable layers when a higher layer is convectively unstable. The physical rationale behind this is that preexisting brine channels through the stable layers allows brine from the unstable layers to flow downwards without interacting with the stable layers. However, the resulting upward welling brine fluxes through the mush advect salt and heat. As long as the temperature decreases towards the ice surface, the upwelling brine leads to a desalination of the stable layers, which in turn reduces the convective instability of the layers above.

This convective parametrization requires a small time step, especially since the bottom layers of SAMSIM are thin. In this paper the bottom layers vary from 2 mm to 5 cm. A basic numerical rule of thumb for 1D advection is that the distance traveled by the fluid per time step should not be larger than a tenth of the grid spacing. Translated to SAMSIM this rule states that the volume of brine moving from layer to layer per time step should not be larger than a tenth of the brine volume in those layers. The brine volume of each layer and the flow are extremely variable, so a small time step is necessary to avoid numerical instabilities. Although a simple flux correction is implemented to ensure that the salt advection remains positive definite, the computational cost of the stand-alone model is small enough that we can chose the time step to be as small as we need.

Recently, a scheme which shares some of our assumptions was successfully implemented into the Los Alamos Sea Ice Model (Turner et al., 2013).

2.3.3 Simple parametrization

The convective parametrization is ill-suited for earth system models as it requires a small time step to avoid instabilities. As an alternative we propose a simpler parametrization as a tool to improve sea-ice thermodynamics and salt release into the ocean for climate models. In this paper we refer to the simpler salinity parametrization as the simple parametrization and to the more complex parametrization that calculates brine fluxes as the convective parametrization.

The simple parametrization is based on the assumption that convectively unstable layers lose salinity until they are stable. This assumption is a simplification of the convective parametrization in which convectively unstable layers lose salt through convection. Instead of losing salt via convection, the simple parametrization directly reduces the amount of salt in the layer until the layer is stable. The simple parametrization always produces a stable salinity profile while the convective parametrization slowly evolves towards a stable salinity profile. Since the simple salinity parametrization does not determine any brine fluxes, it is of very limited use to model biogeochemistry in the ice.

The first step of the simple parametrization is identical to the convective parametrization, the Rayleigh numbers of all layers are calculated. If the Rayleigh number is higher than the critical value, the layer is considered convectively unstable. But instead of calculating brine fluxes and resulting salt transport, in the simple parametrization we reduce the salinity by a certain fraction. So if $R^i > R_{crit}$, then the salinity will be

multiplied with a fixed constant $\gamma < 1$ leading to S^i_{abs} in the following time step being γS^i_{abs}. The resulting parametrization is unconditionally stable and can be summarized in the following line:

$$\textit{If at time step t: } R^i > R_{crit} \qquad \textit{Then: } {S^i_{abs}}^{t+1} = \gamma \cdot {S^i_{abs}}^{t} \tag{2.6}$$

Again we have a parametrization with two free parameters: R_{crit} and γ. For R_{crit} we use the same value as the convective parametrization. γ must have a value between 0 and 1. The closer γ is to 1 the smoother the salinity evolution, but γ must be small enough to ensure that the salinity decreases faster than the surrounding ice conditions evolve. The smaller the time step, the closer γ can be to 1. We recommend keeping γ above 0.9, as large jumps in salinity lead to sudden temperature changes. Our experience indicates that slight changes of γ do not affect the results much.

We expect the largest differences between the two schemes to occur when sea ice grows rapidly, because the simple parametrization forces the salinity profile into equilibrium much quicker than the brine circulation of the convective parametrization. Another difference is that a convectively stable layer below unstable layers can desalinate in the convective parametrization, but not in the simple parametrization.

2.3.4 Permeability

In porous media, permeability is part of the proportionality constant in Darcy's law which relates flow rate to a pressure gradient. In contrast to static materials (such as sandstone) the permeability of sea ice is continuously evolving and is affected by temperature, ice structure, salinity, and flow direction. Brine movement in sea ice causes heat and salt transport, which leads to a change in permeability, which in turn affects the brine movement. This behavior leads to highly non-linear effects which can be exceedingly difficult to capture in numerical models.

The permeability of sea ice is an extremely complex ongoing research topic which has been studied extensively (e.g. Petrich et al., 2006; Golden et al., 2007; Pringle et al., 2009; Büttner, 2011; Jones et al., 2012). In SAMSIM we define permeability as an empirical function of the fluid volume fraction. This commonly used approach neglects the ice structure, which seems justified for our purposes because Gough et al. (2012) concluded that desalination processes are mostly unaffected by the ice structure.

All tests in this paper were conducted using the relationship proposed by Freitag (1999):

$$\Pi^i(\phi^i_l) = 10^{-17}(10^3\phi^i_l)^{3.1}.$$

We believe this empirically derived relationship is similar enough to the $\Pi = \Pi_0(\phi_l)^3$ used by Wells et al. (2010) to avoid issues when transferring the results of Wells et al. (2010) to SAMSIM.

At low liquid fractions sea-ice can become impermeable, and $\phi_{l_{crit}} = 0.05$ is often used as threshold value under which the remaining brine pockets are assumed to be isolated from each other (e.g Golden et al., 1998; Petrich et al., 2006; Golden et al.,

2007; Vancoppenolle et al., 2010). As SAMSIM attempts to represent a spatial average of possibly highly heterogeneous sea-ice, we believe that small permeabilities at low liquid fractions are justifiable. Also, if a low permeability results in a Rayleigh number below R_{crit}, our gravity drainage parametrizations predict no changes. So as long as $R < R_{crit}$, it is irrelevant if the ice is truly impermeable or not. This does not change the fact that the gravity drainage parametrizations react strongly to changes in the assumed permeability as it directly affects the Rayleigh number, and therefore also the values of α and R_{crit}.

2.4 Parameter estimation and evaluation

The convective parametrization introduced in subsection 2.3.2 contains two free parameters, the dimensionless R_{crit} and α with the physical dimension of $kg/(m^3 s)$. In this section we detail how we derived α and R_{crit} from laboratory salinity measurements, and how we determined that both parameters are independent of the vertical resolution of the model.

2.4.1 Salinity measurements

The salinity measurements we use stem from a laboratory experiment that was described in section 8.4 of Notz (2005). In this experiment, an NaCl solution was cooled from above by a cooling plate that was switched from $-5°$ to $-10°$ C every 12 hours. The ice grew to almost 15 cm over the 72 hours of the experiment, which was repeated once under identical conditions. Throughout the experiment, solid fraction and temperature were measured in situ at fixed depths at a high temporal resolution using a so-called wireharp (Notz and Worster, 2008). The measured solid fraction is used to calculate the liquid fraction, and the brine salinity is derived from the measured temperature. Multiplying the liquid fraction with the brine salinity then allows us to calculate the bulk salinity.

Although the precision of the wireharp was never determined thoroughly, tests with solid fractions below 0.8 agreed very well with theoretical expectations. However, at low liquid fractions slight measurement errors of the solid fraction lead to large errors in the bulk salinity. As a rule of thumb we assume that for liquid fractions above 0.2 the total error of bulk salinity is below 5 ppt, and that the relative error of bulk salinity increases with $1/\phi_l$ as the liquid fraction approaches zero.

The three sub panels of figure 2.3 show salinity measurements at three points in time. To what extent the differences between the two experiment repetitions (one marked by black dots, the other by white dots) are due to measurement errors or actual physical differences is impossible to tell. Cottier et al. (1999) showed that growing sea ice can have a high horizontal gradient in salinity linked to the location and morphology of the brine channels. We assume that the experiments were conducted under identical conditions and the differences result from the sampling size of ice between the wires and measurement errors.

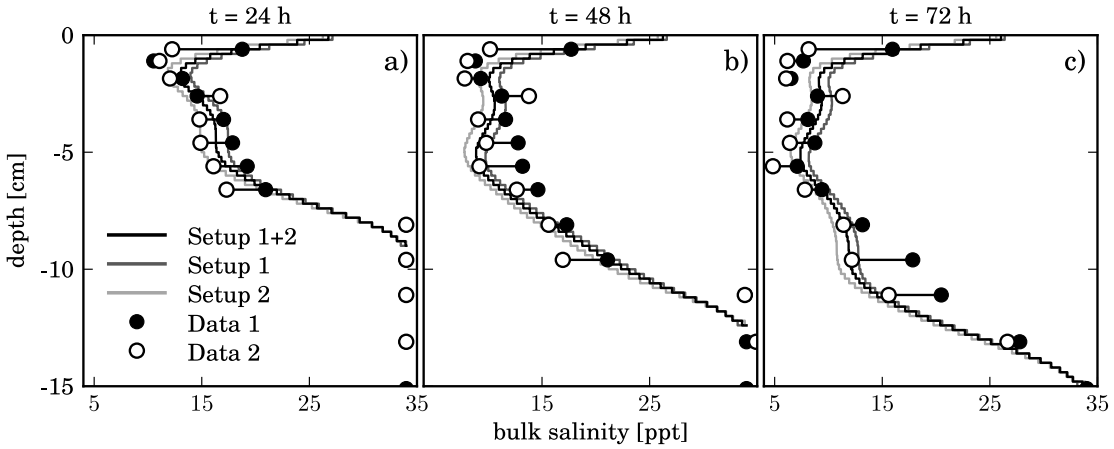

Figure 2.3: Bulk salinity measurements (dots) at different depths and corresponding model profiles at a) t=24h, b) t=48h, c) t=72h. The free parameters of the gravity drainage parametrization of Setup 1 were optimized to fit Data 1, of Setup 2 to fit Data 2, and of Setup 1+2 to fit the average of Data 1 and Data 2. Grid parameters: N=90, $\triangle z_0$=0.2 cm See subsection 2.4.1 for details on experimental setup and instrumentation.

We choose this experiment for multiple reasons. The first, and arguably the most important reason, is the high spatial resolution of the data. Also of great advantage is that the experiment was conducted twice, and that the controlled environment of the experiment can be easily translated to boundary conditions for the model. In contrast, field studies of sea ice contain many unknowns, such as precise heat fluxes and dynamic effects, which makes field measurements difficult to reproduce with a high degree of accuracy.

Although a similar laboratory experiment was conducted with a fixed cooling temperature of $-10°$ C the results are unsuitable for a quantitative evaluation of the model. This results from of a combination of measurement uncertainty and the fact that the experiment was only conducted once. Additionally, inspecting the data uncovered multiple artifacts which further hinder a quantitative evaluation.

The final reason for using this experiment is that the temperature of the cooling plate alternated between -5° and -10° C. Our convective parametrization is based on the results of (Wells et al., 2010), in which a steady cooling temperature was assumed. If SAMSIM can reproduce the experiments, we have shown that our approach can deal with more complex conditions than those of Wells et al. (2010).

A limitation of the data is the rather short duration of the experiment. Also, the experiment would ideally have been conducted more than twice.

2.4.2 Parameter optimization

We use the Levenberg-Marquardt algorithm to determine the optimal values of α and R_{crit} (Levenberg, 1944). The metric which the algorithm seeks to minimize is the difference between the measured and the modeled salinity every twelve hours. If a measurement lies inside a model layer, it is directly compared to that layer. If the

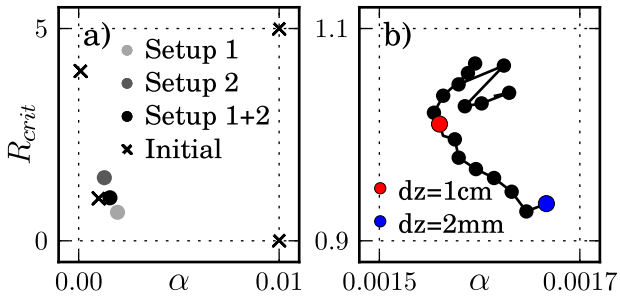

Figure 2.4: a) Values of R_{crit} and α derived by the Levenberg-Marquardt optimization algorithm for given sets of salinity measurements ('1+2' is the average of sets '1' and '2'). For all initial parameter values (marked by an x) the optimization results were identical. (b) Optimization results of R_{crit} and α from a separate experiment for different vertical grid spacing dz. dz increases from 2 to 20 mm in 1 mm steps. Neighboring gird spacings (e.g., 3 mm and 4 mm) are connected by a line. Note the different scales of subfigure a & b.

measurement lies between two layers, it is compared against the arithmetic mean of those two layers.

We optimize the parameters separately for the first and second experiments measured by Notz (2005). To ensure that the optimization results are not local minima, we chose four different initial estimations of α and R_{crit}. All four initial values result in almost identical values for all the data sets, which is by itself a promising sign (figure 2.4a). The differences resulting from using other initial values are smaller than the precision criterion required to stop the algorithm. The two parameters vary by roughly a factor of two from set 1 (α=$1.93 \cdot 10^{-3} kg/(m^3 s)$, R_{crit}=0.67) to set 2 (α=$1.28 \cdot 10^{-3} kg/(m^3 s)$, R_{crit}=1.48).

To get an indication of how sensitive the optimization process reacts to small changes in the data, we create an additional artificial data set by averaging the two experiments (figure 2.4a). Using this artificial data, set the optimization process returns values which lie between the two previous results (α=$1.56 \cdot 10^{-3} kg/(m^3 s)$, R_{crit}=1.01). We use these values as the default setting for SAMSIM.

2.4.3 Resolution dependency

To test the dependency of the parameters on the vertical resolution we conducted a simulation with a reference run at a vertical grid spacing of 1 cm, in which ice was grown from a NaCl solution at a fixed cooling temperature over 6 days. A relatively high salinity of 70 ppt was chosen to increase the strength of gravity drainage and the resulting freshwater signal. Every 12 hours the freshwater content of all layers was saved. The Levenberg-Marquardt algorithm was used to optimize the model with different vertical resolutions to reach the same total freshwater content each 12 hours. In contrast to the previous subsection in which the salinity profile was used to determine the model performance, we choose to compare the freshwater content instead of comparing vertical profiles. This was done because comparing vertical profiles at different

resolutions requires interpolation, and results would depend on the interpolation technique used. We also choose to keep the cooling temperature steady to ensure a linear temperature profile, which minimizes thermodynamic differences due to the changing resolution.

The spacing of the model varied from 2 mm to 2 cm in steps of 1 mm, a range that covers most of the values used in this paper. We find that the variations of α and R_{crit} are smaller than 10 % and show no trend (figure 2.4b). From this we conclude that our parameters α and R_{crit} —which we determined using a 2 mm grid— do not seem to depend on resolution and are valid for vertical resolutions up to at least 2 cm.

2.4.4 Parametrization evaluation

Although we have determined our free parameters by optimizing the model using salinity measurements, parameter fitting only reduces the model error as much as the structure of the parametrization allows. To determine if the parametrization can reproduce the measurements we compare the resulting salinity profiles of the model for the different values of α and R_{crit} against the measurements (figure 2.3). The model output generally agrees very well with measurements, with almost all deviations being smaller than the measured uncertainty. This good agreement indicates that the assumptions on which our convective parametrization is based yield an appropriate model. Additionally, SAMSIM proves itself capable of reproducing the thermodynamics of the experiment.

We cannot verify if the high salinity values directly at the cooling plate predicted by the model occurred during the experiments. But it is to be expected that the ice crystal formation at the beginning of the experiment includes crystalline processes which can not be captured using mushy layer theory. It is also difficult to keep the cooling plate at a constant negative temperature when initially brought in contact with the NaCl solution because of the very rapid initial exchange of latent heat. The resulting initial temperature fluctuations are not included in the boundary conditions of the model simulations.

It is remarkable that despite the rather large spread of α and R_{crit} the model setups 1, 2, and 1+2 behave very similarly. This similar behavior can be attributed to the fact that gravity drainage is a relatively stable process. Increased convection leads to increased salt loss, which results in lower liquid fractions and permeability, which in turn reduces convection. Slow convection leads to ice with a higher permeability, which leads to increased convection.

Although we determined in the previous subsection that the optimal parameter estimates of α and R_{crit} were insensitive to grid size, a further test is conducted to determine the sensitivity of the parametrization and the model to changes in vertical resolution. This test again uses half-daily alternating temperatures of -5° and -10° C as a boundary condition. Comparing the salinity profiles after 10 days for six different vertical resolutions against each other shows two very important results (figure 2.5). Firstly, the bulk salinity values change very little even though the vertical resolution changes by a factor of 32. And secondly, the profiles change only very little once

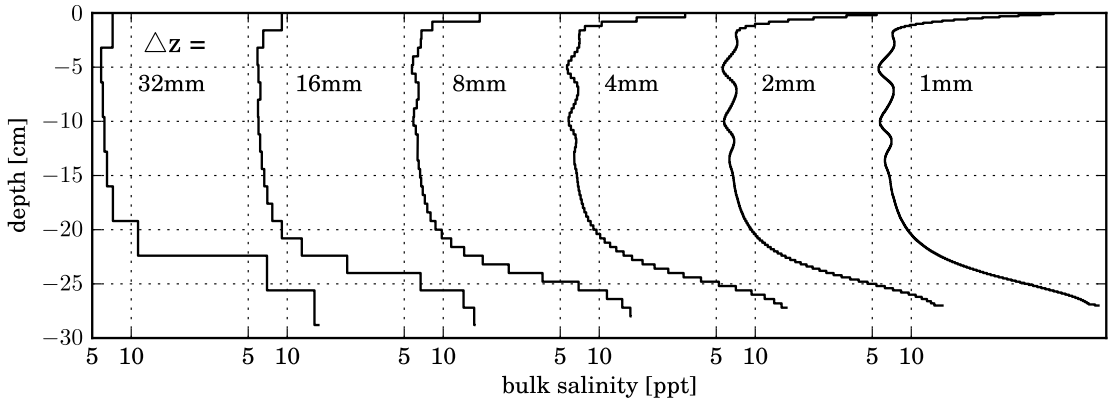

Figure 2.5: Bulk salinity model profiles for six different vertical resolutions after 10 days. Beware that the x-axis of each profile is shifted by 20 ppt to improve visibility, i.e. the 5 ppt line of the 16 mm profile is also the 25 ppt line of the 32 mm profile. Grid parameters: N=300, $\triangle z_0$=1-32 mm

the vertical resolution is sufficient to fully resolve the curves of the salinity profile. This test further demonstrates that the convective gravity drainage parametrization is insensitive to grid sizes.

In conclusion, we derived estimations of α and R_{crit} which are independent of grid resolution. More data from longer experiments is needed to further improve the estimations of α and R_{crit}, which are highly dependent on the assumed permeability. Using these values of α and R_{crit} in the convective parametrization enables the model to reproduce measured salinity profiles.

2.5 Idealized tests

After developing, tuning, and evaluating our convective gravity drainage parametrization with small-scale laboratory data, we now study gravity drainage under various idealized conditions. The tests with idealized boundary conditions are used to study the depth and strength of gravity drainage, to quantify the desalination caused by gravity drainage, and to investigate the relationship between growth speed and the final bulk salinity of sea ice. The conclusions we draw from the idealized test cases are then tested under more realistic conditions in the next section, in which we force SAMSIM with reanalysis data.

2.5.1 Constant cooling

Our first test case is the freezing of a NaCl solution from a constant cooling temperature, which is the most often used setup for laboratory studies (e.g. Tait and Jaupart, 1992; Chen, 1995; Wettlaufer et al., 1997; Notz and Worster, 2009).

We conduct simulations of a NaCl solution freezing at four different cooling temperatures ranging from -5° to -35° C to cover the full range of growth speeds which occur

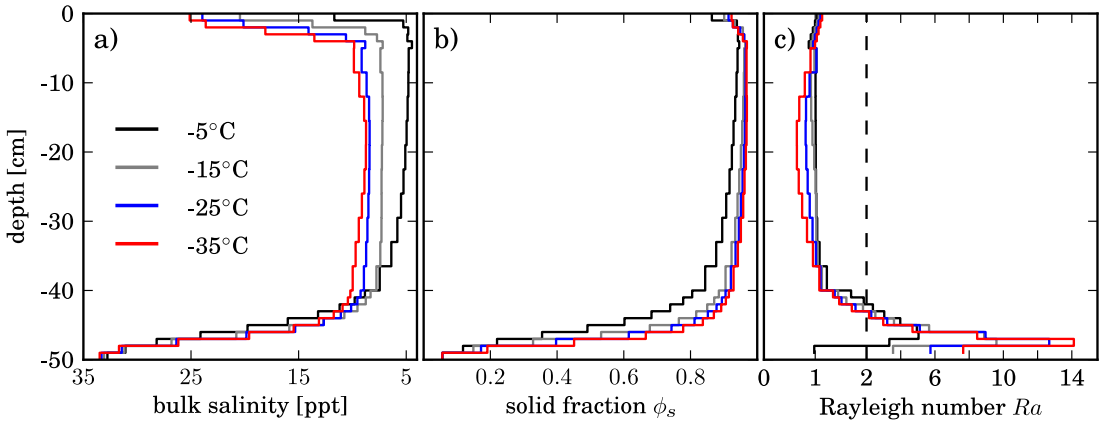

Figure 2.6: a) Bulk salinity, b) solid fraction, and c) Rayleigh number profiles of freezing NaCl from a fixed surface temperature. Simulations were run until the ice thickness reached 50 cm. Please notice that the scale of the x-axis in subfigure c) changes above 2 (marked by dashed line). All layers with R greater than the critical Rayleigh number of 1.01 are convectively unstable. Grid parameters: N=25, N_{top}=5, N_{bot}=10, $\triangle z_0$=1cm

in the Arctic and Antarctic. For these tests SAMSIM's grid is set to N_{top}=5, N_{mid}=10, N_{bot}=10, and $\triangle z_0$=1.0 cm with a time step of 5 s. We wait until the ice grows to a thickness of 50 cm and then compare the resulting profiles of salinity, solid fraction and Rayleigh number. These test cases provide a frame of reference on how the bulk salinity of sea ice is related to growth speed.

We find that more salt is retained in the ice the colder the cooling temperature (figure 2.6a), as was also found in the laboratory experiments of Cox and Weeks (1975) and Wettlaufer et al. (1997). Based on the salinity profiles, we conclude that a layer of growing sea ice cannot retain more than 10 ppt salt once convection has ceased.

Despite the higher salinity, the colder experiments have a slightly higher solid fraction (figure 2.6b). This can easily be understood: because the colder experiments have higher brine salinities, the solid fraction must be higher than in the warmer experiment to inhibit convection and retain salt. In all simulations almost all the convection occurs in the lowest 10 cm regardless of growth speed (figure 2.6c).

The Rayleigh number of the slower-growing ice remains close to the critical value of 1.01 in the top 40 cm of the ice, while the faster-growing ice is more stable there. In contrast, the faster-growing ice is much more unstable in the lowest 10 cm. All simulations remain slightly unstable in the top 5 cm, driving a very weak circulation over the complete 50 cm. Here we can see a clear signature of the semi-adaptive grid, where the depth of the top instability is determined by the amount of thin top layers. This top instability is maintained by the constant surface temperature. Slight fluctuations of this temperature would remove the instability by first increasing the Rayleigh number and convection. The slight increase in convection would desalinate the lower layers enough so that when the top temperature returns to the initial value the reduced permeability would stabilize the flow.

To summarize these results, we find that slow-growing warm ice desalinates more strongly and results in a marginally stable Rayleigh number profile. In contrast, faster-

growing colder ice retains more salt, and the ice becomes convectively stable once gravity drainage ceases. As almost all convection occurs in the lowest 10 cm, we conclude that multiple layers in the lowest 10-20 cm are necessary to properly simulate gravity drainage numerically. The relationship of higher salinity for fast growth speed and lower salinity for lower growth speed was also found in laboratory experiments by Cox and Weeks (1974). These experiments were used to derive a fractionation coefficient based on growth velocity that describes the incorporation of salt into the advancing front. However, our results agree with the findings of Notz and Worster (2009) that such fractionation coefficient does not reflect the underlying physics of the measured relationship between growth speed and sea-ice bulk salinity. We will further examine this relationship for more realistic boundary conditions in section 6.1.

2.5.2 Warming triggered convection

It is currently unclear if gravity drainage can occur in warming sea ice. Measurements of salt fluxes below sea ice (Widell et al., 2006) and of algae behavior in sea ice during autumn (Fritsen et al., 1994) indicate that convection may occur, as do recent observations of short-lived salinity anomalies under warming sea ice (Jardon et al., 2013). In this subsection we introduce an experiment designed to test if it is possible to trigger gravity drainage in sea ice by warming the ice from above and/or below. A secondary goal is to study how gravity drainage affects the sea ice.

In principle, warming sea ice can lead to gravity drainage by increasing the permeability of the ice. However, warming sea ice also causes the brine salinity to fall, which reduces the buoyancy between brine and underlying ocean water which inhibits gravity drainage. If the permeability increase outweighs the buoyancy reduction depends on the nonlinear dependence of the two quantities to temperature. Also, melting at the ice-ocean boundary can increase the buoyancy of the brine. This buoyancy increase is caused by the reduction of the salinity below the ice due to melting ice at the ice-ocean boundary.

To maximize our chance of triggering convection we create initial conditions which are just stable. These initial conditions are reached by growing ice from a fixed temperature of -16.7° C from salt water with a salinity of 34 ppt. The sea ice grows until it reaches a thickness at which the prescribed ocean heat flux of 20 W/m^2 balances the growth. Over the roughly 18 months simulated to reach the equilibrium state, gravity drainage slowly desalinates the ice until the Rayleigh numbers are just below the critical value.

Three different experiments were applied using the stable initial conditions to trigger deep convection. Experiment I raises the top temperature from -16.7° to -5° C to increase permeability while reducing buoyancy. Experiment II increases the oceanic heat flux from 20 to 100 W to increase buoyancy by melting ice at the ice-ocean boundary. Experiment III is a combination of the atmospheric and the oceanic forcing in experiments I and II.

All three experiments succeeded in triggering convection in SAMSIM, with each experiment resulting in different convection patterns and salinity profiles (figure 2.7). Experiment I mostly destabilizes the upper half of the ice (figure 2.7-I-C), but the

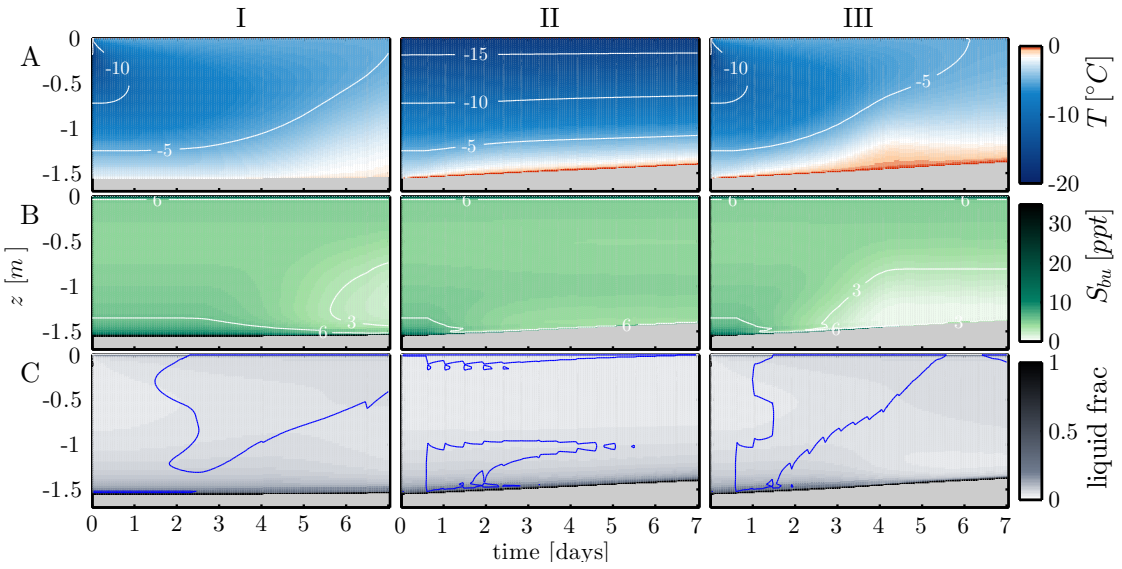

Figure 2.7: (A) Temperature, (B) bulk salinity, and (C) liquid volume fraction over one week. The blue line in row C encloses convectively unstable layers. Beginning from identical stable initial conditions: experiment I raises the top temperature from -16.7° to -5° C, experiment II increases the oceanic heat flux from 20 to 100W, and experiment III combines experiment I and II. Grid parameters: N=70, N_{top}=5, N_{bot}=5, $\triangle z_0$=1cm

strongest desalination occurs in the bottom half of the ice (figure 2.7-I-B). The increased oceanic heat flux of forcing II destabilizes the lowest 50 cm and the top 10 cm (figure 2.7-II-C). The desalination caused in experiment II is weaker than the desalination of experiment I and is mostly confined to the lowest 40 cm (figure 2.7-II-B). This desalination caused by an increased oceanic heat flux is possibly what was observed by Widell et al. (2006), who linked salt release to upward oceanic heat fluxes.

The convection and desalination results of experiment III can be interpreted as an accelerated linear combination of the convection and desalination of experiment I and II. The resulting desalination is strong enough that it leads to a visible warming in the lower 40 cm after four days, as the ice solidifies and warms at the same time (figure 2.7-III).

From these three experiments we conclude that gravity drainage can occur during top warming and bottom melt under ideal conditions. Warming the ice from above creates a stronger effect than melting the ice from below, and a combination of both leads to the strongest effects. In contrast to the gravity drainage that occurs during growth, the resulting deeper convection can span the whole ice layer. The desalination caused by the deep convection is strongest in the lower half for two reasons. Firstly, as the amount of upwelling brine in each layer n equals the sum of all brine flowing downward from above the layer n, the amount of upwelling is always largest in the lowest layer and decreases upward. Secondly, the temperature gradient is steeper in the lower than in the upper half due to the top warming. The combination of more upwelling and a higher gradient leads to a stronger salt advection, which results in a stronger desalination in the lower layers (equation 2.5).

In nature, atmospheric and oceanic forcing could easily be as strong or stronger than

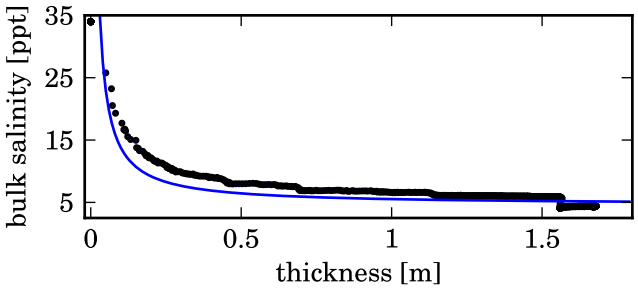

Figure 2.8: Reanalysis-forced daily model values of bulk salinity vs ice thickness (dots) and empirical relation of Kovacs (1997).

the idealized forcings we used in this experiment. However, it is highly unlikely that the initial ice conditions of the idealized experiments occur naturally. From these two statements we conclude that deep convection is possible in reality, but the resulting convection will likely be weaker than in the idealized experiments. The desalination of the lower half of sea ice after the onset of flushing, which was already noted by Malmgren (1927) and Holt and Digby (1985), could be the result of such warming-induced deep convection.

2.6 Seasonal growth under reanalysis forcing

To examine how gravity drainage occurs under more realistic conditions, we conduct a case study of a single growth season using reanalysis data. We use this test case to determine which of our results from the idealized tests (such as those concerning deep convection and the link between growth speed and final salinity) are also valid under realistic conditions (subsection 2.6.1). This test case is also used to compare the simple against the convective gravity drainage parametrization and to quantify the effect of gravity drainage on the thermal properties of sea ice (subsections 2.6.2 and 2.6.3).

To force SAMSIM with reanalysis data, the surface temperature is derived by balancing outgoing long wave radiation with three-hourly ERA-interim fluxes. Both the fluxes and precipitation were taken from a grid point close to where the SHEBA campaign was conducted (Perovich et al., 1999), namely at 75 N and 217.5 E. We randomly chose the year 2005 to simulate the total growth season from ice formation to maximum thickness. Snow accumulates over time in the single snow layer of variable thickness (see subsection 2.2.2). To avoid numerical instabilities the comparatively small heat flux into the snow and the sensible heat flux to the atmosphere are not included in the surface energy balance.

As we have no reanalysis data of oceanic heat fluxes we approximate the oceanic heat flux as a simple sine curve with a period of 1 year, which is based loosely on the values Huwald et al. (2005b) derived from the SHEBA measurements. The oceanic heat flux reaches 14 W/m^2 in Autumn and sinks to 0 W/m^2 in Spring. For SAMSIM's grid we choose N_{top}=10, N_{mid}=40, N_{bot}=20, and $\triangle z_0$=1.0 cm to highly resolve the bottom 20 cm of the ice. To avoid numerical issues in these small layers we use a time step of

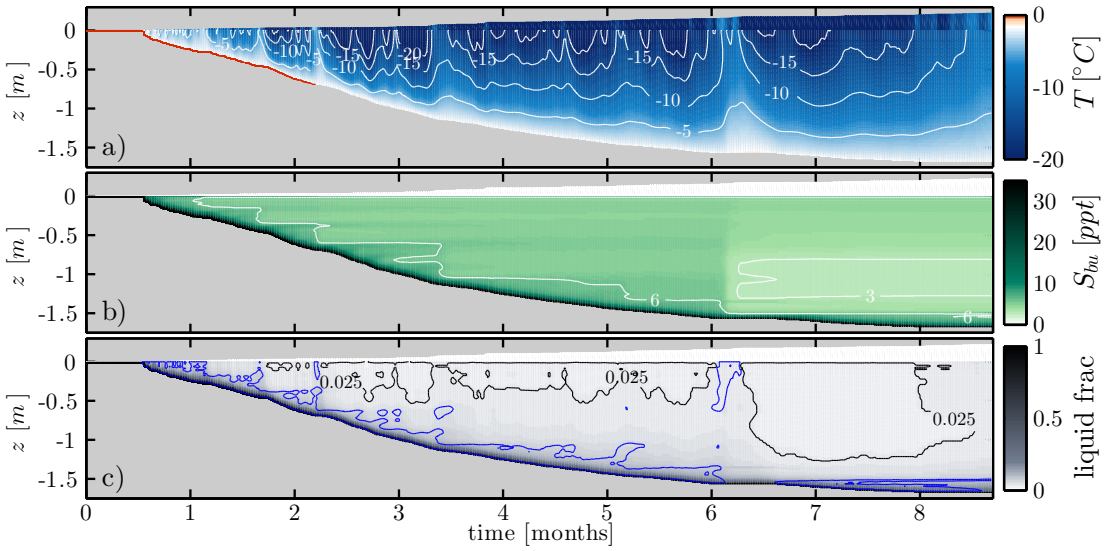

Figure 2.9: a) Temperature, b) bulk salinity, c) and liquid volume fraction over a growth season (see section 2.6). In subfigure c) the blue line encloses convectively unstable layers, and the black line encloses regions with a liquid fraction below 2.5 %. The single snow layer on top of the sea ice lies above $z = 0$. Grid parameters: N=70, N_{top}=10, N_{bot}=20, $\triangle z_0$=1cm

10 seconds. Aspects we neglect in this simulation are the initial formation of frazil ice and the feedbacks of the sea ice on oceanic, sensible, and latent heat fluxes.

To determine if the model output is realistic, we evaluate the test case against data from the SHEBA Baltimore site and against the empirical relationship derived from over 400 Arctic ice cores by Kovacs (1997). Our model produces a similar dependence of mean bulk salinity on ice thickness as given by the empirical function of Kovacs (1997) (figure 2.8). In thin ice, modeled bulk salinity is slightly higher, which could also be related to the outflow of brine during sampling, which causes an underestimate of sampled bulk salinity in thin sea ice.

A comparison with buoy data of first year ice from the SHEBA Baltimore site (Perovich et al., 2009) shows a good general agreement between simulated and measured temperature profiles (not shown). In the case study, the model grows 1.8 m of ice and accumulates approximately 30 cm of snow (figure 2.9). The simulated sea ice is somewhat thicker than the maximum thickness of 1.5 m measured at the Baltimore site, but the Baltimore site is likely somewhat thinner due to the thicker snow cover of 50 cm compared to the 30 cm of snow in our case study. From the general similarities of the model with the SHEBA data and the empirical salinity-thickness relationship of Kovacs (1997) we conclude that the model results fulfill basic expectations.

2.6.1 Gravity drainage under reanalysis forcing

The high spatial and temporal resolution of the case study simulation supplies a wealth of information on how gravity drainage, salinity, and temperature interact (figure 2.9). From this data we draw conclusions on the depth and variability of gravity drainage,

the salinity evolution in growing sea ice, how gravity drainage responds to temperature, and how salinity is linked to growth speed.

From the blue line in subfigure 2.9c we can see that although gravity drainage occurs mostly in the lowest 20 cm, there is a great amount of variation. Not only does the convection depth at the bottom vary, but also additional layers separated from the lower convection become unstable now and then. Most notable is the full depth convection after six months when top warming destabilizes the top 50 cm of ice. Similar events of smaller magnitude occur shortly after two months and after roughly three and a half months. This variance of gravity drainage is not a simple reaction to temperature forcing or random model behavior. Instead, this variance results from the complicated interplay of salinity, buoyancy, and permeability.

Comparing the 6 ppt salt contour of subfigure 2.9b to the blue line of subfigure 2.9c shows that the 6 ppt contour roughly outlines the lower convective ice layers. The 6 ppt contour shows a stepwise shape at approximately 1.2, 1.6, 2.2, 3.3, 5.2, and 6 months. These steps all coincide with a warming of the ice, as can be seen in subfigure 2.9a. At the same time, the depth of gravity drainage increases for a short time and then collapses. From this behavior we conclude that gravity drainage reacts in cycles to the temperature evolution. The cycle begins when the surface temperature drops and ice grows faster at the ice-ocean boundary. While the ice continues to grow, the newly formed ice remains convectively unstable. At some point in time the surface temperature rises again. As the ice warms, the convection depth increases or remains constant. When the ice once again begins to cool, most of the convectively unstable regions stabilize and the cycle repeats itself. Such a cycle in figure 2.9 begins shortly before and ends slightly after two months, during which the top temperature drops from above -5° C to below -20° C and returns above -10° C. These cycles are visible as slight kinks or jumps when the bulk salinity is compared against the thickness (figure 2.8).

We will now turn to comparing these results to those from the idealized test case described in section 2.5. Doing so, it is interesting to note that in the simulation under realistic forcing, gravity drainage reduces the salinity to a stable value below 6 ppt. This value of 6 ppt lies below the upper threshold of 10 ppt which we determined from idealized experiments in section 2.5 to be the absolute maximum salinity possible in stable sea ice. In addition, the link between faster growth speed and higher salinity that we found in section 2.5 no longer holds: Such a link would result in a nonlinear relationship of salt flux to growth rate, which we do not find for the realistic forcing (figure 2.10). The cyclic interaction of temperature and convection discussed in the above paragraph both disrupts the link between growth speed and salinity and causes a reduced stable bulk salinity in comparison to the experiments with a constant cooling temperature (figure 2.6).

In section 2.5 we concluded from idealized experiments that top warming can lead to gravity drainage over the whole ice layer. We also concluded that such convection would lead to a desalination which is strongest in the lower ice layers. The full depth convection which occurs after six months in the reanalysis-forced test case shows that both of these conclusions still hold for realistic boundary conditions. The resulting desalination is clearly visualized by the 3 ppt contour of salinity (subfigure 2.9b).

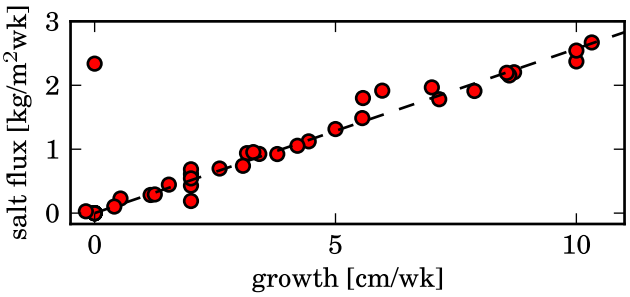

Figure 2.10: Reanalysis-forced weekly summed values of modeled salt flux vs growth speed.

Comparing the 2.5 % contour (subfigure 2.9c) before and after the event highlights the reduction in liquid fraction caused by the desalination.

2.6.2 Convective versus simple parametrization

To study how closely the simple parametrization (introduced in subsection 2.3.3) mimics the convective parametrization we compare salinity profiles resulting from both parametrizations for the reanalysis-forced case study. As the simple parametrization is intended for use in coupled models in which using 70 levels is unthinkable, we also run SAMSIM at a lower resolution for this analysis. For the high-resolution case, we chose N_{top}=10, N_{mid}=40, N_{bot}=20, and $\triangle z_0$=1.0 cm (figure 2.11a). The low-resolution is based on N_{top}=3, N_{mid}=3, N_{bot}=4, and $\triangle z_0$=5 cm (figure 2.11b).

The simple convection provides a reasonable salinity profile approximation, especially at low resolution (figure 2.11b and d). Although the convective parametrization desalinates growing sea ice somewhat slower, the differences are rather small. Two characteristics of the high resolution convective parametrization are not reproduced by the simple parametrization: the high salinity in the top layer, and the desalination caused by deep convection after six months. The high salinity in the top layer can not be reproduced by the simple parametrization because it has no sense of the speed of desalination and stabilizes the salinity profile almost immediately. The deep convection can not be captured by the simple parametrization as it arises from the convective nature of gravity drainage.

2.6.3 Relevance to climate models

In this subsection we seek to quantify how relevant gravity drainage is for climate models. To achieve this, we compare the reanalysis-forced simulations using the convective and simple parametrization against simulations without gravity drainage. Due to their relevance in climate models we choose to evaluate ice thickness, enthalpy, thermal resistance, and freshwater column.

The freshwater column describes the amount of freshwater contained in the sea ice and snow. It is calculated by melting the ice and snow and separating the resulting meltwater into freshwater and ocean water with a salinity of 34 ppt. For example, two meter thick sea ice with a bulk salinity of 8 ppt has a freshwater column of about one

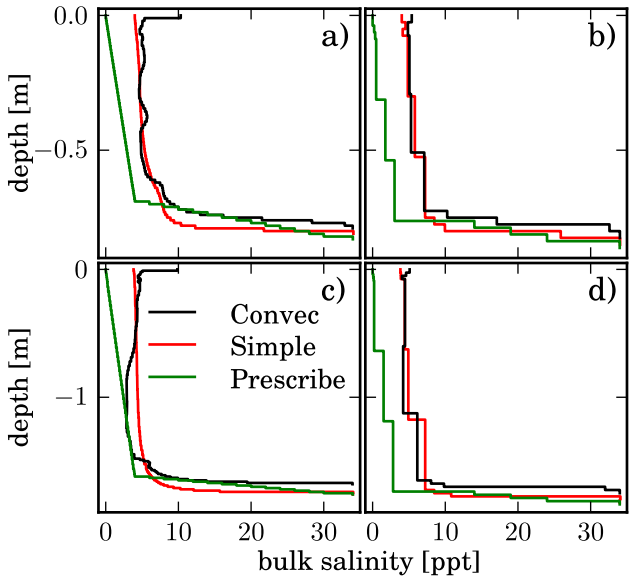

Figure 2.11: Case study salinity profiles of the convective and simple parametrization for two different vertical grids at two different times. The prescribed profile used in subsection 2.6.3 is also included. a) and b) t ≈ 3 months, c) and d) t ≈ 9 months. a) and c) Grid parameters: N=70, N_{top}=5, N_{bot}=5, $\triangle z_0$=1cm. b) and d) Grid parameters: N=10, N_{top}=3, N_{bot}=4, $\triangle z_0$=5cm

and a half meters. The freshwater column grows when salt leaves sea ice and enters the ocean. Thermal resistance is the reciprocal of thermal conductance and is a measure of how strongly the sea ice resists the flow of heat between the ocean and atmosphere.

The salinity of the comparison runs are determined by setting the salinity of the lowest layer where ice forms to 4 or 7 ppt because these are plausible values of the bulk salinity of first-year ice. However, setting an initial salinity is not identical to the constant salinity approach often used in front tracking models. The most significant difference is that in our model the freezing temperature at the ice-ocean interface is determined by the salinity of the water in the lowest layer into which the ice grows (4 or 7 ppt in this case), while front-tracking models can set the ice-ocean interface temperature independently of the sea-ice and ocean salinity. Also, brine expulsion redistributes small amounts of salt.

An additional comparison run is computed using a prescribed salinity profile which can be seen in figure 2.11. In the lowest 15 cm the salinity decreases linearly from 34 too 4 ppt, and above that the salinity decreases to 0 ppt at the surface. This setup is an imitation of prescribing a multi-year salinity profile in a front tracking thermodynamic model, as is currently done in the Los Alamos Sea Ice Model (Bitz and Lipscomb, 1999).

The brine fluxes from the ocean to the ice of the convective gravity drainage parametrization transport heat, which leads to a slight increase of oceanic heat flux. To ensure that the runs are comparable, the amount of heat transported by the moving brine is subtracted from the prescribed oceanic heat flux at each time step.

In the rest of this subsection we will refer to the run using the full convective parametriza-

	Griewank & Notz	Vancoppenolle et al. (2006)
forcing	three-hourly reanalysis	idealized climatological
comparison period	growth season	first year & equilibrium annual cycle
model	SAMSIM	Bitz and Lipscomb (1999)
vertical layers	70	5-10
metrics	total enthalpy, thermal resistance freshwater column	thickness & salt flux
desalination processes included	gravity drainage	gravity drainage & flushing

Table 2.1: Comparison of our approach against the approach of Vancoppenolle et al. (2006) to determine the effect of the salinity evolution on the thermal properties of sea ice.

tion as the convec run, the run using the simple parametrization as the simple run, the run with the prescribed profile as prescribe, and the comparison runs as 4 and 7 ppt run in reference to their initial salinities. The same terminology is used in figure 2.12.

Vancoppenolle et al. (2006) conducted a similar experiment to quantify the effect of the full salinity evolution on the thermodynamic properties of the sea ice using a 1D model with a parametrized salinity evolution. Although the aims of Vancoppenolle et al. (2006) were similar, our approaches differ in many crucial aspects detailed in table 2.1. We believe the most important differences are that Vancoppenolle et al. (2006) forced their runs with idealized climatological data, and that they ran their simulations until they reached an equilibrium, i.e. a constant annual cycle. Vancoppenolle et al. (2006) conclude that including a dynamic salinity component would significantly improve large-scale sea-ice models. **?** studied the effects of adding a dynamic sea-ice salinity component to the coupled NEMO-LIM3 ice-ocean model, and concluded that the impact is similar to a 10 % change of sea-ice albedo, and advised accounting for varying sea-ice salinity when simulating possible future climates.

As expected, the 4 and 7 ppt runs produce thicker ice than the full convective run, in part owing to the higher freezing temperature and the higher thermal conductivity of fresher ice (figure 2.12a). In the simulations with the simple parametrization and in those with a prescribed salinity profile, the ice grows slightly slower during the first month, but reaches the same thickness as simulated by the complex parametrization over the remaining 7 months.

To study both short-term variations and long-term trends of the evaluated quantities, we subtract the running monthly mean of the convec run from all five runs. These differences are then smoothed by a weekly running average and plotted in subfigure b to e of figure 2.12. The short-term variations of all runs agree well with two exceptions. The first exception occurs during ice formation because the constant salinity runs freeze sooner and quicker. The second exception is visible in subfigure 2.12e after six months when the deep convection occurs. Only the convec run shows a short-term freshening.

At the end of the growth season the evaluated quantities of the simple run are 0-3 %

lower than the convec run. The prescribed and simple run are very similar, with the exception that the prescribed run has a higher freshwater column, which is reasonable since the prescribed profile is an approximation of a multi-year profile and saltless at the surface. Although the 4 and 7 ppt runs have a similar thickness, the 4 ppt run's thermal resistance is in better agreement with the convec run. In contrast, the enthalpy of the 7 ppt run agrees better than the 4 ppt run with the convec run. This shows that although the initial salinity can be varied to fit one quantity, no value can fit all. At

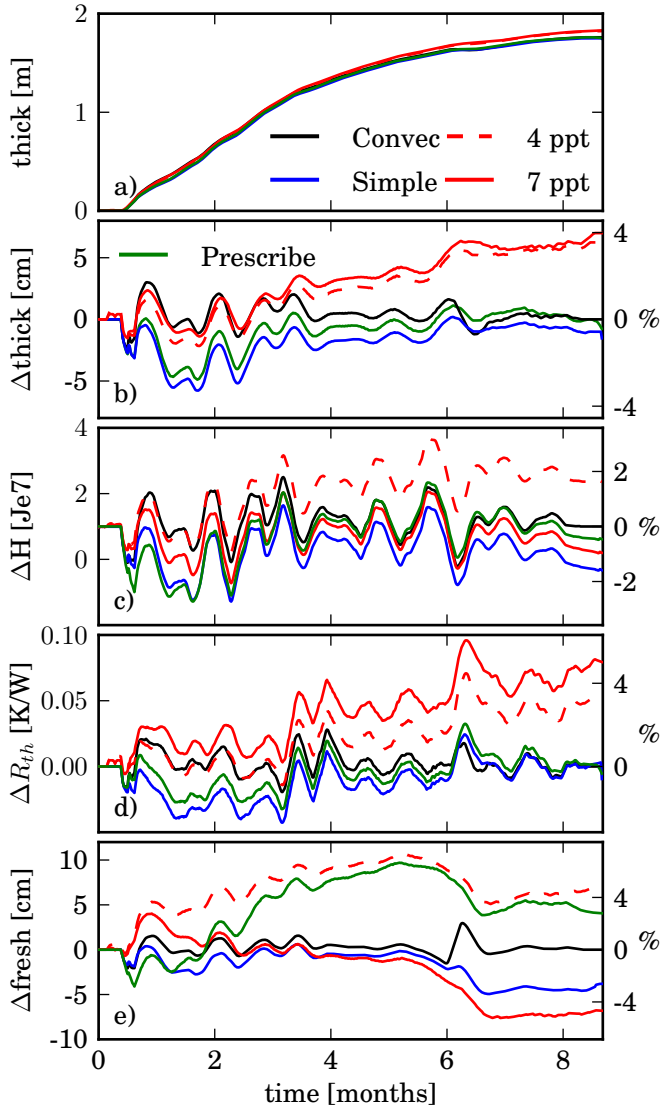

Figure 2.12: a) Thickness, and differences b) of thickness, c) of total enthalpy, d) of thermal resistance, and e) of fresh water column for the four salinity approaches. 'Convec': convective parametrization, 'Simple': simple parametrization, '4 ppt': initial salinity of 4 ppt, '7 ppt': initial salinity of 7 ppt. Differences are calculated by first subtracting a moving monthly average of the convective parametrization, and then applying a moving weekly average to reduce the noise. The percentages marked on the right y-axis of subfigures b) to e) are the left y-axis values divided by the end values of 'convec'.

the end of the growth season the average of all discrepancies over both the 4 and 7 ppt salinity runs is approximately 3 % compared to the convec run.

In conclusion, in our test case the short-term variations of all approaches are similar, with the notable exception of the deep convection which only occurs in the simulation with the complex parametrization. The total effect of gravity drainage on the thermodynamic properties of the ice is rather modest, and differences between all runs and compared properties seldom exceed 4 % (figure 2.12).

2.7 Summary & Discussion

2.7.1 Summary

In this paper we have studied gravity drainage using a convective parametrization with two free parameters, namely the critical Rayleigh number and a proportionality constant α. Values for these two parameters were determined using the Levenberg-Marquadt optimization algorithm and salinity measurements from laboratory experiments. The optimization results were robust against changes in the initial values but the uncertainties should be reduced with more data, especially from longer experiments. Our derived value of the critical Rayleigh number (1 ± 0.5) agrees well with theoretical expectations but is difficult to compare to the value of 5 used by Vancoppenolle et al. (2010) or the values of 0.5-2 which Gough et al. (2012) derived from ice-core measurements because slightly different definitions of the Rayleigh number were used. Vancoppenolle et al. (2010) and Gough et al. (2012) both use the thermal diffusivity of sea ice which is highly temperature and salinity dependent instead of the thermal diffusivity of brine we use in our definition of the Rayleigh number (Schwerdtfeger, 1963).

The link between growth speed and resulting bulk salinity as indicated from laboratory experiments (Cox and Weeks, 1975; Wettlaufer et al., 1997) and field studies (Gough et al., 2012) is simulated by SAMSIM for sea ice growing from a fixed surface temperature. In contrast to the findings of these measurements, comparing salt release versus growth rate of a reanalysis-forced test case shows no indication that more salt is retained at faster growth speeds. In our model the strong temperature variations of the test case and the resulting destabilization of stable layers disrupt the link between growth speed and resulting bulk salinity.

We show that SAMSIM allows for deep convection in sea ice, and deep convection can be found in both idealized and more realistic runs. The strongest salinity signal from deep convection is found in the lower and middle ice layers, which could explain observations of desalination near the ice-ocean interface during the melt season (Malmgren, 1927; Holt and Digby, 1985). However, all results related to deep convection are somewhat speculative because deep convection is very sensitive to various model assumptions (e.g. permeability) and no direct measurements are available to compare SAMSIM's results against reality. We also show that under idealized conditions a freshening of the water directly under the ice caused by an increased oceanic heat flux can

lead to gravity drainage near the ice-ocean interface. This mechanism could explain the link between salt flux and oceanic heat measured in the field by Widell et al. (2006).

We compared a model run using the full convective gravity drainage parametrization against runs with fixed salinities and showed that the total enthalpy, thermal resistance, and freshwater column differ over the growth season (by ≈ 3 %) but have similar short-term variations. Only at ice formation and during deep convection —the processes most difficult to reproduce correctly in a 1D model— does model behavior diverge. As gravity drainage is the dominant but not sole desalination processes in sea ice, the effect of the total salinity evolution has yet to be assessed. Also, since the ocean and incoming atmospheric heat fluxes were prescribed, possible feedbacks were not included in this study.

As a computationally cheap alternative to the convective parametrization we also developed an unconditionally stable and numerically cheap parametrization referred to as the simple parametrization. It is based on the assumption that the salinity profile evolves to reduce convective instability. The simple parametrization is capable of reproducing the general salinity profile of the convective parametrization and leads to an approximately 1 % discrepancy of total enthalpy, thermal resistance, and freshwater column compared to the complex parametrization.

An additional reference run was generated by prescribing a crude approximation of a multi-year salinity profile. The resulting thickness, total enthalpy, and thermal resistance evolution are very similar to those produced by the simple parametrization. However, the freshwater column is roughly 4 % higher, which is to be expected since the prescribed profile is more similar to multi-year than first-year ice.

2.7.2 Discussion

The convective parametrization of gravity drainage we presented provides a 1D estimate of brine fluxes that is consistent with our physical understanding of the underlying processes. As such, it can aid researchers conducting detailed process studies of sea-ice biogeochemistry and ice-ocean interaction.

Our results provide insight into the relevance of gravity-drainage parameterizations for coupled climate models, but they can not quantify the effect of the full salinity cycle including ice-ocean-atmosphere feedbacks. Given these limitations, our test case indicates that large-scale models would not profit greatly from the inclusion of a gravity drainage parametrization. The complex parametrization is much too computationally demanding to be included in a large-scale model, and the effect on the thermal properties is rather small. The simple parametrization which was designed as a numerically effective alternative for large-scale models produces results achievable by directly prescribing a salinity profile. Especially for models with few layers (such as those proposed by Semtner (1976) and Winton (2000)) possible improvements are small compared to the overall model uncertainties (Wilkins, 2010).

Chapter 3

A 1D model study of Arctic sea-ice salinity

In this paper we explore how sea-ice surface melt can be incorporated into 1D models and how the salinity evolves in Arctic sea ice. We also quantify the relevance of explicitly parametrizing the temporal evolution of sea-ice salinity for climate models and use model simulations to gain general insight on desalination processes, sources of inter-annual salinity variability, the link between bulk salinity and ice thickness, and the transformation of first-year to multi-year ice. We incorporate surface melt into the 1D thermodynamic SAMSIM sea-ice model presented by Griewank and Notz (2013) and introduce a flushing parametrization which treats sea ice as a hydraulic network of horizontal and vertical fluxes. Flooding is also parametrized, allowing SAMSIM to simulate the full salinity evolution. Idealized experiments reveal that in SAMSIM the ratio of horizontal to vertical flushing oscillates over time. We investigate the sea-ice salinity evolution over 36 years by forcing SAMSIM with reanalysis data taken from throughout the Arctic. We show that the modeled salinity agrees well with ice-core data, and that the brine fluxes close to the ice surface are the least well captured. After ice growth has ceased 1.5-4 g/kg of bulk salinity are transported to the ocean via gravity drainage before flushing sets in. Most of the salinity variability of first-year ice is restricted to the top 20 cm. In assessing the impact of parametrizing salinity on the ice thickness, thermal resistivity, freshwater column, and stored energy we find that runs with a prescribed salinity profile differ from the full parametrization by less than 5 % on average, with maximum differences up to 11 %. We conclude that the impact of fully parametrizing the temporal salinity evolution in an earth system model is too small to justify the necessary additional computational cost.

3.1 Introduction

Sea ice is a multi-phase material consisting of salty brine, fresh ice, and gas bubbles and is far from static. Brine moves through the ice and across the ice-ocean interface transporting dissolved tracers such as salt. The thermal properties of sea ice change along with the phase composition, bubbles form, dissolve, and escape into the atmosphere

while chemical and biologic processes occur in the brine. Salt is a core component of sea ice as it determines the liquidus point of the brine which along with temperature dictates the phase composition of sea ice through the liquidus relationship. It also influences the brine density, the chemical properties, the small scale sea-ice structure, and the vertical stratification of the underlying ocean via salt transport to the mixed layer. Unfortunately, the salinity of sea-ice is an elusive quantity which is difficult to observe. Many open questions related to the salinity evolution can not be answered due to the limited amount and the isolated nature of ice-core measurements, such as to what extent gravity drainage occurs during ice melt, what causes inter-annual salinity variability, how first-year ice transforms to multi-year ice, and how bulk salinity is linked to ice thickness. To fill these gaps in our understanding we study the salinity evolution of Arctic sea ice and quantify the impact of the salinity evolution on various sea-ice properties using an expanded version of the 1D SAMSIM thermodynamic sea-ice model introduced in Griewank and Notz (2013).

The surface of melting sea ice is complex and highly heterogeneous. Melt water flows horizontally through snow and ice into melt ponds and cracks or percolates vertically through the ice. The properties of melting wet snow differ strongly from those of dry fresh snow, and the ice surface also deteriorates during melt and can form a layer of with white deteriorated ice which is visually similar to snow (Eicken et al., 2002). Due to the large influence the ice albedo has in climate models, the sea-ice modelling community has produced many albedo and melt pond parametrizations (e.g. Flocco and Feltham, 2007; Pedersen et al., 2009), but otherwise surface melt has received very little attention. All 1D thermodynamic models since Maykut and Untersteiner (1971) have disregarded the physical structure and high gas fraction of the surface during melt, and treat melting sea ice as freshwater ice with modified thermal properties.

Surface melt is linked to the salinity evolution via flushing. Over the last decade researchers have begun to parametrize the sea-ice salinity evolution (e.g. Vancoppenolle et al., 2006, 2007, 2009; **?**; Wells et al., 2011; Rees Jones and Worster, 2013a; Turner et al., 2013) to study the biogeochemical and physical processes in and below sea ice (e.g. Vancoppenolle et al., 2010; Tedesco et al., 2010; Saenz and Arrigo, 2012; Tedesco et al., 2012; Jardon et al., 2013). Despite these developments, the only sea-ice model with a fully parameterized salinity evolution is the LIM 1D model of Vancoppenolle et al. (2007) based on the 1D thermodynamic model of Bitz and Lipscomb (1999). Accordingly, many possible approaches to model surface melt and parametrize salinity remain unexplored in 1D sea-ice models. After the implementation of surface melt, flooding, and flushing, SAMSIM is capable of simulating the full growth and melt cycle of sea ice including the salinity evolution.

We force SAMSIM with Arctic reanalysis data to study the desalination processes and the resulting salinity evolution in the Arctic. This is the first general multi-year model study of sea-ice salinity throughout the Arctic. The only previous model study of sea-ice salinity is the study by Vancoppenolle et al. (2007) which focuses on two ice-core sites of land fast ice from 1999-2001. Model studies are necessary as measurement campaigns can only provide brief glimpses of the full salinity evolution, whereas we can easily explore a far greater diversity of conditions over a longer time frame. The simulated salinity profiles are compared to ice-core measurements to evaluate the model

performance and to determine which processes are not well represented.

The final topic we address is how parametrizing the salinity effects various sea-ice properties important to climate models. This is a highly relevant question as sea-ice components of climate-models are slowly becoming more sophisticated and modelers have begun to treat sea-ice salinity as a variable instead of a prescribed value or profile (e.g Vancoppenolle et al., 2009; Turner et al., 2013). It remains unclear how much model performance can be improved by fully parametrizing the temporal salinity evolution, and how sophisticated the parametrizations should be to balance the improvements against the increase in computational cost.

This paper is organized as follows. In section 3.2 we detail how surface melt, flooding, and flushing are implemented in SAMSIM. The section ends with a description of the three separate approaches used to parametrize salinity in SAMSIM and a discussion of the relative numerical costs associated with these approaches. In section 3.3 we conduct an idealized melting experiment to study flushing and to determine how sensitive SAMSIM responds to changes of key parameters. In section 3.4 we study the salinity evolution of 36 years of simulated sea ice forced with ERA-interim reanalysis data taken from throughout the Arctic. The simulations are split into first-year and multi-year ice which are analyzed separately and compared to ice-core data. The final section 3.5 uses the same atmospheric forcing as section 3.4 to quantify the impact of the various salinity approaches on quantities relevant to climate-models in order to evaluate if climate models would benefit from a fully parametrized temporal salinity evolution in their sea-ice sub models.

3.2 Model description

For the purpose of this paper, we expand the SAMSIM model which we first described in Griewank and Notz (2013). SAMSIM (Semi-Adaptive Multi-phase Sea-Ice Model) is a 1D column model which employs a semi-adaptive grid. In this section we will introduce how SAMSIM treats surface ablation and processes related to surface melting as well as flooding.

We provide a very brief description of the fundamentals of SAMSIM in subsection 3.2.1, a detailed description can be found in Griewank and Notz (2013). Following the brief description of SAMSIM we address how sea-ice melts in reality and in SAMSIM in subsection 3.2.2. The last addition to SAMSIM are the parametrizations of flushing and flooding in subsection 3.2.3. In subsection 3.2.4 we describe the three salinity setups used in SAMSIM. Subsection 3.2.4 includes a discussion of the numerical costs and merits of each of the salinity approaches.

3.2.1 SAMSIM

Each layer of SAMSIM is defined by the four fundamental variables mass m, absolute salinity S_{abs}, absolute enthalpy H_{abs}, and thickness $\triangle z$. Absolute values are simply the integral over the mass weighted bulk salinity S_{bu} and enthalpy H. The solid and liquid

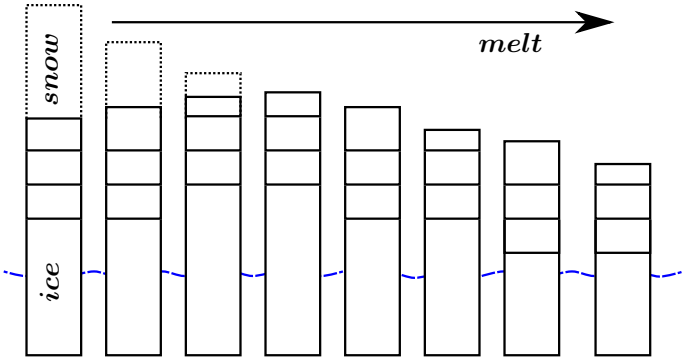

Figure 3.1: Sketch of SAMSIM grid evolution for three top layers during snow melt and following surface ablation as explained in subsection 3.4.1

.

mass fractions ψ_s and ψ_l, as well as the solid, liquid, and gas volume fraction ϕ_s, ϕ_l, and ϕ_g are derived from the fundamental variables. A salt-free snow layer can exist on the ice, which has a variable density that affects the snow thermal conductivity. However, the only process currently implemented in SAMSIM which affects the snow density is rainfall into snow. In this paper, we refer to a specific layer by an upper right index counting from top to bottom, with the exception of the snow layer which is marked with *snow*. E.g. m^6 is the mass of the sixth layer from the surface, m^1 is the mass of the top layer, and m^{snow} is the mass of the snow layer.

SAMSIM employs a unique semi-adaptive grid which grows and shrinks in discrete steps of $\triangle z_0$ at the ice-ocean interface (Griewank and Notz, 2013). However, at the ice-atmosphere boundary it is necessary to have a freely adjustable boundary to deal with incremental surface ablation and snow to ice conversion. This is addressed by letting the top layer thickness vary freely between $1/2\ \triangle z_0$ and $3/2\ \triangle z_0$. Once the top layer grows thicker than $3/2\ \triangle z_0$ it is split into two layers, the lower layer of the two with a thickness of $\triangle z_0$. Similarly when the top layer shrinks below $1/2\ \triangle z_0$ it is merged together with the second layer. A sketch of how a grid with three top layers evolves during melt is shown in figure 3.1.

The short wave radiation properties of the ice are set with a number of parameters. These parameters are the albedo *alb*, the fraction of penetrating short wave radiation *pen*, and the optical thickness of the ice κ. Various parametrizations have been proposed which define the optical properties based on the surface temperature, ice thickness, and ablation rates. In SAMSIM the gas volume fraction could also be used to parametrize the optical properties, as the amount of air bubbles has a large impact on the optical properties of the ice (Light et al., 2008). However, because the focus of this paper is on the salinity evolution we will use constant values of *alb*, *pen*, and κ for sea ice to remove a source of variability in the model results (values shown in table 3.1).

Table 3.1: Default model settings and free parameter values of salinity parametrizations.

$\triangle z_0$	1 cm
dt	10 s
N_{top}	20
N_{mid}	60
N_{bot}	20
$\phi_{s,min}$	0.05
$\phi_{s,melt}$	0.4
$\phi_{g,melt}$	0.2
alb	0.75
pen	0.3
κ	2 1/m
α	$1.56 \cdot 10^{-3} kg/m^3 s$
R_{crit}	1.01
γ	0.99
β	1
δ	0.5
ϵ	0.1
ζ_{max}	5 cm

3.2.2 Sea-ice surface melt

There are two main difficulties which complicate simulating surface melt in a 1D thermodynamic sea-ice model. The first is the strong spatial heterogeneity of melting sea ice. Although certain aspects such as melt ponds can be parametrized, there is no way to overcome the fact that a 1D approximation is less valid for melting sea ice than for growing sea ice. The second major difficulty is that many physical processes which occur at the surface during sea-ice melt are poorly understood. This is especially true for processes which occur at the snow-ice boundary and processes which involve capillary forces in snow or ice.

We have decided against separating the 1D column into a ponded and non-ponded fraction, as this is impossible without sacrificing physical consistency in a number of ways. A possible compromise is to couple a 1D column with a melt pond cover to another 1D column with no pond. A melt pond and albedo parametrization could be introduced to modify short-wave radiation penetration and reflectance without any effect on sea-ice permeability, freeboard, or melt water formation. However, we have decided to not introduce such an albedo parametrization for two reasons. Firstly, most albedo parametrizations are not suitable for SAMSIM. For example, some parametrizations change the albedo as an empirical function of surface temperature. If the parametrization assumes that the surface layer is salt free, the parametrization will assume that the surface temperature during melt will always be at 0 °C. However in SAMSIM, the surface temperature varies during melt depending on the salinity of the top layer. Other parametrizations rely on the surface melt speed, which is not a variable in SAM-

SIM. Instead SAMSIM has melt water formation and surface ablation, which are linked but not identical. The second reason is that slight albedo changes would overshadow the effects of the sea-ice salinity. If the albedo parametrization were fully physically consistent with SAMSIM this would be acceptable. However, albedo parametrizations mostly rely on empirical measurements and are intended to improve large-scale models and are ill-suited to determine how the albedo would react to a 5% increase of gas volume fraction or a 0.1 °C increase of temperature in the top ice layer of SAMSIM. Including an albedo parametrization would result in a high non-physical source of variability which would greatly complicate interpreting the results. Extending SAMSIM by an albedo parametrization that is compatible with SAMSIM physics remains, however, desirable and will be subject to future work.

From the measurements taken at the SHEBA site, Eicken et al. (2002) identified three stages of melt for Arctic multi-year ice. During stage I melt ponds form, fed by horizontally transport of melting snow. The snow cover still persists and while most of the melt water movement is horizontal, some melt water drains to the bottom of the ice through cracks and flaws in the ice. Stage II begins when the snow cover has completely melted away. During stage II melt water flows horizontally to reach flaws as well as vertically through the ice. In stage III the flaws have enlarged to the point of ice disintegration. Melt water moves vertically through the ice as well as horizontally to reach cracks and the edge of the ice flows, and convective overturning occurs close to the ice-ocean interface.

In SAMSIM, surface melt is implemented by separating melt into two separate stages. The first stage is snow melt, in which snow is converted to slush. This process thins the snow layer by transforming a fraction of the snow into slush, which is then added to the top sea ice layer as described in subsection 3.2.2.1. The second stage is surface ablation in which a fraction of the liquid volume of the top ice layer is designated as melt water as described in subsection 3.2.2.1. This melt water is either transported directly into the ocean, or flows through the ice and cracks according to the flushing parametrization introduced in subsection 3.2.3.2.

3.2.2.1 Snow melt

The physics of snow is very complex and a scientific field of its own. The snow layer in SAMSIM is intended to simulate only the most basic aspects of snow on sea ice. In contrast to the widely used 1D thermodynamic sea-ice model of Bitz and Lipscomb (1999) which is implemented in both the Los Alamos (CICE) and the Louvain-la-Neuve (LIM) sea-ice models, snow does not turn directly into melt water in SAMSIM. Instead, melted snow from the snow surface percolates downward and accumulates on the sea-ice surface forming a slush layer of depth B as illustrated in figure 3.2. This snow to slush conversion in SAMSIM is based on two core assumptions. The first assumption is that the snow can only retain a maximum liquid mass fraction ($\psi_{l,max}$) which is a function of the snow solid mass fraction. The function we use is

$$\psi_{l,max} = 0.057\frac{(1-\psi_s^{snow})}{\psi_s^{snow}} + 0.017,$$

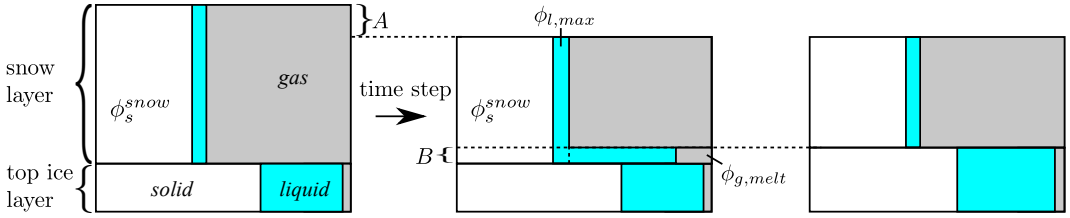

Figure 3.2: Sketch of snow melt by snow to slush conversion as described in subsection 3.2.2.1. B is the thickness of the slush layer, and A is the thickness lost by snow to slush conversion. At the end of the time step the top ice layer thickness increases by B while the snow layer thickness is reduced by $A + B$. The white, blue, and grey areas represent the solid, liquid, and gas volume fractions of each model layer.

which we take from the laboratory study of Coleou and Lesaffre (1998). In figure 3.2 the volume fractions are shown instead of the mass fractions, because the volume fractions are proportional to the area depicted. The second core assumption is that when the liquid water content surpasses the retainable amount, the excess water pools at the bottom of the snow layer forming a layer of slush. At each time step the depth of the slush layer is determined and then the slush layer is added to the top ice layer.

Two additional assumptions are required to determine the slush depth which is marked as B in figure 3.2, namely the gas fraction of the slush $\phi_{g,melt}$, and the solid fraction of the slush layer and remaining snow layer. We assume that the solid volume fraction equals the solid fraction of the previous time step, and that $\phi_{g,melt}$ is a constant. In this paper we set $\phi_{g,melt}$ to 20 %, which we base on the measured surface sea-ice densities of Eicken et al. (1995).

Following these assumptions, when the liquid volume fraction of the snow layer exceeds $\phi_{l,max}$ the slush depth B is calculated from the snow solid fraction of the last time step (ϕ_s^{snow}) and the gas content as

$$B = \triangle z \frac{\phi_l^{snow} - \phi_{l,max}}{1 - \phi_{l,max} - \phi_s^{snow} - \phi_{g,melt}}.$$

As a result the top ice layer grows thicker by B, and mass and enthalpy are transfered according to the composition of the slush layer. To maintain the solid fraction of the last time step the snow needs to be compacted by A as illustrated in figure 3.2. In total the snow to slush conversion shrinks the snow layer by $A + B$, the total snow and ice column shrinks by A, and the top ice layer grows by B.

To our current knowledge, the approach of converting snow into slush before it can run off as melt water is unique. Compared to the standard approach in which melted snow is directly removed as melt water, our approach leads to a slight delay in the onset of flushing. In reality sea-ice has a varying surface height, which causes the melt water in the slush to flow into melt ponds. In SAMSIM, by the time the snow layer has melted away, the top model layers which were formed by snow to slush conversion are predominantly liquid and salt free but also contain the solid fraction of the flooded snow. These top layers can be interpreted as a spatial average over melt ponds and

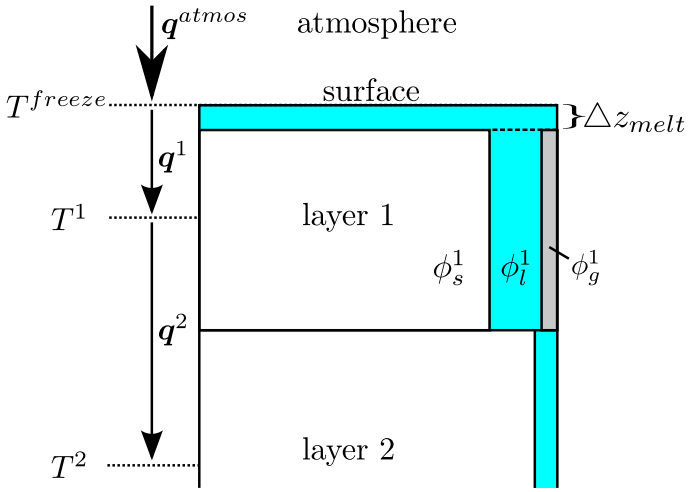

Figure 3.3: Sketch of melt water formation caused by surface melting as described in subsection 3.2.2.2. The white, blue, and grey areas represent the solid, liquid, and gas volume fractions of each model layer (ϕ_s, ϕ_l, and ϕ_g). $\triangle z_{melt}$ is determined by the amount of latent heat release necessary to balance the energy difference between the atmospheric heat flux to the surface $\vec{q}^{atmos}$ and the flux from the surface into the top ice layer $\vec{q}^1$.

snow remnants. As a result the snow melt stage of SAMSIM is shorter than the first melt stage of Eicken et al. (2002). Although the implemented snow to slush conversion neglects many of the finer aspects of snow physics, we trust that it captures snow melt more realistically than the standard approach of turning snow directly into melt water.

Two additional processes also convert snow to slush, flooding as introduced in subsection 3.2.3.4 and melt water wicking. Wicking occurs when the top ice layer is so liquid that excess brine seeps into the snow. This process is incorporated into the model as introduced in the following subsection.

3.2.2.2 Surface ablation

Surface ablation begins once the snow layer has been completely transformed to slush and the top ice layer is in direct contact with the atmosphere. Surface ablation in SAMSIM requires deciding how much of the liquid fraction runs off as melt water and how much of the departing melt water is replaced by gas. In reality the ice surface varies immensely in space and time, from dark deep melt ponds to deteriorated white ice which looks like snow from afar (Eicken et al., 2002). In contrast, the ice surface in SAMSIM is solely represented by the phase composition of the top ice layer.

Melt water runoff in SAMSIM is restricted to the top ice layer and is based on three assumptions. The first is that ice melted at the ice surface directly turns into melt water. The second is that if the solid fraction of the top ice layer sinks below a minimal low value, excess brine is free to flow off as melt water. The third is that over time the gas fraction increases until it reaches the value of $\phi_{g,melt}$.

Melt water can form by surface melting as soon as the surface temperature surpasses the freezing temperature of the top layer. The amount of melt water formed is determined

by the amount of latent heat release necessary to balance the atmospheric heat flux to the surface and the diffusive heat flux from the surface into the top layer (depicted in figure 3.3). This approach is commonly used in sea-ice thermodynamic models (e.g. Bitz and Lipscomb, 1999) but needs to be adapted to incorporate the varying density and gas fraction of SAMSIM. The discretized diffusive heat flux from the ice surface into the top layer is

$$\vec{q}^1 = -k^1 2 \frac{T^{freeze} - T^1}{\triangle z^1}.$$

The thermal conductivity of the top layer k^1 is a linear combination of the liquid and solid phases, while the gas phase is treated as an insulator. The depth of the melt water film for a given atmospheric energy flux $\vec{q}^{atmos}$ is then

$$\triangle z_{melt} = \frac{\vec{q}^{atmos} - \vec{q}^1}{\phi_s^1 \rho_s L}.$$

The second way melt water can form is when the solid fraction of the top layer ϕ_s^1 to fall below a minimal low value $\phi_{s,melt}$. When this occurs the solid fraction is compacted by $\triangle z_{melt}$ until the solid fraction reaches $\phi_{s,melt}$ as shown in figure 3.4. From volume conservation it follows that

$$\triangle z_{melt} = \triangle z^1 \left(1 - \frac{\phi_s^1}{\phi_{s,melt}}\right).$$

This extreme simplification ensures that melt water forms before the top layer is fully liquid. Not shown in the figure is that a similar limit exists on the gas fraction. If the gas fraction exceeds $\phi_{g,melt}$ then the top layer is compacted to reduce ϕ_g^1 to $\phi_{g,melt}$. $\phi_{g,melt}$ is the same parameter which determines the amount of air captured in the slush during snow melt, and is set to 0.2 based on density measurements at the surface of Eicken et al. (1995). To our knowledge there are no measurements from which to estimate $\phi_{s,melt}$. A range of values will be explored later in this paper, but as a first guess we assume a value of 0.4, which is slightly above the solid fraction assigned to fresh snow in SAMSIM. If the ice melts primarily through compacting due to low solid fractions, the top layer will approach the given values of $\phi_{g,melt}$ and $\phi_{s,melt}$ over time.

If the melt water forms due to a low solid fraction while snow is present, the melt water is assumed to wick up into the snow and creates a slush layer which is then added to the top layer again. We refer to this as wicking which is similar to snow melt (figure 3.2), except that the amount of water available to form slush is given by the amount of melt water present in the top layer.

3.2.3 Salinity parametrizations

There are three known relevant desalination processes in sea ice: gravity drainage, flushing, and flooding (Notz and Worster, 2009). We addressed how gravity drainage is implemented into SAMSIM in our previous publication (Griewank and Notz, 2013). In this subsection we introduce parametrizations for flushing and flooding, making

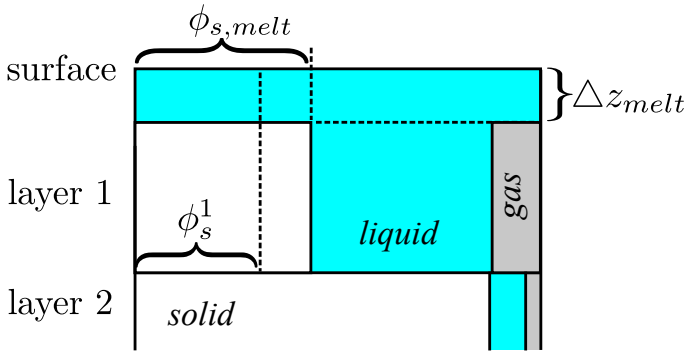

Figure 3.4: Formation of melt water in the top layer when $\phi_s^1 < \phi_{s,melt}$ as described in subsection 3.2.2.2. $\triangle z_{melt}$ is determined by how much the solid fraction has to be raised to equal $\phi_{s,melt}$. The white, blue, and grey areas represent the solid, liquid, and gas volume fractions of each model layer.

SAMSIM the second 1D model capable of capturing the full salinity evolution. The first model capable of capturing the full salinity cycle is the 1D LIM sea-ice model of Vancoppenolle et al. (2006).

Parametrizing flushing faces the same challenges that modeling surface melting faces, namely high horizontal heterogeneity, insufficient data, and a lack of theoretical understanding. No quantitative laboratory studies of flushing have been published to this date, and due to sampling issues and difficult conditions field studies have been limited to studies of dye dispersion and ice-core salinity (Eicken et al., 2002). The understanding of flooding is even poorer, and is limited to the analysis of ice cores which contain flooded snow-ice.

3.2.3.1 Flushing

The first and only published flushing parametrization incorporated in a full thermodynamic sea-ice model by Vancoppenolle et al. (2006) assumes that once the ice reaches a certain permeability, a fraction of the melt water flows downward through the sea ice and into the ocean below. Although this approach neglects many aspects of flushing, it is able to reproduce field measurements of salinity (Vancoppenolle et al., 2007). In this subsection we will introduce two parametrizations. The complex parametrization attempts to model flushing as a physically consistent hydraulic system, and the simple parametrization is a numerically cheap alternative based on the assumption that the liquid fraction increases towards the surface during surface melt.

3.2.3.2 Complex flushing

It is known from the field observations of Eicken et al. (2002) that much of the brine movement during flushing occurs horizontally in the upper layers. The horizontal flows drain through flaws and cracks beneath the sea-ice which can lead to underwater ice formation. The parametrization of Vancoppenolle et al. (2006) has no explicit

treatment of horizontal fluxes. Our goal is to design a flushing parametrization which is as physically consistent as possible in a 1D model and includes horizontal brine fluxes which are highest close to the ice surface. Additionally the parametrization should have as few free parameters as possible. The resulting parametrization (sketched in figure 3.5) treats sea ice as a hydraulic network in which each model layer has a vertical and horizontal hydraulic resistance (R_v and R_h). The assumptions on which the parametrization is based are:

1. Cracks always exist in the ice, and the average horizontal distance between these flaws grows linearly with ice thickness.
2. Once brine reaches such a crack it drains away to the ice-ocean interface without interacting with the underlying ice layers.
3. The vertical resistance represents the resistance to brine flowing from the top to the bottom of a layer. The horizontal resistance represents the resistance which brine needs to overcome to reach a crack.
4. Flushing melt water flows vertically from layer to layer and horizontally to the cracks. The specific amount for each layer are determined by the hydraulic resistances and the hydraulic head.
5. The hydraulic head is assumed to be equal to the freeboard ζ, resulting in a pressure difference of $\triangle p = \zeta \rho g$ for the brine density ρ and gravitational constant g.

The resulting parametrization has only a single free parameter β which determines the average distance x to the nearest crack for a given ice thickness h through $x = \beta \cdot h$.

The Darcy flow in a porous medium with a hydraulic resistance of R leads to a mass flux f of

$$f = \frac{\triangle p \cdot A}{R} \rho$$

for the pressure difference $\triangle p$ and liquid density ρ. In SAMSIM, for each layer i the vertical hydraulic resistance

$$R_v^i = \frac{\mu}{\Pi(\phi_l^i) A} \triangle z^i$$

is defined by the permeability Π which is a function of the layer's liquid fraction ϕ_l^i, the brine viscosity μ, the column area A, and the layer thickness $\triangle z$.

To define the horizontal hydraulic resistance we take the average distance to the next crack from our assumptions resulting in

$$R_h^i = \frac{\mu}{\Pi(\phi_l^i) A_v^i} x.$$

In contrast to the vertical flow area A which is always 1 m^2 in the column model, the horizontal flow area A_v^i varies with layer thickness as well as with the geometry of the cracks and resulting flow field. As a working assumption we take A_v^i to be equal to the vertical layer surface with an area of $\triangle z^i \cdot 1$ m.

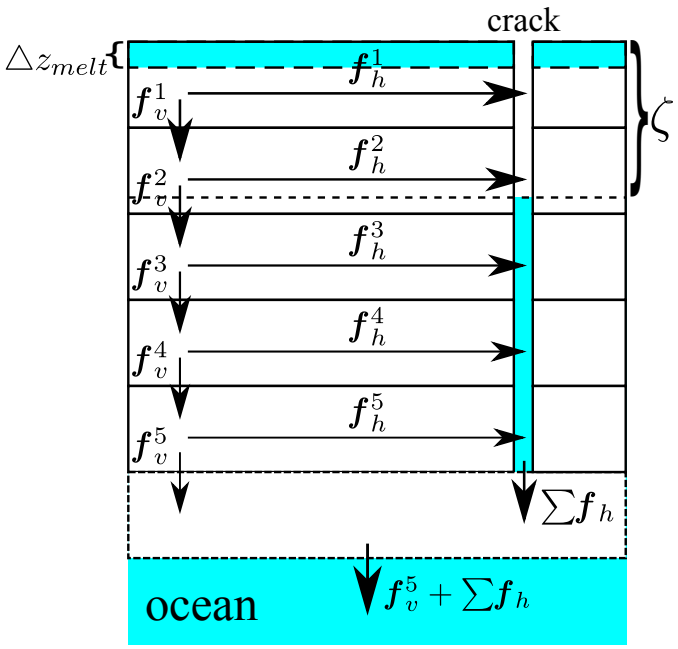

Figure 3.5: Brine fluxes of the complex flushing parametrization resulting from melt water formation at the surface as described in subsection 3.2.3.2. The horizontal fluxes $\vec{f_h}$ transport heat and salt to the lowest layer directly via cracks in the ice, while the vertical fluxes $\vec{f_v}$ advect heat and salt from layer to layer. ζ is the freeboard of the ice and $\triangle z_{melt}$ is the depth of the melt water.

The resulting horizontal and vertical brine fluxes ($\vec{f_h}$ and $\vec{f_v}$ as shown in figure 3.5) are then computed from hydraulic head and resistance. The total resistance over multiple layers is calculated as a sum of parallel and serial resistances, the same method used in resistor ladder circuits. The total flux is limited by the amount of melt water present in the top layer.

Vertical fluxes advect salt and heat from layer to layer using the upstream method, while horizontal fluxes transport both salt and heat directly to the lowest model layer, i.e. the ice-ocean interface. As the thermal profile in melting ice is almost uniform, the vertical fluxes lead to a smaller desalination than the horizontal fluxes.

Although the top layer can accumulate melt water faster than it can flush away, a fully liquid layer is impossible. As the top layer becomes more and more liquid, the permeability increases and the horizontal hydraulic resistance of the top layer decreases, resulting in a strong horizontal flushing in the top layer.

As brine movement always leads to a heat transport, flushing cold brine into the ocean produces a heat sink in the model. Because flushing mostly occurs in ice close to the freezing temperature the energy lost due to flushing is small. When comparing runs using different salinity approaches the amount of heat lost by flushing is added to the oceanic heat flux to keep the runs as comparable as possible. The same approach is applied to the gravity drainage parametrization as discussed in Griewank and Notz (2013).

3.2.3.3 Simple flushing

We propose a second numerically cheaper parametrization which we will refer to as the simple flushing parametrization. In contrast to the complex parametrization which calculates brine fluxes which affect salinity via advection, the simple parametrization directly modifies the salinity to fulfil a stability criterion. This stability criterion is based on the simple assumption that the liquid fraction is highest in the top layer during melt, and decreases into the ice.

The implementation is as follows. At each time step the melt water which forms in the top layer as explained in subsection 3.2.2.2 is removed. As the salinity of the melt water given by the ice-brine liquidus relationship is higher than the bulk salinity of the top layer, the melt water removal desalinates the top layer. At each time step it is checked if $\phi_l^1 > \phi_l^2$. Given that the temperature differences between the top layers is small during surface melt, the second saltier layer gradually become more liquid than the fresher top layer. When this occurs, the salinity of the second layer is simply reduced by a fixed fraction ϵ. The same procedure is then applied the next lower layer as long as $\phi_l^i > \phi_l^{i+1}$. For example if $\phi_l^1 < \phi_l^2 < \phi_l^3 > \phi_l^4 < \phi_l^5$, the salinity of the second and third layer are reduced.

3.2.3.4 Flooding

Flooding can occur when snow pushes the ice below the ocean surface, causing ocean water to well up and flood the snow. The resulting frozen mix of snow and ocean water called snow ice can be identified by various means in ice cores, from which we know that flooding occurs mainly in the Antarctic and contributes up to 25 % of ice production in certain areas (Jeffries et al., 2001; Maksym and Jeffries, 2001). We base our understanding and treatment of flooding on the work of Ted Maksym and Martin O. Jeffries (Maksym and Jeffries, 2000; Jeffries et al., 2001; Maksym and Jeffries, 2001). To readers interested in flooding we recommend the PhD thesis by Maksym (2001).

Although at first glance flooding seems to be the same process as flushing but with a reversed pressure gradient, there are a number of additional uncertainties. Field measurements have shown that a negative freeboard does not automatically lead to flooding, although the chance of flooding is higher the lower the freeboard. Additionally, very little is known about what happens to the flooded brine once it reaches the ice surface. As flooding occurs at the bottom of the snow mantel, direct observations of flooding are extremely difficult to obtain. Snow metamorphism is by itself a complex process, but the interactions between flooding brine and snow are even more complex and little research has been devoted to this specific issue. Brine movement must occur at the ice surface after or during flooding, because otherwise snow-ice salinities would be higher than the measured values.

As for flushing and gravity drainage we again developed two separate parametrizations for flooding. However, the two flooding parametrizations are rather similar. We will simply refer to the slightly more sophisticated parametrization as the *complex* parametrization and the simpler one as the *simple* flooding parametrization.

3.2.3.5 Complex flooding

The complex parametrization assumes that during flooding ocean water passes through cracks and channels in the ice to flood the snow layer. The flooding ocean water does not interact with the brine in the sea ice, because Maksym and Jeffries (2001) showed that if flooding resulted in an upward brine displacement through the whole ice the resulting desalination would quickly turn the ice impermeable. The flux of ocean water to the surface is calculated as a Darcy flow driven by the negative freeboard and limited by the permeability of the least permeable model layer. This approach can lead to a large negative freeboard if the ice layer is impermeable. To avoid this a maximum negative freeboard ζ_{max} is defined. If the freeboard sinks below this threshold, the flux of ocean water necessary to raise the freeboard to the threshold is determined and applied.

The ocean water which is transported to the ice surface forms a slush layer which is added to the top ice layer. This is the same approach SAMSIM uses to imitate snow melt and melt water wicking into the snow layer (described in subsection 3.2.2.1 and 3.2.2.2). However, given a snow solid volume fraction of approximately 30-40 % this approach would result in the flooded slush layer having a very high salinity of roughly 20 g/kg, inconsistent with measurements. To avoid this high salinity, we assume that the ocean water which floods the snow simultaneously wicks upward and dissolves additional snow into the slush which leads to a freshening of the slush. The ratio of dissolved to flooded snow is assumed to be constant, and is defined by an additional free parameter δ.

In this paper we use a value of 5 cm for ζ_{max}, which is based on the freeboard measurements analyzed in Maksym and Jeffries (2000) and for δ we use a value of 0.5 as a preliminary best guess.

3.2.3.6 Simple flooding

The simple parametrization is simply the complex parametrization stripped of the permeability dependent flooding speed and without snow dissolving into the slush layer. The simple parametrization is identical to the complex parametrization if the free parameters are set accordingly, $\zeta_{max} = 0$ m and $\delta = 0$. This means that as soon as a negative freeboard develops flooding sets in right away, and that no snow is dissolved into the forming slush.

3.2.4 Salinity setups

In subsection 3.2.3 we have presented four parametrizations, two for flushing and two for flooding. Together with the two gravity drainage parametrizations introduced in Griewank and Notz (2013) SAMSIM now has two complete sets of desalination processes. The first set consists of the complex flushing, the complex flooding, and the complex gravity drainage parametrization. The second set of parametrizations consists of the simple flushing, the simple flooding, and the simple gravity drainage parametrization. The parametrizations of the first set all compute brine fluxes which result in

salt and heat advection. Accordingly, the rate of salinity change is determined by the strength of brine flow and the salinity gradients between layers. In contrast, the parametrizations of the second set directly adjust the salinity profile to fulfill defined stability criteria.

We will refer to the first set of parametrizations as the *complex* salinity approach, as it consists of the more sophisticated parametrizations which were designed to be as close to reality as possible. The second set will be referred to as the *simple* approach, as the parametrizations included were developed as simpler alternatives to the parametrizations of the complex approach.

The third and final salinity approach employed in this paper is to prescribe a depth dependent salinity profile which is completely independent of the ice properties. The profile used is the same introduced in Griewank and Notz (2013), which consists of a linear decrease from 34 to 4 g/kg in the lowest 15 cm, and a second linear decrease from 4 to 0 g/kg at the surface. This approach is referred to as the *prescribed* approach. The prescribed profile is by choice highly idealized. A more realistic profile could have been derived from simulations using the complex approach, but we prefer the idealized profile as it is independent of SAMSIM and the simulation forcing.

An important aspect of the complex parametrisation set is that the simulated brine fluxes result in heat fluxes both in the ice and into the ocean. This is most relevant during growth when gravity drainage continually moves colder brine to the ocean while taking up relatively warm ocean water, resulting in a small but steady increase of oceanic heat flux in our limited model domain. To keep the results of the three salinity approaches as comparable as possible, the heat fluxes resulting from gravity drainage and flushing are subtracted from the lowest layer at each time step.

Numerically, the complex approach is much more expensive than the simple approach because the brine dynamics and resulting salt advection require a much smaller time step at the same spatial resolution. If the amount of brine flowing into a layer is close to the liquid volume of the layer, sudden salinity changes can lead to layers becoming impermeable and choking off all further flow. As the brine flows and the brine volume in the layers are continuously changing, there is no easy way to predict beforehand what time step is needed for a specific experiment.

In comparison to the prescribed approach, the simple approach is not much more expensive in the 1D model for the same amount of layers. However, because the simple approach is dependent on the vertical structure of the ice column its quality degrades if very few layers are used. Also, while the prescribed approach is only dependent on the total ice thickness, the simple approach also depends on the amount of salt in each layer. This is not of great importance in 1D models, but if implemented in a model with horizontal ice advection the amount of tracers which need to be advected would lead to a large increase of computational demands. In summary, the computational advantage of the prescribed approach over the simple approach is that the number of layers can be smaller and it requires no tracer advection, while the computational advantage of the simple approach over the complex approach is the ability to use longer time steps.

3.3 Idealized flushing experiments

In this section we take a closer look at the complex flushing parametrization and how sensitively it reacts to various parameters. To do so, we use a highly idealized experiment which aims to remove all feedbacks and processes other than flushing. As a full exploration of possible initial and boundary conditions and the parameter space would be a very expensive exercise, we limit ourselves to a single experiment and choose the three parameters which have the greatest influence and vary them independently of one another. The first parameter is the minimum amount of solid fraction $\phi_{s,melt}$ which can be present in the top layer before melt water forms. $\phi_{s,melt}$ affects how permeable the top layer is when melt water forms. The second parameter we vary is β which determines the linear relationship of average horizontal flow distance to ice thickness. The third parameter is the layer thickness $\triangle z_0$. For the idealized experiment we set the total number of layers high enough so that all layers have the uniform thickness of $\triangle z_0$.

The idealized experiment begins with a two meter thick homogeneous slab of ice with a bulk salinity of 5 g/kg and a temperature of roughly -1.3° C. A constant oceanic heat flux of 15 W/m^2 is applied to the bottom while a constant heat influx of 380 W/m^2 is applied to the surface. After subtracting the outgoing thermal radiation at 0° C at the surface, the net heat input into the surface is slightly below 70 W/m^2. All brine fluxes which occur in the experiment are caused by flushing as gravity drainage is deactivated and no flooding occurs. The setup of the idealized experiment was chosen to produce a strong flushing signature with chosen values not too far away from field conditions.

We will first make some general observation of how flushing occurs in the idealized experiment in subsection 3.3.1 before analysing how sensitively the flushing parametrization reacts to the three parameters in subsection 3.3.2, 3.3.3 and 3.3.4.

3.3.1 General observations

In the idealized experiment the homogeneous sea-ice slab melts away over two months (figure 3.6). The constant surface heat input should lead to a constant rate of surface ablation, however SAMSIM's semi-adaptive grid results in a step wise surface ablation, especially at lower resolution (see subfigure 3.7 d). One of two striking features of this idealized experiment is that while flushing reduces the bulk salinity close to the surface it also leads to a high increase of salinity at the bottom (figures 3.6, 3.7 b-d, and 3.8). This is caused by the positive temperature gradient near the ice-ocean interface, which leads to the vertically flushing brine to move from colder to warmer layers. As the brine is saltier in the colder layers due to the liquidus relationship, salt advection leads to a bulk salinity increase in the lowest ice layers. This effect disappears if gravity drainage is activated (figure 3.7 a), which explains why this salinity increase due to flushing has not been observed to our knowledge. To determine if flushing could in principle lead to such an increase in salinity if gravity drainage is absent would require experiments with a multi-phase material in which both phases have a similar density to inhibit convection. An additional requirement needed to generate these high salinities close to the ice-ocean interface is that the oceanic heat flux is relatively small so that

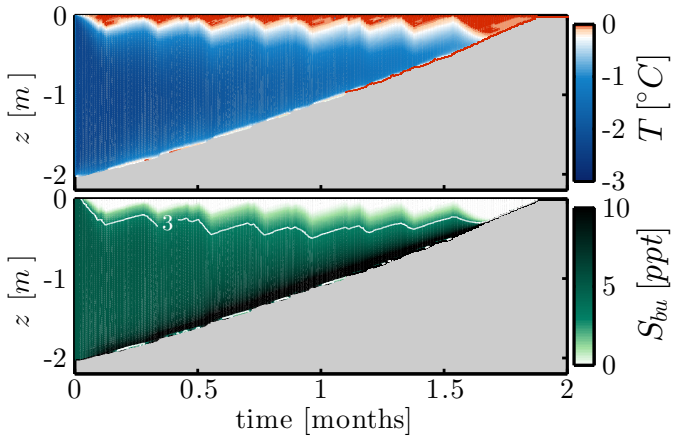

Figure 3.6: Temperature (a) and bulk salinity (b) evolution of the idealized flushing experiment using the default model setup (experiment setup in section 3.3, model setup in table 3.1). Temperature color bar is white at the freezing temperature of the initial ice salinity of 5 g/kg. Plot background is grey.

the salt has time to accumulate in the lower layers before they melt away. The low oceanic heat flux also allows melt water to accumulate in the very lowest layer where melt water is transported by flushing (figure 3.7 b and c).

The second most striking feature is that the desalination near the surface occurs in waves, which can be seen by following the 3 g/kg contour in figures 3.6 and 3.7. As the rate of melt water formation is nearly constant over time, this oscillation shows that the ratio of horizontal to vertical flushing oscillates over time. The speed, form, and strength of these oscillations are dependent on the chosen values of ϕ_s^{top}, β, and $\triangle z_0$, which indicates that the complex flushing parametrization does not reach an equilibrium and is dependent on model parameters (figure 3.7 b-d). The oscillation is also visible when comparing the salinity profiles of the experiment at 30 and 34 days (figure 3.8). At 30 days there is almost no visible difference between $\beta = 1, 5$, and 25. Four days later a smooth progression is visible. Similarly, all the grid spacing 4, 8, and 16 mm are almost identical at 34 days, but at 30 days this is not the case. Such an oscillatory behavior is physically plausible. At the beginning of the experiment flushing penetrates deep into the still saline ice and desalinates the upper layers. The desalination leads to an increase of the solid fraction and a slight warming. The underlying layers which have not yet been desalinated remain cooler. At some point the lowest desalinated layer is cooled enough by the lower layers so that the liquid reduces enough to make the ice totally solid. The now impermeable layer shields the lower layers from vertical flushing and the melt water flows horizontally into cracks and flaws. Over time the surface melt away until the impermeable layer which shielded the lower layers reaches the surface. Once the fresh layer is melted away, flushing melt water penetrates deep into the ice desalinating the upper layers, and the cycle repeats itself.

Local short-term flushing events have been detected in the temperature profiles of both field data (Pringle et al., 2007) and laboratory experiments (Wiese, 2012). However,

averaging horizontally over a large area should average out the local flushing events to a gradual and smooth desalination. Accordingly, to get a representative salinity profile from SAMSIM it is best to perform a short temporal average over one or two oscillations.

3.3.2 Minimal surface solid fraction

The range of possible values of $\phi_{s,melt}$ is constrained by physical and model limitations to be between 0 and 1-$\phi_{g,melt}$. We choose to vary $\phi_{s,melt}$ between 0.2 and 0.5, which we trust to span the range of realistic values with a default value of 0.4. The effect

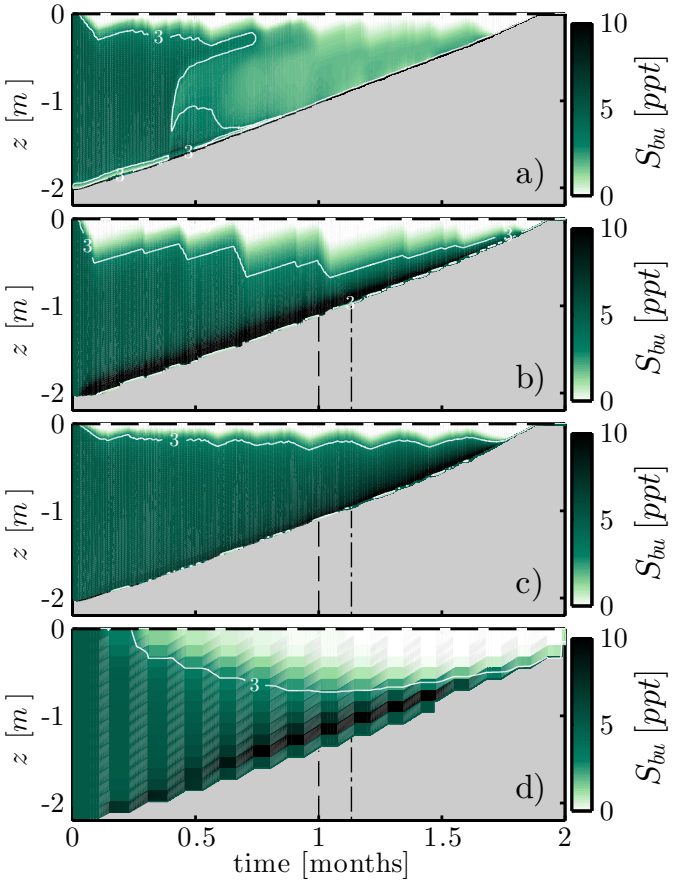

Figure 3.7: Salinity evolution of the idealized melting experiments in which one specific parameter or setting has been changed from the default values (default model results shown in figure 3.6, experiment description can be found in section 3.3, default settings are listed in table 3.1). The white line is the 3 g/kg salinity contour. Subfigure a includes gravity drainage which is otherwise disabled in the experiment. In subfigure b the minimal solid fraction of the top layer $\phi_{s,melt}$ is 0.2 instead of 0.4. In subfigure c the ratio of horizontal to vertical hydraulic resistance β is 0.2 instead of 1.0. In subfigure d the vertical spatial resolution $\triangle z_0$ is 12.8 cm instead of 1 cm. The dashed black lines in subfigure b, c, and d mark the times at which the profiles in figure 3.8 are shown.

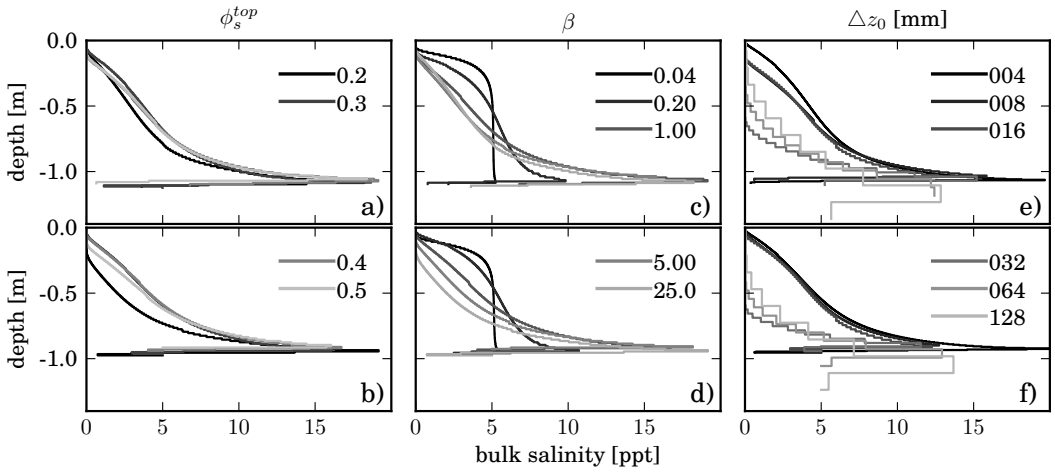

Figure 3.8: Salinity profiles of the idealized melting experiments after 30 days (subfigures a, c, and e) and after 34 days (subfigures b, d, and f). Profiles are shown at two separate times to visualize the short-term variations due to oscillations. The experiment description can be found in section 3.3 and the point of time of the profiles are marked in figure 3.7 by dashed lines. In subfigures a and b the minimal solid fraction of the top layer $\phi_{s,melt}$ is varied (see subsection 3.3.2), in subfigures c and d the ratio of horizontal to vertical hydraulic resistance β is varied (see subsection 3.3.3), and in subfigures e and f the vertical spatial resolution $\triangle z_0$ is changed (see subsection 3.3.4). The subfigures above and below each other share their legend (e.g. a & b).

of $\phi_{s,melt}$ on the complex flushing parametrization seems to be rather small, with only slight differences visible in the resulting salinity profiles (figure 3.8 a & b). In the idealized experiment, lower values of $\phi_{s,melt}$ cause slightly stronger salinity changes in the idealized experiment (figures 3.6 b vs figure 3.7 b and figure 3.8 a & b). As $\phi_{s,melt}$ also affects snow to slush transformation, it is possible that the effect of $\phi_{s,melt}$ is stronger when snow is present.

3.3.3 Free parameter β

In contrast to $\phi_{s,melt}$ we have no definitive physical or model limits on the possible value of β. Based on tracer studies of Eicken et al. (2002), we expect horizontal flows to be on the order of meters. Accordingly, we expect β to be in the single digits. However, to account for unknown biases in the model and parametrization (e.g. permeability) we chose a very wide spread of values from 0.04 to 25 to err on the side of caution. As a working assumption we use 1 as the default value.

As a high β increases the horizontal hydraulic resistance, the higher β is the weaker the horizontal fluxes are and vice versa. In the idealized experiment the low value of β = 0.04 leads to the flushing brine only penetrating a short distance into the ice (figure 3.8 c and d). Higher values of β cause an increased salinity at the ice-ocean interface, which results from vertical brine fluxes in the lowest layers. The results for β = 1, 5, and 25 differ only slightly, indicating that most melt water flows vertically through the

ice. From the idealized experiment we conclude that changing β has the anticipated effect. A wide spread of values was used for β, and the parametrization has a low sensitivity to changes of β close to the default value of 1. This low sensitivity is an advantage for us because although we lack the data to derive the optimal value of β, having a poor estimate of β will only impact our results slightly.

3.3.4 Vertical resolution

The impact of changing the vertical resolution is manifold. $\triangle z_0$ affects melt water formation, the accuracy of the spatial discretizations, and salinity advection. However, the most direct effect of the resolution on the complex flushing parametrization is that changing $\triangle z_0$ changes the distance between parallel connected hydraulic resistances in the ladder circuit, enabling a more refined flow separation.

In the idealized experiment higher resolution leads to a quicker onset of flushing, faster oscillations of the 3 g/kg contour, and a shallower desalination at the surface (see figures 3.6 b, and 3.7 d, and 3.8 e & f). No strict convergence like behavior is visible, but at vertical spacings below 2 cm the simulations change only slightly. Given the lack of experimental data or theoretical expectation we can not validate our decision to use a $\triangle z_0$ of 1 cm as our default value, but we expect small changes in resolution to not substantially affect results.

3.3.5 Summary

In the idealized experiment the ratio of deeper penetrating vertical fluxes versus shallower horizontal fluxes oscillates, which is clearly visible in the 3 g/kg salinity contour. In the absence of gravity drainage salt accumulates in the lowest layers leading to high salinities of up to 20 g/kg.

The complex flushing parametrization responds weakly to changes of the parameter β, and the parameter $\phi_{s,melt}$ only has a minor effect. Changing β has the expected effect, but no theoretical expectations or data are available to determine the optimal value. Accordingly, the chosen default value of 1.0 is highly uncertain and may be off by more than an order of magnitude. However, given the low sensitivity to β even a change of magnitude would not qualitatively change our results. The vertical model resolution has a strong influence on the parametrized flushing with higher resolution leading to quicker oscillations and a shallower desalination at the surface. It is possible that the complex parametrization performs most realistically at a specific layer thickness or that the optimal value of β is resolution dependent, but this can not be determined until more precise data is available.

3.4 Arctic sea ice

In this section we study how SAMSIM simulates the salinity evolution in the Arctic using the complex salinity approach, and compare the model output with ice-core data.

We have decided to limit the study to the Arctic because flooding and the corresponding snow ice formation play a large role in the Antarctic. As explained in subsection 3.2.3.4, we treat the flooding parametrizations currently implemented in SAMSIM as ad hoc solutions only suitable for dealing with isolated and sporadic flooding events. Accordingly, we will refrain from studying Antarctic ice until flooding is better understood.

Although a basic understanding of the salinity evolution has existed for many decades, the main processes driving this desalination still pose many unanswered questions. Using a model has the major advantage of being able to track the evolution consistently over long periods of time, while sea-ice cores can only provide snapshots. Simulating the salinity evolution with SAMSIM is an exercise of reproducing a vaguely known result of poorly understood origin. We aim to understand the impact and interactions of the various processes better, while at the same time discovering the limitations of the developed parametrizations or the existence of neglected relevant processes.

3.4.1 Model setup

To imitate Arctic conditions we use three-hourly ERA-interim radiative fluxes and precipitation to provide the surface conditions for SAMSIM. Nine simulations, each forced with ERA-interim reanalysis data taken from one of nine locations spread over the Arctic, are run from July 2005 till December 2009. The coordinates of the chosen locations from South to North are: 70° N & 0° W, 72°N & 155° E, 75° N & 180° E, 75° N & 0° E, 75° N & 145° W, 80° N & 0° E, 80° N & 90° E, 85° N & 180° E, and 90° N. A simulation period of 4.5 years was chosen because it enables four yearly cycles of growth and melt, which covers the age of most Arctic sea ice (Lietaer et al., 2011).

SAMSIM also requires oceanic boundary conditions in the form of ocean salinity and oceanic heat flux. Due to the scarcity of oceanic heat flux measurements and for simplicity's sake all runs share the same prescribed yearly heat-flux cycle, based loosely on the heat fluxes Huwald et al. (2005b) derived from the SHEBA measurements. Similarly, a standard ocean salinity of 34 g/kg is used for all runs. The model settings and parameters used are listed in table 3.1.

It is important to state that the boundary conditions we use are not necessarily a realistic approximation of the true conditions at the specific locations and time from which we chose the reanalysis data. Not only are the oceanic heat fluxes a strong approximation, the precision of the reanalysis data is limited by the lack of observations in the Arctic. Additionally, the influences of dynamic processes such as frazil formation, lead opening, melt ponds, and ice drift can not be accounted for in the 1-D SAMSIM model. Given the lack of melt pond formation and lead openings SAMSIM will tend to underestimate the amount of melt compared to reality.

3.4.2 Ice-core data

We begin analyzing the SAMSIM salinity evolution by comparing the output against salinity traits derived from ice-core measurements. Despite its drawbacks, taking ice

cores is by far the oldest and most wide spread method of measuring sea ice salinity. Gough et al. (2012) provide a thorough overview of statistical and physical sampling issues associated with ice-core salinity measurements. Due to the high horizontal heterogeneity of sea ice we will only use means over multiple ice-cores. It is to be expected that the core measurements underestimate the salinity near the ocean interface due to brine loss (Notz and Worster, 2008).

After over a century of sporadic measurement campaigns beginning with Nansen's Fram expedition, the observational record of Arctic sea-ice salinity is sparse in time and space and no comprehensive compilation of the conducted measurements has been published in the last decades (e.g. Weeks and Lee, 1958; Cox and Weeks, 1974; Nakawo and Sinha, 1981; Eicken et al., 1995). We do not attempt to provide a rigorous model versus field data comparison in this paper. Instead, we select three characteristic traits of sea-ice salinity to compare SAMSIM's results against. The three traits we compare against are the link between bulk salinity and ice thickness, the first-year salinity evolution from January to June, and the multi-year salinity profile.

3.4.2.1 Bulk salinity against thickness

The first trait we selected is the link between salinity and thickness which was studied by Cox and Weeks (1974) and Kovacs (1997). For the single growth season studied in Griewank and Notz (2013) the model results agreed well with the fit of Kovacs (1997) for first-year ice up to two meters.

We separate first-year from multi-year ice before comparing the bulk salinity against thickness (figure 3.9). A single simulation was singled out and highlighted allowing the reader to track the progress over 4 years as the first-year ice turns into multi-year ice and becomes less saline and thicker each further year. Both first-year and multi-year ice show a distinctly different behavior during growth and melt. The gradual transition from growth to melt is visible as a drop in bulk salinity at a constant thickness. A closer examination reveals that a slight thickness increase is visible in many simulations before ablation sets in. This bump in ice thickness arises from SAMSIM's definition of sea-ice which includes melting snow that has turned into slush (for details see subsection 3.2.2.1). That this little bump appears at the end of the downward drop signals that until then no flushing has occurred. From that we can conclude that gravity drainage is what causes the drop in salinity.

Ice thinner than 20 cm has a wide spread in bulk salinity caused by melting and flooding at the onset of the growth season. First-year ice thicker than 20 cm agrees well with the empirical results of Cox and Weeks (1974) and Kovacs (1997) during growth, although the model tends to have a higher salinity. This bias is especially high for ice thinner than 0.5 m, which may be partially due to the fact that the underestimation of bulk salinity due to brine loss is higher for thin cores. After melt sets in the bulk salinities are comparable to the estimates of Cox and Weeks (1974), which were based on a limited amount of cores which were at least a meter thick.

As expected multi-year sea ice shows a much smaller range of bulk salinities. During growth the bulk salinities show no coherent dependence on thickness, but during melt

there appears to be a linear dependence on thickness going from 1 g/kg at 0.5 m to 2 g/kg at 2.5 m. This is not far off from the estimation of Cox and Weeks (1974).

In conclusion, the thickness-salinity relationship of growing first-year ice agrees well with the empirical fits to measurements of both Cox and Weeks (1974) and Kovacs (1997). Although growing multi-year ice tends to be less salty when thicker, there is no uniform dependence on thickness. Both melting first-year and multi-year ice show a linear dependence of salinity on thickness. The transition from growing to melting ice leads to a loss in bulk salinity at a constant thickness which is caused by gravity drainage in the warming ice.

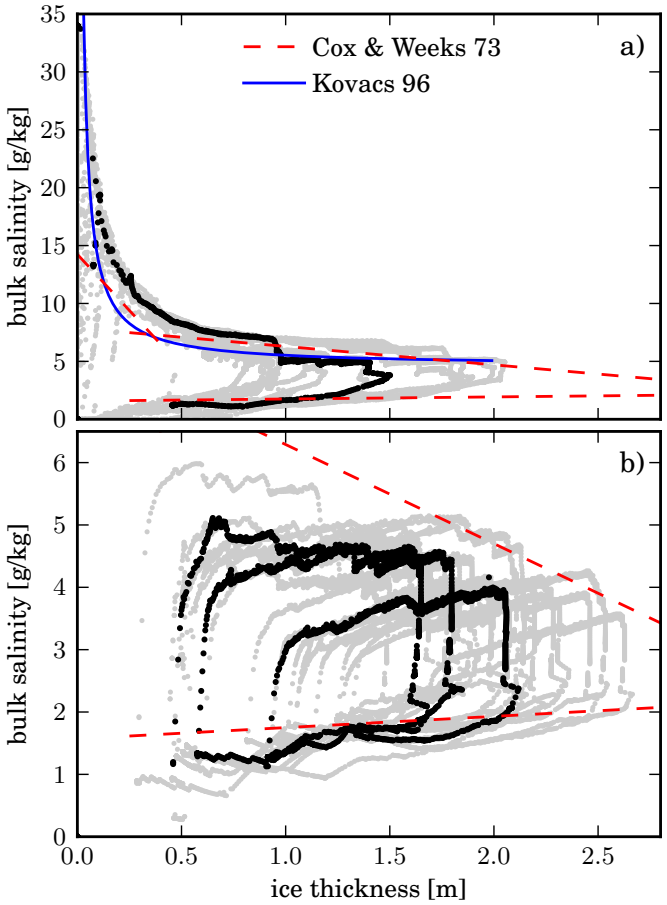

Figure 3.9: The vertically integrated vertical bulk salinity as a function of ice thickness for all reanalysis forced runs as described in 3.4.1. Each grey dot represents a 12-hourly snapshot. Subfigure a contains all 15 years of first-year ice and subfigure b contains all 21 years of multi-year ice in grey. Of all nine simulations a single simulation is plotted in black (80° N, 90° E) to enable tracking the evolution over time. The blue curve in subfigure a is the empirical relationship for first-year ice published by Kovacs (1997) for ice up to 2 meters. The red dashed lines mark the empirical linear relationships found by Cox and Weeks (1974) for growing (upper lines) and melting Arctic ice (lower line).

3.4.2.2 First-year salinity evolution

The second trait we evaluate with core data is the evolution of first-year ice salinity from January until June. A longer time frame was not possible due to data availability, but none the less the period allows us to study the salinity changes after gravity drainage is mostly restricted to the lower layers. We use the ice-core data taken as part of the Seasonal Ice Zone Observing Network and the Alaska Ocean Observing System by the sea-ice research group at the Geophysical Institute at the University of Fairbanks from 1999-2011 (Eicken et al., 2012). The great advantage of these measurements other than the shear number of cores taken is that by measuring repeatedly over a decade a large spread of conditions were captured. After rejecting all cores which did not include an ice thickness measurement or contained gaps in the salinity profile, a total of 86 first-year profiles remained between January and June.

The comparison of the model salinity against the Barrow cores is not ideal because SAMSIM is forced with conditions from throughout the Arctic while the cores where all taken close to the Alaskan coast as part of an ongoing effort to understand and alleviate the impact of changing sea-ice on the human settlements along the coast (Druckenmiller et al., 2009). However, as we will show in the following subsection on inter-annual salinity variability the salinity variations resulting from atmospheric conditions are strongest in the upper most 20 cm (subsection 3.4.4). Because of this, we believe that the comparison should work well for the rest of the ice.

To compare the core profiles against the model profiles both are first normalized to a depth of 0 to 1 before averaging over time. Often the salinity measurements did not extend all the way to the bottom of the ice, in which case the lowest measurement was extrapolated downwards. This extrapolation will contribute to the underestimation of salinity at the ice-ocean interface common to ice cores. We group the 86 core measurements into three bins of similar size based on the dates they were taken. The first bin spans from January to March (27 cores), the second from April to Mai (29 cores), and the final bin contains the remaining 29 cores taken in June.

As expected, even though the core profiles have a sharp increase of salinity at the ice-ocean interface they are still less saline at the ice-ocean boundary than SAMSIM (figure 3.10). In the upper 90 % SAMSIM and the Barrow cores never differ by more than 2 g/kg, which is in itself a mentionable model feat. Especially the June profiles share a very similar shape.

Other than the general agreement this comparison highlights some limitations of SAMSIM's complex salinity approach. One of these limitations is that flushing and snow melt by design lead to a zero salinity at the surface, which is clearly not present in the core data (figure 3.10). However, it is likely that core values at the surface would be lower if the sampling resolution were higher than the 2.5 to 5 cm used.

This total desalination at the surface is rooted in two of SAMSIM's design choices. The first design choice is that the snow layer in SAMSIM has zero salinity, and that melting snow forms slush which is treated as sea ice. Accordingly, when snow melts the top layer will consist of melted snow slush and be absolutely salt free. The second design choice which leads to zero salinity at the surface is the implementation of flushing in

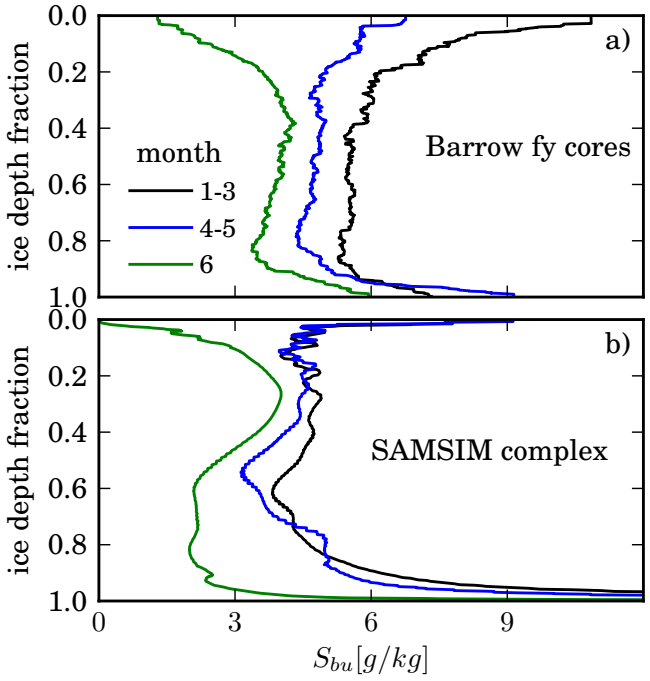

Figure 3.10: Time-averaged and vertically-normalized salinity profiles from first-year ice cores (described in subsection 3.4.2 and shown in subfigure a) and first year ice from reanalysis forced simulations using the complex brine dynamic parametrizations (subfigure b). Both were averaged from January to March (1-3), April to May (4-5), and over June (6).

SAMSIM. One of the core assumptions of the complex flushing parametrization is that the melt water leaving the top layer has a brine salinity determined by the liquidus relationship. Accordingly, as the brine salinity of the top layer is by definition always higher than the bulk salinity of the top layer, flushing always results in zero salinity at the surface over time as shown by the idealized flushing experiments (section 3.3).

The second distinct difference between model and core salinity is that SAMSIM has a high surface salinity with a very strong salinity gradient (figure 3.10 b). The sharp salinity gradient could be a numerical artifact arising from SAMSIM's semi-adaptive grid. The first centimeters of ice are formed when only few layers are active, which might be insufficient to parametrize gravity drainage. A different explanation is snow wicking, a process which transfers some of the surface salinity into the snow layer. In the model wicking only occurs when melt water forms in the top layer beneath snow.

The third discrepancy between the cores and SAMSIM is that the bulk salinity in the upper 40 % is higher in January-March. There are many possible explanations for this discrepancy, such as the non-ideal comparison itself, insufficient simulations or core measurements, and errors of the core salinity measurements. Another explanation is that the model is unable to simulate the salinity evolution correctly close to the surface during winter. A likely candidate to explain that the salinity remains constant near the surface is that the gravity drainage parametrization desalinates too quickly. The modeled salinity is quickly reduced to 5 g/kg after which it stabilizes, instead of a less strong initial desalination followed by a gradual desalination over time (figure

3.10). The discrepancy between model and data could also arise from the neglect of frazil or pancake ice formation in SAMSIM. It is also possible that the freeboard plays an important role, and that brine from above the waterline drains away by an unknown mixture of gravity drainage or flushing. The differences between the cores and SAMSIM as well as our poor understanding of what happens during flooding indicates that unknown yet relevant brine movements may occur at the ice-snow interface.

3.4.2.3 Multi-year salinity profile

The final and most well documented trait we selected to compare is the mean multi-year salinity profile. The most widely used multi-year profile in the sea-ice modelling community is based on 40 ice cores taken at the drifting ice station A in 1958 (Schwarzacher, 1959). Although later studies have incorporated additional measurements (e.g. Cox and Weeks, 1974; Eicken et al., 1995), the basic shape has remained similar. The fitted bulk salinity profile of Schwarzacher (1959) on a normalized vertical coordinate z from zero to one

$$S_{bu}(z) = 1.6(1 - \cos)(\pi z^{\frac{0.407}{0.573+z}}))$$

is used in the 1D models of Maykut and Untersteiner (1971) and Bitz and Lipscomb (1999). Although the fitted profile has a 3.2 g/kg salinity at the ice-ocean interface (figure 3.11), in the measurements an increase is clearly visible, similar to the salinity increase of the eight multi-year salinity cores taken at Barrow. Due to this ignored increase and the repeatedly mentioned salinity loss in cores we only compare against the upper 80 % the Schwarzacher profile.

We compare the mean of all normalized multi-year profiles, and find that in the upper 50 % of the ice the multi-year mean and the profile of Schwarzacher (1959) agree very well (figure 3.11 b). This indicates that the complex flushing parametrization predicts the desalination depth and strength reasonably correctly. Given that the complex flushing parametrization contains large parameter uncertainties and was developed without any data or underlying theory, this comparison to field data is the closest we can come to evaluating the flushing parametrization until controlled laboratory measurements are available. In the lower 50 % of the ice SAMSIM gradually becomes more and more saline, until the two profiles diverge in the lowest 20 %. How much of this is due to core sampling issues (location and season) or the previously mentioned loss of salt is unknown.

3.4.2.4 Summary

According to SAMSIM there is a clear link between ice thickness and bulk salinity in growing first-year ice as described by Kovacs (1997). However, after the ice stops growing, gravity drainage in the warming ice causes a thickness independent desalination. Both melting first-year and multi-year ice show an approximately linear dependence of bulk salinity on ice thickness as suggested by Cox and Weeks (1974). The mean multi-year salinity profile of SAMSIM agrees well with the core data of Schwarzacher (1959) and the evolution of salinity in first-year ice measured at Barrow is comparable

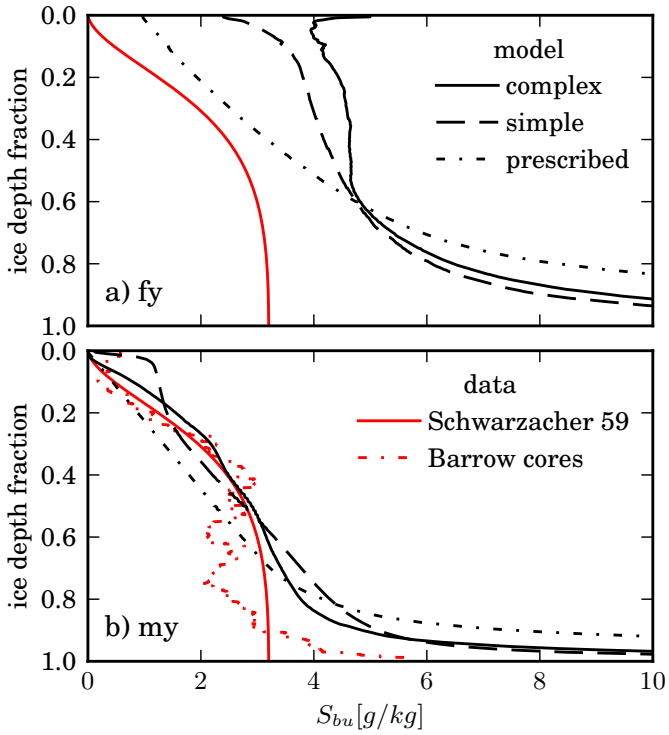

Figure 3.11: Yearly mean of vertically-normalized salinity profiles of reanalysis forced simulations using the complex brine dynamic parametrizations, the simple salinity parametrizations, and the prescribed SAMSIM salinity profile. Schwarzacher 59 refers to the fitted profile of Schwarzacher (1959). The simulations were split into first-year ice (subfigure a) and multi-year ice (subfigure b).

to model results (Eicken et al., 2012). However, the modeled salinity close to the ice surface in first-year ice desalinates faster than the Barrow core data, indicating that brine fluxes occur close to the surface which are poorly captured by the complex set of parametrizations.

All comparisons between SAMSIM and ice cores show that SAMSIM captures the general salinity evolution well, both qualitatively and quantitatively. Keep in mind that no tuning was used to reach these results and that all parametrizations were developed without any field data. Additionally, all parametrizations were developed separately, with no regard to possible interactions. From the comparison to ice cores we conclude that our parametrizations and understanding of desalination processes are sufficient to use SAMSIM as a valuable tool to study Arctic sea ice.

3.4.3 Mean salinity profile

In this subsection we analyze the mean salinity evolution of the complex approach. In total the model simulations yield 36 years of sea-ice growth and melt. Of those 36 years 21 years are multi-year ice and 15 are first-year ice. Of the 15 years of first-year ice 8 years end in open water while 7 form multi-year ice in the following year.

To process and visualize the salinity evolution we first normalize all salinity profiles of the model output between 0 and 1. This allows averaging over multiple normalized profiles and simplifies comparing profiles of varying thicknesses. To resolve the mean

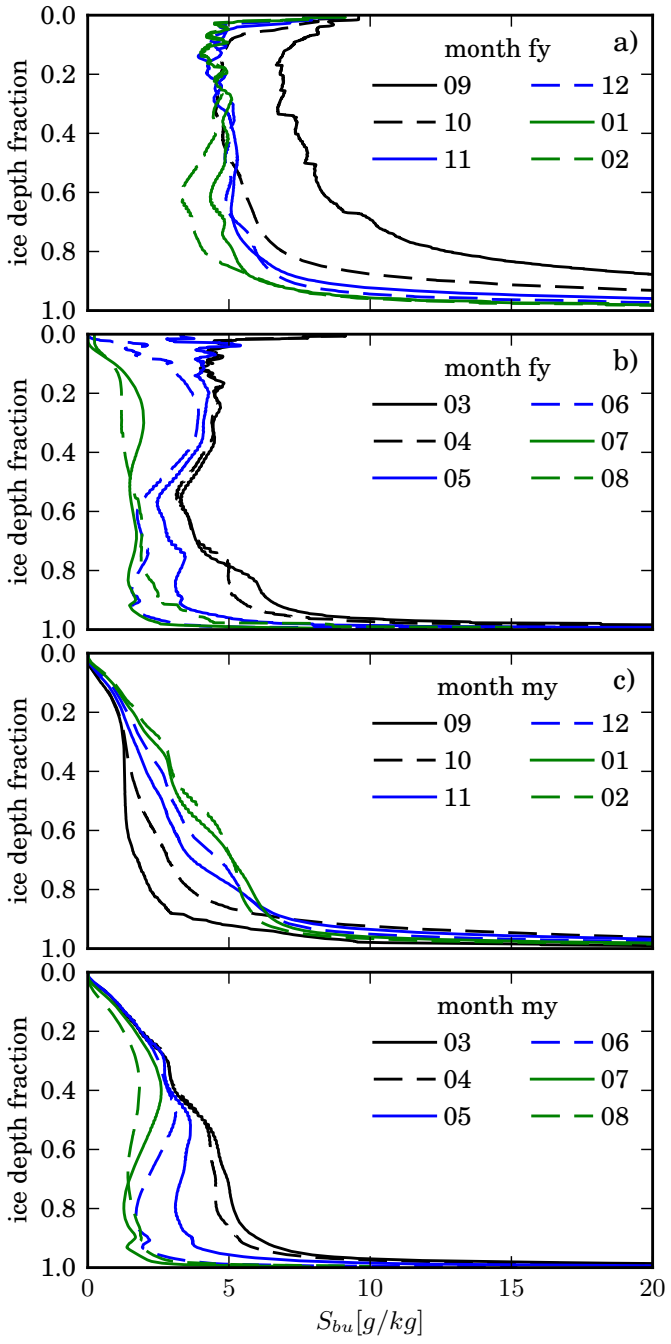

Figure 3.12: Monthly mean of vertically-normalized salinity profiles of reanalysis forced simulations using the complex brine dynamic parametrizations as described in subsection 3.4.1. The simulations were split into annual cycles beginning in September (month 9) and sorted into 15 years of first-year ice (subfigures a & b) and 21 years of multi-year ice (subfigures c and d). The corresponding ice thickness of the monthly means are shown in figure 3.13.

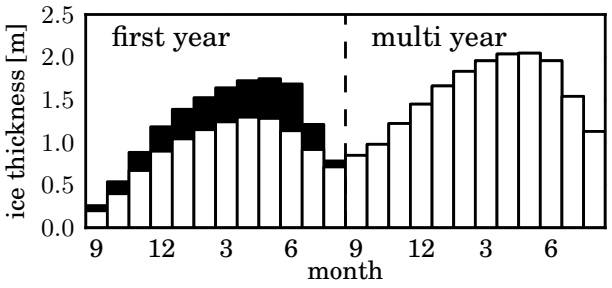

Figure 3.13: The white columns show he thickness of all monthly mean salinity profiles shown in figure 3.12. The black columns represent only first-year ice which evolves into multi-year ice the following year. To be included in the monthly average ice must be present, meaning that model output of ice-free water with an ice thickness of zero is excluded from the mean.

annual cycle we sort all first-year and multi-year profiles into monthly bins beginning in September, which we then average (figure 3.12). A side effect of this averaging approach is that when there is no ice in the model output this output does not affect the mean salinity profile. This is especially important for the August profiles of first-year ice when many of the first-year simulations are already ice free. As a consequence the mean August profile consists mostly of first-year ice which will turn into multi-year ice the following year. An advantage of this averaging effect is that there is a smooth transition from the August first-year profile to the September multi-year profile. The effect of this selection is clearly visible when comparing the mean ice thickness of all first-year simulations excluding ice free output against the mean thickness of first-year ice which turns into multi-year ice next September (figure 3.13).

During the growth season the salinity of the first-year ice decreases to 5 g/kg after about two months with a sharp increase to 10 g/kg in the upper 5 % of the ice thickness (figure 3.12 a). As the ice grows thicker the lower layers retain less salt, indicating that on average the lower growth speed of thicker ice does lead to a reduced amount of salt being retained as was proposed by Cox and Weeks (1975) and Wettlaufer et al. (1997). In contrast, in our previous study using the same parametrization of gravity drainage this behaviour of retaining less salt at slower growth speeds was only present in idealized experiments but not in the single growth season studied (Griewank and Notz, 2013).

The salinity profile remains pretty stable between February and April, followed by a slight desalination in May at the onset of melt. The desalination accelerates during June and July until the lowest 80 % of the ice have an almost uniform salinity of approximately 2 g/kg (subfigure 3.12 b). The influence of flushing is clearly visible by the total loss of salt at the surface from June onwards. Given that the maximal salinity occurs between an ice-depth fraction of 0.2 and 0.4, the desalination caused by flushing in the model occurs mostly in the top third of the ice. Although there is little indirect experimental evidence of gravity drainage occurring as the ice warms (e.g Widell et al., 2006; Jardon et al., 2013) the salinity reduction in the lower half of the ice from April to June shows that gravity drainage is active in SAMSIM during the onset of melt. This desalination is consistent with results from idealized experiments we conducted

that show a reduction of bulk salinity from above 5 g/kg to below 3 g/kg from gravity drainage when sea-ice begins to warm (Griewank and Notz, 2013).

At the end of the melt season the multi-year ice salinity is lowest. While the surface salinity remains low the newly formed ice at the bottom retains up to 5 g/kg. During the melt season the lower half of the ice is desalinated by gravity drainage while flushing maintains the low surface salinity. That this desalination is not only due to the loss of the saltier lower layers through melt is visible in the curve that develops in the lower half of the normalized profile. With the exception of the gravity drainage during melt the overall multi-year salinity agrees well with expectations already voiced by Cox and Weeks (1974).

For readers interested in analytical approximations of the mean first-year and multi-year profile as shown in figure 3.11 we chose two functions $S_{bu,fy}(z)$ and $S_{bu,my}(z)$. Both are a function of the normalized ice depth $0 \leq z \leq 1$ and are shown in figure 3.14. The fitted first-year ice profile is

$$S_{bu,fy}(z) = a + \frac{b}{(b-z)^2}$$

for $a = 4.17$, $b = 0.170$, $c = 1.08$ and the fitted multi-year ice profile is

$$S_{bu,my}(z) = a(1 - e^{bz}) + c(1 - e^{dx})$$

with $a = -1.284 \cdot 10^{-17}$, $b = 42.07$, $c = 5.411$, $d = -15.56$.

The transition from first-year to multi-year ice over the melt season can be approximated by a time dependent combination of the two profiles, in the form

$$S_{bu}(z,t) = (1-t) \cdot S_{bu,my}(z) + t \cdot S_{bu,my}(z)$$

for $t = 0$ at the beginning of the melt season in June and $t = 1$ at the onset of growth in September.

3.4.4 Variability

While the last subsection studied the mean salinity properties, in this subsection we will take a brief look at the salinity variability in SAMSIM using the complex approach. The model variability arises from two sources, the main one being the atmospheric forcing. Although the location at which the reanalysis data was selected has the largest impact, interannual variability ensures that all 36 years of simulated sea ice have a unique forcing. The second source for variability is the initial ice conditions at the beginning of the growth season. This second source only applies to the 21 years of multi-year ice, since all first-year ice grows from ice-free water. The variance of the model can not be directly compared to ice-core variability, because the variability in ice cores additionally contains a large amount of variability due to small scale horizontal heterogeneity (Gough et al., 2012).

To visualize the variability we have plotted all normalized salinity profiles at two dates in time, as well as the mean over all profiles at that time point in figure 3.15. With few

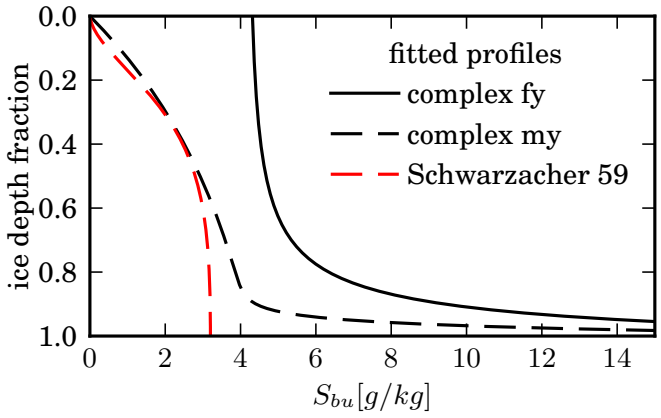

Figure 3.14: Fitted salinity profiles to the yearly mean complex first-year and multi-year sea-ice profiles as shown in figure 3.11. The profile of Schwarzacher (1959) is included as a reference. The fitted functions are listed in subsection 3.4.3.

exceptions the first-year ice only deviates a few g/kg from the mean in the lowest 80 % of the ice. However, at the surface the spread is much higher, with values reaching from 0 to above 10 g/kg (see figures 3.15 a & b). There are two main reasons for the higher variability at the surface. The first is that after 10 to 20 cm of ice has formed, the variability of the atmospheric forcing is severely dampened before it reaches the ice-ocean interface. As a result, the ice formed after the initial 10-20 cm grows under roughly similar conditions in all simulations. The second reason is that flooding and flushing both occur mainly at the surface of the ice. That such a similar high variability near the surface is not visible in the multi-year ice is because both processes are far less likely to occur in multi-year ice during the winter than in first-year ice. Farther south where first-year ice seldom survives the melt season, rainfall and above-freezing surface temperatures occur during the growth season, both of which can cause flushing. As the first-year ice is less thick, strong snow fall which slows ice growth can lead to flooding more easily than in multi-year ice.

As all multi-year ice has experienced at least one melt season, it is not surprising that multi-year simulations have a salinity of zero at the surface (figure 3.15 c and d). That all 21 years have zero surface salinity shows that flooding of multi-year ice does not occur in any of the simulations. Most of the variability in multi-year ice arises from the different ice thickness and salinity of the ice at the end of the melt season. The spikes visible in roughly 5 simulations between 0.4 and 0.6 in the November profiles arise from sudden quick growth in the beginning of the growth season beneath comparably fresh ice (figure 3.15 c). This growth can be quicker than in first-year ice of similar thickness due to the following reasons. The first reason is that by the time first-year ice reaches the same thickness, it has likely accumulated an insulating snow layer which slows ice growth. Secondly, the fresher multi-year ice has a higher thermal conductivity and lower thermal capacity which enhances heat transport from the ice-ocean interface to the ice-atmosphere boundary.

Over the next half year the profiles are smoothed out and the salinity sinks to 5 g/kg

or lower except in the lowest 10 percent (subfigure 3.15 d). Visible in both first-year ice and multi-year ice is that the salinity in the lowest layers is higher in November when ice growth is stronger than in April.

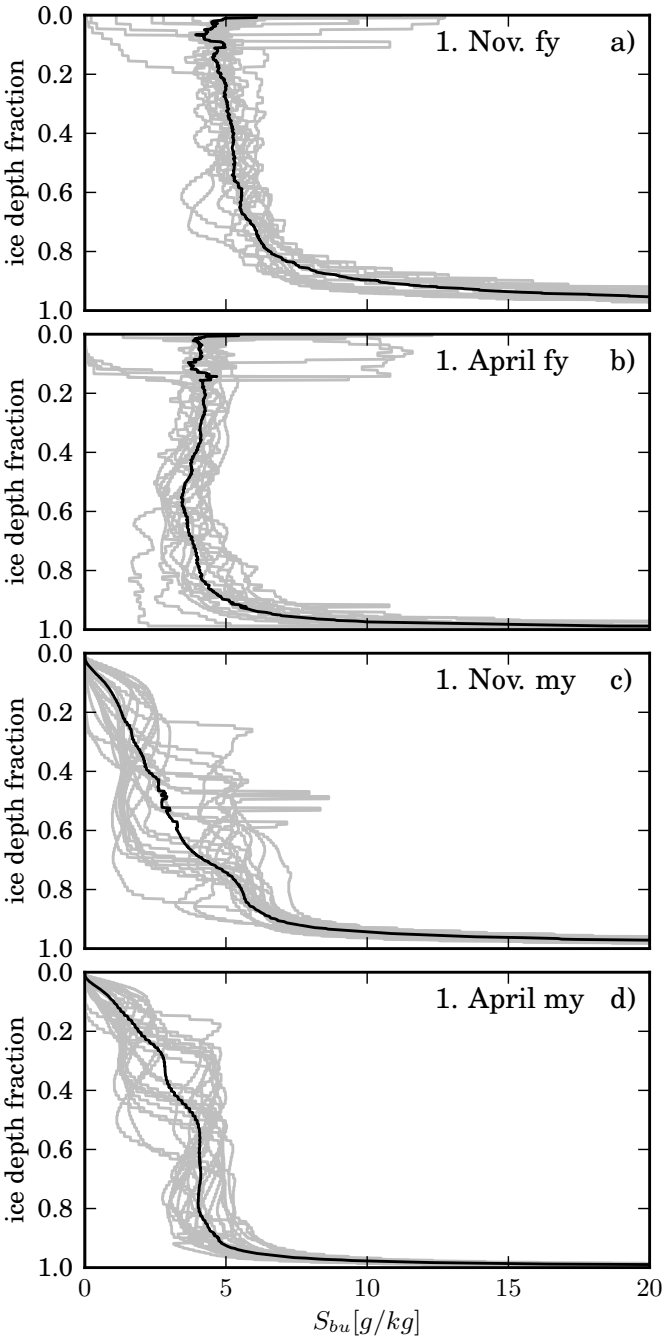

Figure 3.15: Vertically-normalized salinity profiles of the reanalysis forced simulations (described in subsection 3.4.1) using the complex salinity parametrizations at the first of November (subfigures a & c) and the first of April (b and d). First-year ice (subfigures a & b) and multi-year ice (subfigures c & d) are shown separately. The grey lines are the individual model realizations and the black line is the average over all profiles.

In conclusion, the variability in first-year ice is strongest at the surface and arises from the atmospheric forcing, while the variability in multi-year ice is mostly due to the thickness of the ice at the beginning of the growth season. A third possible source of variance is the variation in the oceanic heat flux. This is not included in this study as all simulations share the same prescribed annual cycle of oceanic heat flux.

3.4.5 Simple and prescribed salinity approach

As both the simple and prescribed approach are relevant in the following chapter, we briefly compare the mean first-year and multi-year profile of all approaches. The mean first-year profiles of the three approaches differ far more than the mean multi-year profiles (figure 3.11 a). The simple approach has a lower first-year salinity than the complex run in the upper ice half, and has a slightly higher salinity in the upper 20 % and in-between the depth fraction of 0.6 and 0.8 for multi-year ice (figure 3.11 a). The prescribed approach is lower in the upper half and more saline in the lower 20-30 % of the ice in comparison to the other approaches in both first-year and multi-year ice.

3.5 Impact of parametrizing salinity

While the previous section focused on the salinity evolution and the processes which drive it, this section aims to quantify how parametrizing salinity affects sea-ice properties relevant to the climate system. We address this question, which is highly relevant to modellers seeking to improve climate models, by using the same runs used in the previous section (see subsection 3.4.1).

To asses the total impact of parametrizing salinity in a climate model it is not sufficient to quantify the impact on the sea ice itself. It is also necessary to determine resulting feedbacks with the ocean and atmosphere. So far the only coupled model featuring a partially parametrized salinity is the NEMO-LIM model which uses a prescribed atmospheric forcing. Using the NEMO-LIM model Vancoppenolle et al. (2009) found that the large-scale sea-ice mass balance and the upper ocean characteristics are quite sensitive to sea-ice salinity. Salinity variations introduced to NEMO-LIM increased sea ice volume by up to 28 % in the Southern Hemisphere because changes to the ice-ocean interactions stabilized the ocean leading to a reduced oceanic heat flux. In the Arctic the ocean stratification was not influenced by the implemented sea-ice variations, but Vancoppenolle et al. (2009) discovered increases in ice thickness of up to a meter due to changes of the sea-ice thermal properties.

From Vancoppenolle et al. (2009) we conclude that in the Arctic the oceanic feedbacks will be small owing to the stable stratification of the Arctic Ocean. Although the atmospheric feedbacks remains unknown, we can use SAMSIM's more advanced salinity parametrizations with a much higher spatial and temporal resolution to take a more detailed look than Vancoppenolle et al. (2009) at how the salinity evolution affects the sea ice.

A further piece of information needed to weigh introducing salinity parametrizations into a coupled model is the resulting increase in computational cost. As there are almost

unlimited options where to invest additional computational resources (e.g. increasing spatial resolution, more ice thickness categories per grid cell, more complex radiation schemes) it would be ideal to give an estimation of the computational increase along with the estimated improvement so modelers can gauge where to invest free resources most efficiently. A brief description of the numerical costs associated with the salinity approaches can be found in subsection 3.2.4.

To quantify the impact of parametrizing salinity we compare quantities of the nine reanalysis forced simulations using the three salinity approaches introduced in subsection 3.2.4. The specific quantities we use based on their importance for the climate system are the same four used in Griewank and Notz (2013). These are the ice thickness, the freshwater column stored in the ice and snow, the thermal resistance R_{th}, and the total enthalpy H integrated over the whole ice and snow column. Each of the nine runs is evaluated separately over the full 4.5 simulation years to ensure that opposing biases at different locations do not average out.

The metrics we use to compare the time dependent quantities against each other are a time integrated ratio and a time integrated, weighted absolute difference. The ratio r of the quantity $x_i(t)$ using the salinity approach i against the same quantity using the different salinity approach $x_j(t)$ over the simulated 4.5 years is calculated as

$$r = \frac{\int_{t=0}^{t=4.5\ a} x_i(t)\ dt}{\int_{t=0}^{t=4.5\ a} x_j(t)\ dt}.$$

The second metric used, the weighted absolute difference d, is determined by

$$d = \frac{\int_{t=0}^{t=4.5\ a} x_i(t) - x_j(t)\ dt}{\int_{t=0}^{t=4.5\ a} x_j(t)\ dt}$$

and is a measure of how large the differences between the two quantities at each time step compared to the total value of the second quantity. The ratio is chosen to indicate if and by how much x_i is greater or smaller than x_j over time, while the absolute difference is chosen to detect compensating errors not apparent in the ratio.

We quantify the impact by comparing the simple and prescribed approach against the complex approach. Although our data comparisons show that the complex salinity approach provides a more realistic estimation of the salinity evolution than the simple and prescribed, which approach provides the most realistic salinity evolution is of no consequence to the determined impact.

The computed ratios for each simulation reveal that the prescribed approach with few exceptions leads to a lower ice thickness, freshwater column, thermal resistance, and total enthalpy than the complex approach (figure 3.16). Ratios range from 0.90 to 1.05, with enthalpy having the largest spread. The mean over all ratios and quantities of the prescribed approach is 0.971, accordingly the quantities of the complex approach are approximately 3 % higher on average. The ratios of the simple approach have a slightly lower spread and are on average higher with a mean of 1.017.

The absolute differences paint a similar picture, with the prescribed approach having a slightly larger spread with differences up to 11 % (figure 3.17). On average the simple

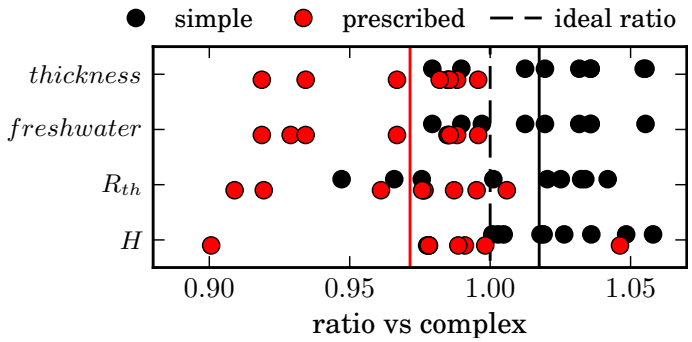

Figure 3.16: Ratios of the time integrated ice thickness, freshwater column, thermal resistance R_{th}, and enthalpy H of the simple and the prescribed SAMSIM salinity approach compared against the complex approach (details in section 3.5). The ratios were calculated separately for each of the nine reanalysis forced simulations over 4.5 years. Each dot shows the ratio of a specific simulation, while the lines show the mean over all runs and quantities.

approach has slightly lower differences with a mean of 3.6 % in comparison to the prescribed mean of 4.3 %. Because the absolute differences are only slightly larger than the ratios, we can deduce that most of the discrepancy between two simulations is in one direction.

Given that the prescribed approach does not distinguish growing from melting ice and that the prescribed profile was not optimized or tuned in any way, the prescribed approach is unexpectedly close to the complex approach. We also expected the prescribed approach to have a wider spread when compared to the complex approach, because the prescribed approach treats all ice the same regardless of its history while the complex approach is dependent on previous conditions.

From our results we conclude that the possible improvements achievable by fully parametrizing salinity in the Arctic are not worth the numerical costs, especially because the impact of parametrizing salinity will be smaller when fewer layers are used. Instead we recommend using either a prescribed profile or a hybrid approach. The salinity approach used by Vancoppenolle et al. (2009) is such a hybrid, in which the total bulk salinity of the whole column is parametrized and the salinity profile is prescribed based on the bulk salinity. Prescribed profiles can also be thickness, time, or even location dependent. If a model can distinguish first-year and multi-year ice this information could also be used to prescribe the salinity.

3.6 Summary and conclusions

We have incorporated surface melt, flooding, and flushing into SAMSIM. In contrast to the thermodynamic models derived from Maykut and Untersteiner (1971), such as Bitz and Lipscomb (1999) and Huwald et al. (2005a), surface melt in SAMSIM is implemented as a two stage process. The first stage is the conversion of snow to slush followed by the second stage of surface ablation by melt water runoff. All desalination

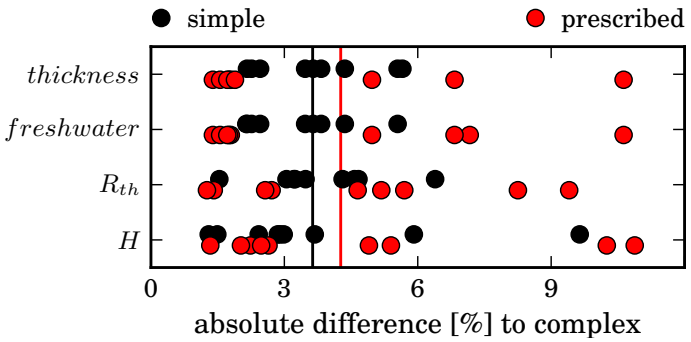

Figure 3.17: Time integrated absolute differences of the ice thickness, freshwater column, thermal resistance R_{th}, and enthalpy H of simulations using the simple and prescribed SAMSIM salinity approach compared against simulations using the complex approach (details in section 3.5). The absolute differences were calculated separately for each of the nine reanalysis forced simulations over 4.5 years. Each dot shows the ratio of a specific simulation, while the lines show the mean over all runs and quantities.

processes are parametrized twice in SAMSIM. The *complex* parametrizations calculate brine fluxes and are physically consistent, while the *simple* parametrizations attempt to imitate the effects of the complex parametrizations with less numerical overhead.

SAMSIM is the only 1D thermodynamic sea-ice model other than the 1D LIM model of Vancoppenolle et al. (2007) which has a fully prognostic salinity. In contrast to the flushing parametrization of Vancoppenolle et al. (2007), the complex flushing parametrization of SAMSIM explicitly includes both horizontal and vertical brine movements. A detailed discussion of why the complex gravity drainage parametrization of SAMSIM agrees better than the gravity drainage of LIM 1D with both theoretical and numerical expectations is included in Griewank and Notz (2013). The complex flooding parametrization based on the results of Maksym and Jeffries (2000) is an ad hoc solution as the current understanding of flooding is insufficient to develop a more realistic parametrization. Nevertheless, SAMSIM is the first 1D model to include flooding as well as flushing and gravity drainage, and the flooding parametrization does capture the basics of flooding and forms snow ice with reasonably salinities in a physically consistent manner.

Under idealized conditions, the complex flushing parametrization leads to oscillations of the salinity profile close to the surface. If gravity drainage is deactivated flushing also leads to a strong increase of salinity close to the ice-ocean interface. Although we do not have data available to determine optimal values of the ratio of vertical to horizontal hydraulic resistance β and the melt solid fraction $\phi_{s,melt}$, sensitivity experiments show that the flushing parametrization is only weakly sensitive to changes close to the default values. At higher vertical resolution the flushing onset occurs sooner and the salinity oscillations have a higher frequency.

No idealized study of the flooding parametrization is shown due to the ad hoc nature of the parametrization and the lesser importance of flooding compared to flushing in the Arctic.

We study the salinity evolution of Arctic sea ice using 36 years of SAMSIM output. To imitate Arctic conditions we force SAMSIM with ERA-interim reanalysis precipitation and radiation fluxes from throughout the Arctic. The 36 years are separated into 16 years of first-year and 21 years of multi-year sea-ice and then compared against ice-core data. The mean multi-year salinity profile of Schwarzacher (1959) and the salinity evolution of first-year ice cores from Barrow Alaska agree well with SAMSIM. However, while the first-year ice-core salinity at the surface decreases from January to May, the modelled salinity at the surface remains constant until the onset of melt. This discrepancy indicates that brine fluxes close to the ice-snow boundary are captured poorly by SAMSIM. Possible reasons for this discrepancy are discussed in detail in subsection 3.4.2.2.

We deduce from the 36 years of simulated sea-ice that ice thickness is a good indicator of bulk salinity for growing first-year ice. The model results agree well with the empirical results of Cox and Weeks (1974) and Kovacs (1997). That the modeled bulk salinities of thin ice are higher than the ice-core data is at least partially due to the fact that brine loss during coring is especially high from thin and more saline ice. The transition from growth to melt is accompanied by a 1.5-4 g/kg reduction of bulk salinity caused by gravity drainage before the onset of flushing. This onset of gravity drainage as the ice warms is consistent with earlier findings by Griewank and Notz (2013) and Jardon et al. (2013). The onset contradicts the general melt evolution depicted by Eicken et al. (2002) in which gravity drainage sets in at the end of the melt season. In general thicker multi-year ice tends to be fresher, but during growth the bulk salinity increases with thickness. During melt both multi-year and first-year ice have a linear relationship of bulk salinity and thickness as Cox and Weeks (1974) hypothesized on a limited set of cores, but the slope of the linear relationship in the model is steeper than that proposed by Cox and Weeks (1974).

Our results show the largest inter-annual variations of salinity occur at the surface of first-year ice and are caused by rain, surface melt, and flooding. In contrast, the lower 80 % of the salinity profile of first-year ice are similar to each other, despite being forced with reanalysis data taken from different locations. The multi-year ice profiles vary depending on the ice thickness at the onset of growth and become more similar over the growth season. First-year and multi-year ice profiles can be approximated using the mean normalized profiles shown in figure 3.14, and a smooth transition of first-year to multi-year ice can be achieved by linearly transitioning from the first-year to the multi-year profile as shown in subsection 3.4.3.

We compare the ice thickness, freshwater column, thermal resistance, and total stored energy of the nine 4.5 year long simulations of Arctic sea-ice using the three different salinity approaches against each other. Although certain quantities differ by up to 10 % for a specific simulation, on average the differences between the complex salinity approach and the others are below 5 %. The simple approach is slightly closer to the complex approach than the prescribed approach, but only by 1 %. We conclude that fully parametrizing the temporal sea-ice salinity evolution in the Arctic for climate models is not worth the computational cost. Instead, we recommend using a parametrized-prescribed hybrid such as that proposed by Vancoppenolle et al. (2009). The most crucial aspect of a parametrized-prescribed hybrid is the ability to distin-

guishing multi-year from first-year ice. This can be done by tracking the bulk salinity of the whole ice column as Vancoppenolle et al. (2009) did, or by tracking the ice age in some fashion (e.g. Lietaer et al., 2011). Once the model is able to distinguish first-year from multi-year ice, empirical profiles of first-year and multi-year, such as the mean normalized profiles shown in figure 3.14 or the multi-year profile of Schwarzacher (1959), can be prescribed. A smooth transition from first-year to multi-year ice can be achieved by linearly transitioning from the first-year to the multi-year profile as discussed in subsection 3.4.3. Further temporal refinement can be achieved by taking the annual cycle into account (figure 3.12).

Comparisons to laboratory and field salinity measurements have shown that the parametrized brine fluxes in SAMSIM are a reasonable approximation of reality. SAMSIM's semi-adaptive grid is convenient when studying processes which occur close to the ice-atmosphere or ice-ocean boundary, as it avoids numerical diffusion through layer advection in the surface and bottom layers. All dissolved tracers in brine can be easily advected similar to salt, and the gas volume fraction in each layer can be used to compute outgassing and uptake. Thanks to these properties SAMSIM is a valuable tool to study small-scale thermodynamic and biogeochemical aspects of sea ice.

Chapter 4

Final conclusions

4.1 Answers to key research questions

How and with which precision can brine fluxes be parametrized in a 1D sea-ice model?

I have successfully parametrized **gravity drainage** to such a degree that when simulating the laboratory experiments of Notz (2005) I can not distinguish model errors from measurement uncertainty. From this I conclude that I can reproduce gravity drainage when it occurs close to the ice-ocean interface with a high degree of precision and better than other parametrizations from the literature. From the good agreement between modeled and measured bulk salinity against ice thickness I know that the complex gravity drainage parametrization also predicts the depth of gravity drainage reasonably well. No measurements are available that can confirm if gravity drainage also occurs deep in the ice as the parametrization predicts.

My **flushing** parametrization produces multi-year salinity profiles which agree with field measurements and also explicitly computes horizontal brine fluxes which are high close to the ice-ocean surface as expected. The ratio of horizontal to vertical flushing tends to oscillate over time, which is physically plausible for a specific location but undesirable in a 1D model which attempts to provide a representative profile for a large horizontal area. More detailed laboratory and field measurements are needed to understand flushing better and to tune and evaluate my parametrization. The high horizontal variability and inherent instability of melting ice indicate that a 1D model will never be able to parametrize flushing with the same precision as gravity drainage.

Flooding is currently too poorly understood and observed to develop a high quality parametrization or evaluate the current parametrization included in SAMSIM. Until we have a better picture of how brine moves at the ice-snow boundary, I must rely on guesswork and ad hoc approximations. Despite the limitations, the flooding scheme I implemented does capture the basics of flooding and forms snow ice with reasonably salinities in a physically consistent manner.

In conclusion, I have succeeded to parametrize the brine fluxes in accordance with the current understanding of the underlying processes. Although brine movements

at the snow-ice interface are only poorly understood, the current parametrizations enable highly detailed and physically consistent studies of sea-ice thermodynamics and biogeochemical processes.

When and how do brine movements occur in sea ice, and how does sea-ice salinity evolve over time as a result?

I find that the depth of gravity drainage varies during growth as a reaction to surface temperature, and can even span the full ice depth (section 2.6). This full depth desalination indicates that gravity drainage can replenish the whole ice column with nutrients from the ocean. I also find that gravity drainage is active during the transition from growth to melt, and that the amount of desalination caused by gravity drainage in warming ice is comparable to that caused by flushing (figure 3.12). It is also clearly visible in the normalized profiles that flushing only desalinates the upper ice while the lower half is desalinated by gravity drainage.

From the model output I conclude that the inter-annual salinity variability of first-year ice is highest in the top 20 % and is caused by raining, flooding, and flushing on thin ice (subsection 3.4.4). The lower 80 % of ice grow under similar conditions, and gravity drainage leads to similar salinity profiles with a low inter-annual variability. The salinity profile of the lower 80 % can be approximated using the mean normalized profile I introduced in subsection 3.4.3. All multi-year ice have zero salinity at the surface and 5 [g/kg] bulk salinity close to the ice-ocean interface (figure 3.15). The highest inter-annual salinity variability is in the middle of the ice shortly after the onset of growth. This variability arises from the different ice states at the end of the growth season. The multi-year salinity profile can be reasonably well approximated through the empirical mean I provide in subsection 3.4.3.

The model shows a clear relationship of ice thickness to bulk salinity for growing sea ice which agrees well with the empirical results of Cox and Weeks (1974) and Kovacs (1997) (figure 3.9). The relationship between bulk salinity and thickness breaks down when the ice warms at the end of growth season. Gravity drainage reduces the bulk salinity of the warming ice by 1.5-4 g/kg while the thickness remains constant. In general thicker multi-year ice tends to be fresher, but during growth the bulk salinity increases with thickness. During melt both multi-year and first-year ice have a linear relationship of bulk salinity and thickness as Cox and Weeks (1974) hypothesized on a limited set of cores, but the slope of the linear relationship in the model is steeper than that proposed by Cox and Weeks (1974).

How much could climate models benefit from fully parametrizing salinity, and which salinity approach provides the best improvement at a reasonable computational cost?

My results from multi-year simulations show that under Arctic conditions parametrizing or prescribing the salinity in SAMSIM leads to differences smaller than 5% on average. For specific simulations certain quantities differ by up to approximately 10 %. Given the large uncertainties in the model representations of sea-ice dynamics, sub-grid scale representation, lead formation, snow thermal conductivity, and snow distribution, I do not recommend large-scale models attempt to fully parametrize the temporal evolution of sea-ice salinity. Instead I recommend either prescribing a sea-ice salinity profile based on age and season or using a prescribed-parametrized hybrid

which combines a prescribed profile with a parametrized bulk salinity. As discussed in the previous paragraph, the ice thickness is a poor proxy for bulk salinity outside of the melt season. The most crucial aspect of a prescribed-parametrized hybrid is the ability to distinguishing multi-year from first-year ice. This can be done by tracking the bulk salinity of the whole ice column as Vancoppenolle et al. (2009) did, or by tracking the ice age in some fashion. Once the model is able to distinguish first-year from multi-year ice, further refinement can be achieved by taking the annual cycle into account.

4.2 Outlook

As the salinity parametrizations are currently limited by lack of understanding and data, they can not be improved or refined until more measurements or theoretical insight become available. The wire harp instrument first used by Notz (2005) has been revised recently and will hopefully soon provide non-invasive time series of salinity profiles from both field campaigns and laboratory studies of melting sea ice. Researchers have also managed to take optical measurements of chemical sea-ice properties (e.g. Rysgaard et al., 2008), which could in future be used to take 2D measurements of salinity.

Researchers are currently seeking to quantify chemical and biological processes in the ice to reproduce and understand field and laboratory measurements, and to determine which processes are relevant over large time and length scales. SAMSIM is well suited for these tasks as it currently provides the most accurate estimation available of brine movements in sea ice. The semi-adaptive grid is helpful when studying processes at the ice surface and close to the ice-ocean interface, as no numerical diffusion through layer advection occurs in the surface and bottom layers. An additional advantage of SAMSIM is that in contrast to all other 1D sea-ice models the gas volume fraction is treated explicitly, which enables calculating the amount of outgassing and uptake needed to achieve pressure equilibrium. Thanks to all these attributes SAMSIM is a valuable tool to study the small-scale biogeochemical and thermodynamic aspects of sea ice.

List of Figures

List of Tables

Bibliography

Bitz, C. M. and W. H. Lipscomb, 1999: An energy-conserving thermodynamic model of sea ice. *J. Geophys. Res.*, **104 (C7)**, 15 669–15 677, doi:10.1029/1999JC900100.

Büttner, J., 2011: Permeability of young sea ice from microtomographic images. M.S. thesis, Geophysical Institute, University of Bergen, Bergen, Norway.

Carsey, F. D., 1992: *Microwave remote sensing of sea ice*, Vol. 68. American Geophysical Union.

Chen, C. F., 1995: Experimental study of convection in a mushy layer during directional solidification. *J. Fluid Mech.*, **293**, 81–98, doi:10.1017/S0022112095001649.

Chiareli, A. and M. Worster, 1995: Flow focusing instability in a solidifying mushy layer. *J. Fluid Mech.*, **297**, 293–305, doi:10.1017/S0022112095003107.

Cole, D. M. and L. H. Shapiro, 1998: Observations of brine drainage networks and microstructure of first-year sea ice. *J. Geophys. Res.*, **103 (C10)**, 21 739–21 750.

Coleou, C. and B. Lesaffre, 1998: Irreducible water saturation in snow: experimental results in a cold laboratory. *Ann. Glaciol.*, **26**, 64–68.

Cottier, F., H. Eicken, and P. Wadhams, 1999: Linkages between salinity and brine channel distribution in young sea ice. *J. Geophys. Res.*, **104 (C7)**, 15 859–15 871, doi:10.1029/1999JC900128.

Cox, G. and W. Weeks, 1975: Brine drainage and initial salt entrapment in sodium chloride ice. Tech. rep., DTIC Document.

Cox, G. F. and W. F. Weeks, 1974: Salinity variations in sea ice. *J. Glaciol.*, **13**, 109–120.

Cox, G. F. N. and W. F. Weeks, 1988: Numerical simulations of the profile properties of undeformed first-year sea ice during the growth season. *J. Geophys. Res.*, **93 (C10)**, 12 449–12 460, doi:10.1029/JC093iC10p12449.

Druckenmiller, M. L., H. Eicken, M. A. Johnson, D. J. Pringle, and C. C. Williams, 2009: Toward an integrated coastal sea-ice observatory: System components and a case study at barrow, alaska. *Cold Reg. Sci. Technol.*, **56 (2)**, 61–72.

Eicken, H., R. Gradinger, M. Kaufman, and C. Petrich, 2012: Sea-ice core measurements (sizonet). *UCAR/NCAR CISL ACADIS*, doi:http://dx.doi.org/10.5065/D63X84KG.

Eicken, H., H. Krouse, D. Kadko, and D. Perovich, 2002: Tracer studies of pathways and rates of meltwater transport through arctic summer sea ice. *J. Geophys. Res.*, **107 (C10)**, 8046.

Eicken, H., M. Lensu, M. Lepparanta, W. B. Tucker, A. J. Gow, and O. Salmela, 1995: Thickness, structure, and properties of level multiyear ice in the eurasian sector of the arctic-ocean. *J. Geophys. Res.*, **100 (C11)**, 22 697–22 710, doi:10.1029/95JC02188.

Feltham, D. L., N. Untersteiner, J. S. Wettlaufer, and M. G. Worster, 2006: Sea ice is a mushy layer. *Geophys. Res. Lett.*, **33 (14)**, L14 501, doi:10.1029/2006GL026290.

Flocco, D. and D. L. Feltham, 2007: A continuum model of melt pond evolution on arctic sea ice. *Journal of Geophysical Research: Oceans*, **112 (C8)**, doi:10.1029/2006JC003836, URL `http://dx.doi.org/10.1029/2006JC003836`.

Freitag, J., 1999: The hydraulic properties of arctic sea ice - implications for the small scale particle transport (in german). *Berichte zur Polarforschung, Alfred-Wegener Institut f r Polar- und Meeresforschung, Bremerhaven.*, **325**.

Fritsen, C. H., V. I. Lytle, S. F. Ackley, and C. W. Sullivan, 1994: Autumn bloom of antarctic pack-ice algae. *Science*, **266 (5186)**, 782–784.

Golden, K., S. Ackley, and V. Lytle, 1998: The percolation phase transition in sea ice. *Science*, **282 (5397)**, 2238–2241.

Golden, K. M., H. Eicken, A. L. Heaton, J. Miner, D. J. Pringle, and J. Zhu, 2007: Thermal evolution of permeability and microstructure in sea ice. *Geophys. Res. Lett.*, **34 (16)**, L16 501, doi:10.1029/2007GL030447.

Gough, A. J., A. R. Mahoney, P. J. Langhorne, M. J. M. Williams, and T. G. Haskell, 2012: Sea ice salinity and structure: A winter time series of salinity and its distribution. *J. Geophys. Res.*, **117 (C3)**, C03 008.

Griewank, P. J. and D. Notz, 2013: Insights into brine dynamics and sea ice desalination from a 1-d model study of gravity drainage. *J. Geophys. Res.*, **118 (7)**, 3370–3386, doi: 10.1002/jgrc.20247, URL `http://dx.doi.org/10.1002/jgrc.20247`.

Gu, W., Y. Lin, Y. Xu, S. Yuan, J. Tao, L. Li, and C. Liu, 2012: Sea ice desalination under the force of gravity in low temperature environments. *Desalination*, **295 (0)**, 11–15.

Holt, B. and S. A. Digby, 1985: Processes and imagery of first-year fast sea ice during the melt season. *J. Geophys. Res.*, **90 (C3)**, 5045–5062, doi:10.1029/JC090iC03p05045.

Hunke, E. C., D. Notz, A. K. Turner, and M. Vancoppenolle, 2011: The multiphase physics of sea ice: a review for model developers. *The Cryosphere*, **5 (4)**, 989–1009, doi:10.5194/tc-5-989-2011.

Huwald, H., L.-B. Tremblay, and H. Blatter, 2005a: A multilayer sigma-coordinate thermodynamic sea ice model: Validation against surface heat budget of the arctic ocean (sheba)/sea ice model intercomparison project part 2 (simip2) data. *J. Geophys. Res.*, **110 (C5)**, C05 010.

Huwald, H., L. B. Tremblay, and H. Blatter, 2005b: Reconciling different observational data sets from surface heat budget of the arctic ocean (sheba) for model validation purposes. *J. Geophys. Res.*, **110 (C5)**, doi:10.1029/2003JC002221.

Jardon, F., F. Vivier, M. Vancoppenolle, A. Lourenco, P. Bouruet-Aubertot, and Y. Cuypers, 2013: Full-depth desalination of warm sea ice. *J. Geophys. Res.*, **118**, 1–13.

Jeffery, N., E. C. Hunke, and S. M. Elliott, 2011: Modeling the transport of passive tracers in sea ice. *J. Geophys. Res.*, **116 (C7)**, C07 020, doi:10.1029/2010JC006527.

Jeffries, M. O., H. Roy Krouse, B. Hurst-Cushing, and T. Maksym, 2001: Snow-ice accretion and snow-cover depletion on antarctic first-year sea-ice floes. *Ann. Glaciol.*, **33 (1)**, 51–60.

Jones, K. A., M. Ingham, and H. Eicken, 2012: Modeling the anisotropic brine microstructure in first-year arctic sea ice. *J. Geophys. Res.*, **117 (C2)**, C02 005.

Kaleschke, L., X. Tian-Kunze, N. Maaß, M. Mäkynen, and M. Drusch, 2012: Sea ice thickness retrieval from smos brightness temperatures during the arctic freeze-up period. *Geophys. Res. Lett.*, **39 (5)**.

Kovacs, A., 1997: Sea ice. part 1. bulk salinity versus ice floe thickness. *CRREL Report*, **96-7**.

Kwok, R., H. J. Zwally, and D. Yi, 2004: Icesat observations of arctic sea ice: A first look. *Geophys. Res. Lett.*, **31 (16)**.

Lecomte, O., T. Fichefet, M. Vancoppenolle, and M. Nicolaus, 2011: A new snow thermodynamic scheme for large-scale sea-ice models. *Ann. Glaciol.*, **52 (57)**, 337–346.

Lei, R., Z. Li, B. Cheng, Z. Zhang, and P. Heil, 2010: Annual cycle of landfast sea ice in prydz bay, east antarctica. *J. Geophys. Res.*, **115 (C2)**, C02 006.

Lemieux, J.-F., B. Tremblay, J. Sedlek, P. Tupper, S. Thomas, D. Huard, and J.-P. Auclair, 2010: Improving the numerical convergence of viscous-plastic sea ice models with the jacobian-free newton-krylov method. *J. Comput. Phys.*, **229 (8)**, 2840–2852.

Levenberg, K., 1944: A method for the solution of certain non-linear problems in least squares. *QJ of Appl. Math*, **II (2)**, 164–168.

Lietaer, O., E. Deleersnijder, T. Fichefet, M. Vancoppenolle, R. Comblen, S. Bouillon, and V. Legat, 2011: The vertical age profile in sea ice: Theory and numerical results. *Ocean Model.*, **40 (34)**, 211–226.

Light, B., T. C. Grenfell, and D. K. Perovich, 2008: Transmission and absorption of solar radiation by arctic sea ice during the melt season. *J. Geophys. Res.*, **113 (C3)**.

Losch, M. and S. Danilov, 2012: On solving the momentum equations of dynamic sea ice models with implicit solvers and the elastic-viscous-plastic technique. *Ocean Model.*, **41 (0)**, 42–52, URL `http://www.sciencedirect.com/science/article/pii/S1463500311001673`.

Maas, N., L. Kaleschke, X. Tian-Kunze, and M. Drusch, 2013: Snow thickness retrieval over thick arctic sea ice using smos satellite data. *The Cryosphere Discussions*, **7 (4)**, 3627–3674.

Maksym, T., 2001: Brine percolation, flooding and snow ice formation on antarctic sea ice. Ph.D. thesis, University of Alaska Fairbanks, U.S.A.

Maksym, T. and M. O. Jeffries, 2000: A one-dimensional percolation model of flooding and snow ice formation on antarctic sea ice. *J. Geophys. Res.*, **105 (C11)**, 26 313–26 331.

Maksym, T. and M. O. Jeffries, 2001: Phase and compositional evolution of the flooded layer during snow-ice formation on antarctic sea ice. *Ann. Glaciol.*, **33**, 37–44, WOS:000173446300006.

Malmgren, F., 1927: On the properties of sea-ice: Norwegian north polar expedition with the maud, 1918-1925, sci. Results.

Maykut, G. A. and N. Untersteiner, 1971: Some results from a time-dependent thermodynamic model of sea ice. *J. Geophys. Res.*, **76 (6)**, 1550–&, doi:10.1029/JC076i006p01550.

Nakawo, M. and N. K. Sinha, 1981: Growth-rate and salinity profile of 1st-year sea ice in the high arctic. *J. Glaciol.*, **27 (96)**, 315–330.

Notz, D., 2005: Thermodynamic and fluid-dynamical processes in sea ice. Ph.D. thesis, Univ. of Cambridge,Cambridge, U.K.

Notz, D. and M. G. Worster, 2006: A one-dimensional enthalpy model of sea ice. *Ann. Glaciol.*, **44 (1)**, 123–128, doi:10.3189/172756406781811196.

Notz, D. and M. G. Worster, 2008: In situ measurements of the evolution of young sea ice. *J. Geophys. Res.*, **113 (C3)**, C03 001, doi:10.1029/2007JC004333.

Notz, D. and M. G. Worster, 2009: Desalination processes of sea ice revisited. *J. Geophys. Res.*, **114 (C5)**, C05 006, doi:10.1029/2008JC004885.

Oertling, A. B. and R. G. Watts, 2004: Growth of and brine drainage from nacl-h2o freezing: A simulation of young sea ice. *J. Geophys. Res.*, **109 (C4)**, C04 013, doi:10.1029/2001JC001109.

Pedersen, C. A., E. Roeckner, M. Luthje, and J. G. Winther, 2009: A new sea ice albedo scheme including melt ponds for echam5 general circulation model. *Journal of Geophysical Research-atmospheres*, **114**, D08 101, doi:10.1029/2008JD010440.

Perovich, D., J. Richter-Menge, B. Elder, T. Arbetter, K. Claffey, and C. Polashenski, 2009: Observing and understanding climate change: Monitoring the mass balance, motion, and thickness of arctic sea ice. URL `http://imb.crrel.usace.army.mil`, URL `http://imb.crrel.usace.army.mil`.

Perovich, D. K., et al., 1999: Year on ice gives climate insights. *Eos Trans. AGU*, **80 (41)**, 481–486, doi:10.1029/EO080i041p00481-01.

Petrich, C., P. J. Langhorne, and Z. F. Sun, 2004: Numerical simulation of sea ice growth and desalination. *Proceedings of the 17th International Symposium on Ice*, International Association of Hydraulic Engineering and Research, Vol. 3, 68–78.

Petrich, C., P. J. Langhorne, and Z. F. Sun, 2006: Modelling the interrelationships between permeability, effective porosity and total porosity in sea ice. *Cold Reg. Sci. Technol.*, **44 (2)**, 131–144, doi:10.1016/j.coldregions.2005.10.001.

Pringle, D. J., H. Eicken, H. J. Trodahl, and L. G. E. Backstrom, 2007: Thermal conductivity of landfast antarctic and arctic sea ice. *J. Geophys. Res.*, **112 (C4)**, C04 017, doi:10.1029/2006JC003641.

Pringle, D. J., J. E. Miner, H. Eicken, and K. M. Golden, 2009: Pore space percolation in sea ice single crystals. *J. Geophys. Res.*, **114**, C12 017, doi:10.1029/2008JC005145.

Rees Jones, D. W. and M. G. Worster, 2013a: Fluxes through steady chimneys in a mushy layer during binary alloy solidification. *J. Fluid Mech.*, **714**, 127–151.

Rees Jones, D. W. and M. G. Worster, 2013b: A simple dynamical model for gravity drainage of brine from growing sea ice. *Geophys. Res. Lett.*, 1–5.

Roscoe, H. K., B. Brooks, A. V. Jackson, M. H. Smith, S. J. Walker, R. W. Obbard, and E. W. Wolff, 2011: Frost flowers in the laboratory: Growth, characteristics, aerosol, and the underlying sea ice. *J. Geophys. Res.*, **116 (D12)**, D12 301.

Rysgaard, S., R. N. Glud, M. K. Sejr, M. E. Blicher, and H. J. Stahl, 2008: Denitrification activity and oxygen dynamics in arctic sea ice. *Polar Biol.*, **31 (5)**, 527–537.

Saenz, B. T. and K. R. Arrigo, 2012: Simulation of a sea ice ecosystem using a hybrid model for slush layer desalination. *J. Geophys. Res.*, **117 (C5)**, C05 007.

Schwarzacher, W., 1959: Pack-ice studies in the arctic ocean. *J. Geophys. Res.*, **64 (12)**, 2357–2367.

Schwerdtfeger, P., 1963: The thermal properties of sea ice. *J. Glaciol.*, **4 (36)**, 789–807.

Semtner, A. J., 1976: Model for thermodynamic growth of sea ice in numerical investigations of climate. *J. Phys. Oceanogr.*, **6 (3)**, 379–389, doi:10.1175/1520-0485(1976)006⟨0379:AMFTTG⟩2.0.CO;2.

Tait, S. and C. Jaupart, 1992: Compositional convection in a reactive crystalline mush and melt differentiation. *J. Geophys. Res.*, **97 (B5)**, 6735–6756.

Tedesco, L., M. Vichi, J. Haapala, and T. Stipa, 2010: A dynamic biologically active layer for numerical studies of the sea ice ecosystem. *Ocean Model.*, **35 (1-2)**, 89–104.

Tedesco, L., M. Vichi, and D. N. Thomas, 2012: Process studies on the ecological coupling between sea ice algae and phytoplankton. *Ecol. Model.*, **226**, 120–138.

Turner, A. K., E. C. Hunke, and C. M. Bitz, 2013: Two modes of sea-ice gravity drainage: A parameterization for large-scale modeling. *J. Geophys. Res.*, **118 (5)**, 2279–2294.

Vancoppenolle, M., C. M. Bitz, and T. Fichefet, 2007: Summer landfast sea ice desalination at point barrow, alaska: Modeling and observations. *J. Geophys. Res.*, **112 (C4)**, C04 022, doi:10.1029/2006JC003493.

Vancoppenolle, M., T. Fichefet, and C. M. Bitz, 2006: Modeling the salinity profile of undeformed arctic sea ice. *Geophys. Res. Lett.*, L21 501–1–5, doi:10.1029/2006GL028342.

Vancoppenolle, M., T. Fichefet, H. Goosse, S. Bouillon, G. Madec, and M. A. M. Maqueda, 2009: Simulating the mass balance and salinity of arctic and antarctic sea ice. 1. model description and validation. *Ocean Model.*, **27 (1-2)**, 33–53, doi:10.1016/j.ocemod.2008.10.005.

Vancoppenolle, M., H. Goosse, A. de Montety, T. Fichefet, B. Tremblay, and J.-L. Tison, 2010: Modeling brine and nutrient dynamics in antarctic sea ice: The case of dissolved silica. *J. Geophys. Res.*, **115 (C2)**, C02 005, doi:10.1029/2009JC005369.

Weeks, W., 2010: *On sea ice*. University of Alaska Press.

Weeks, W. F. and O. S. Lee, 1958: Observations on the physical properties of sea-ice at hopedale, labrador. *Arctic*, **11 (3)**, 134–155.

Wells, A. J., J. S. Wettlaufer, and S. A. Orszag, 2010: Maximal potential energy transport: A variational principle for solidification problems. *Phys. Rev. Lett.*, **105 (25)**, 254 502, doi:10.1103/PhysRevLett.105.254502.

Wells, A. J., J. S. Wettlaufer, and S. A. Orszag, 2011: Brine fluxes from growing sea ice. *Geophys. Res. Lett.*, **38 (4)**, L04 501.

Wettlaufer, J. S., M. G. Worster, and H. E. Huppert, 1997: Natural convection during solidification of an alloy from above with application to the evolution of sea ice. *J. Fluid Mech.*, **344**, 291–316, doi:10.1017/S0022112097006022.

Widell, K., I. Fer, and P. M. Haugan, 2006: Salt release from warming sea ice rid g-2701-2010. *Geophys. Res. Lett.*, **33 (12)**, L12 501, doi:10.1029/2006GL026262.

Wiese, M., 2012: Laboratory experiments on the thermodynamics of melting sea ice. M.S. thesis, Meteorologisches Institut, Department Geowissenschaften,University Hamburg.

Wilkins, N., 2010: Thermodynamics of thin sea ice. M.S. thesis, Meteorological Institut, University of Hamburg, Germany.

Winton, M., 2000: A reformulated three-layer sea ice model. *J. Atmos. Oceanic Technol.*, **17 (4)**, 525–531.

Acknowledgements

I was lucky enough to conduct my PhD research under ideal conditions. The level of scientific as well as administrative support I received from my panel, the IMPRS-ESM & MPI-M, and CIS is very appreciated.

I would like to thank my many competent and helpful colleagues who were willing to provide solid advice, honest criticism, and lend a sympathetic ear to the first world problems of a young scientist. This applies especially to my fellow and former doctoral candidates, the Hamburg sea-ice experts, the MPI Allstars, the sea-ice group, my office mate and fellow mate addict Mathias, and Einar the world leading expert on land fast ice in the Kara sea.

Thanks Dirk for letting me approach problems in my own way while also pushing me in some directions I did not want to go, for almost always making time to be available when needed, and for having such a short name for easy citation.

Lastly, I would like to thank everybody who contributes to all the free and open software on which I relied throughout my PhD, my anonymous and non-anonymous reviewers & proofreaders, the international sea-ice community for their warm welcome, and the German taxpayers for funding basic research such as my PhD.



ISSN 1614-1199